

ATOMIC FORCE MICROSCOPY
Imaging/spectroscopy of Biological
Membranes

Purple membranes

Light activation of these proteins modulates cellular excitability with millisecond precision

The so-called **Purple Membranes (PM)** are part of the membrane of the archaea *Halobacterium salinarium*, an extremophile naturally found in salt saturated water.

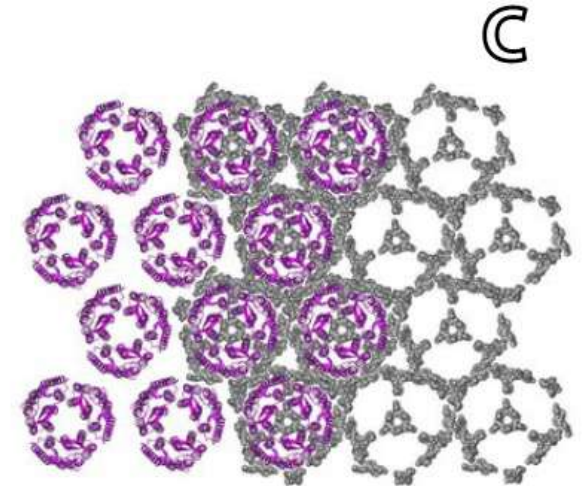
This particular biological membrane **contains only one protein, bacteriorhodopsin (bR) and about seven different unusual membrane lipids** assembled in a hexagonal lattice of bR trimers (p3 crystallographic point group, 6.2 nm lattice constant).

The protein-lipid ratio has recently been determined to be **10 lipids per bR**.

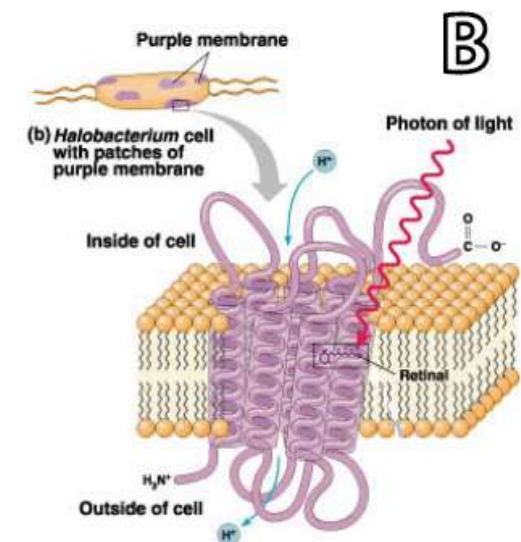
The proteins represent 75% of PM mass and cover 50% of the membrane surface.

bR acts as a **light-driven vectorial proton pump** which converts photonic energy into a proton gradient across the membrane. The induced electrochemical gradient is subsequently used by ATP-synthase as an alternative driving force to produce ATP in mediums particularly poor in oxygen.

The absorption spectrum of bR in its ground state (maximum absorption at 565 nm) is responsible for the purple colour of PM



2D hexagonal lattice



Purple membranes

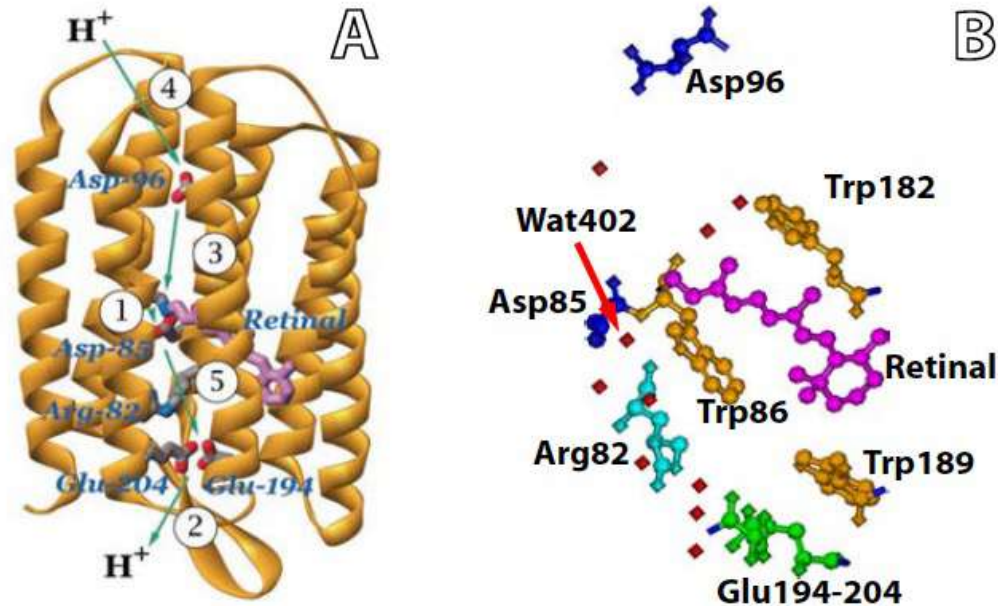
PM is one of the best known biological membranes and an important model system to confront new theories and experimental methods.

bR was indeed the first integral membrane protein whose structure was determined by X-ray crystallography of three-dimensional crystals grown in cubic lipid phase (non-soluble proteins: difficulty in crystallization!)

N.B: membrane proteins are either peripheral (at the surface) and soluble in high ionic strength aqueous solution (1 M salt) or integral, and can be solubilized only with detergent

All the proteins in membranes are coded by 20-30 % of the genome! But of all the known protein structures, only 5 % are of membrane proteins!

Purple membranes

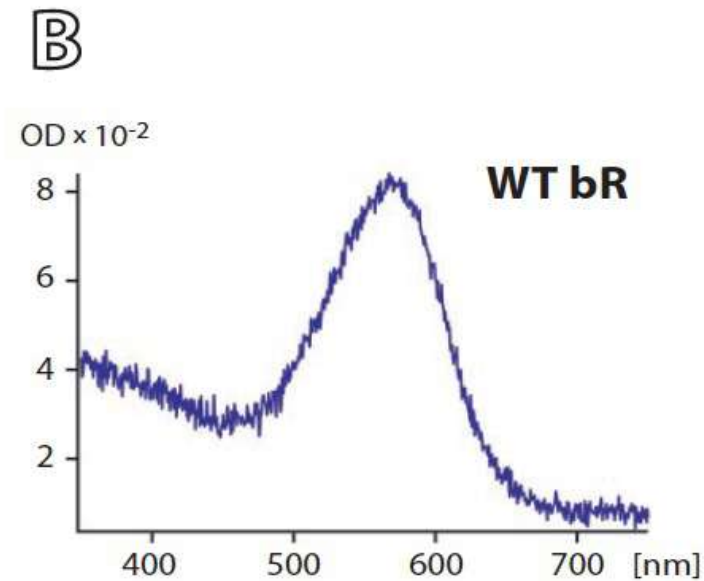
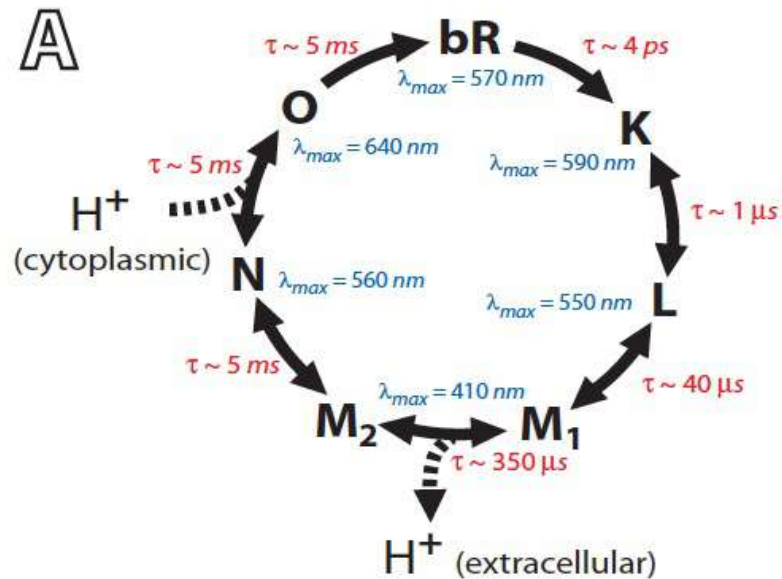


bR is an integral 26 KDa membrane protein composed 248 amino acids arranged in 7 transmembrane α -helices that surround a central cavity which encloses a chromophore, the retinal, linked to the protein backbone (Lys216 residue, helix G) via a Schiff base.

When the protein is in its fundamental/ground state (called bR state), the retinal chromophore adopts an all-trans configuration. Upon light absorption by the protein, the retinal can isomerize around its $C_{13} = C_{14}$ double bond, adopting a 13-cis configuration. This new chromophore conformation triggers a series of structural rearrangements in bR leading to the pumping of a proton from the inside to the outside of the archa.

Purple membranes

The isomerization of the retinal chromophore modify temporarily the position of charged residues within the protein allowing directional pumping of one proton over a \sim **10-20 ms photo-cycle**. The modifications of the retinal local electrical environment can be observed spectroscopically



Purple membranes

In PM, **bR molecules lateral and rotational movements are prevented by the crystalline assembly**. PM is rather rigid with a viscosity typically 10^3 - 10^4 higher than that of halobacterial membrane lipids.

Within one **trimer**, the proximity between the bR molecules allows direct protein-protein interactions through the formation of salt bridges, hydrogen bonds and van der Waals interactions between the α -helices of the different proteins involved.

These interactions are however not sufficient to explain the **important trimer stability in which specific protein-lipid interactions are involved**. The exceptional cohesion within a single trimer is believed to be related to the protein activity through cooperativity.

Purple membranes

PM contains many different lipids some of which are not found in any other membrane and are necessary for bR activity, also in reconstituted membranes. To date, seven different lipids have been reported :

three phospholipids, two glycolipids, squalene and traces of vitamin MK8.

The requirement of a fixed membrane composition indicates that **selective interactions occur between bR and certain lipid molecules** and that these interactions are essential for lattice assembly and bR function.

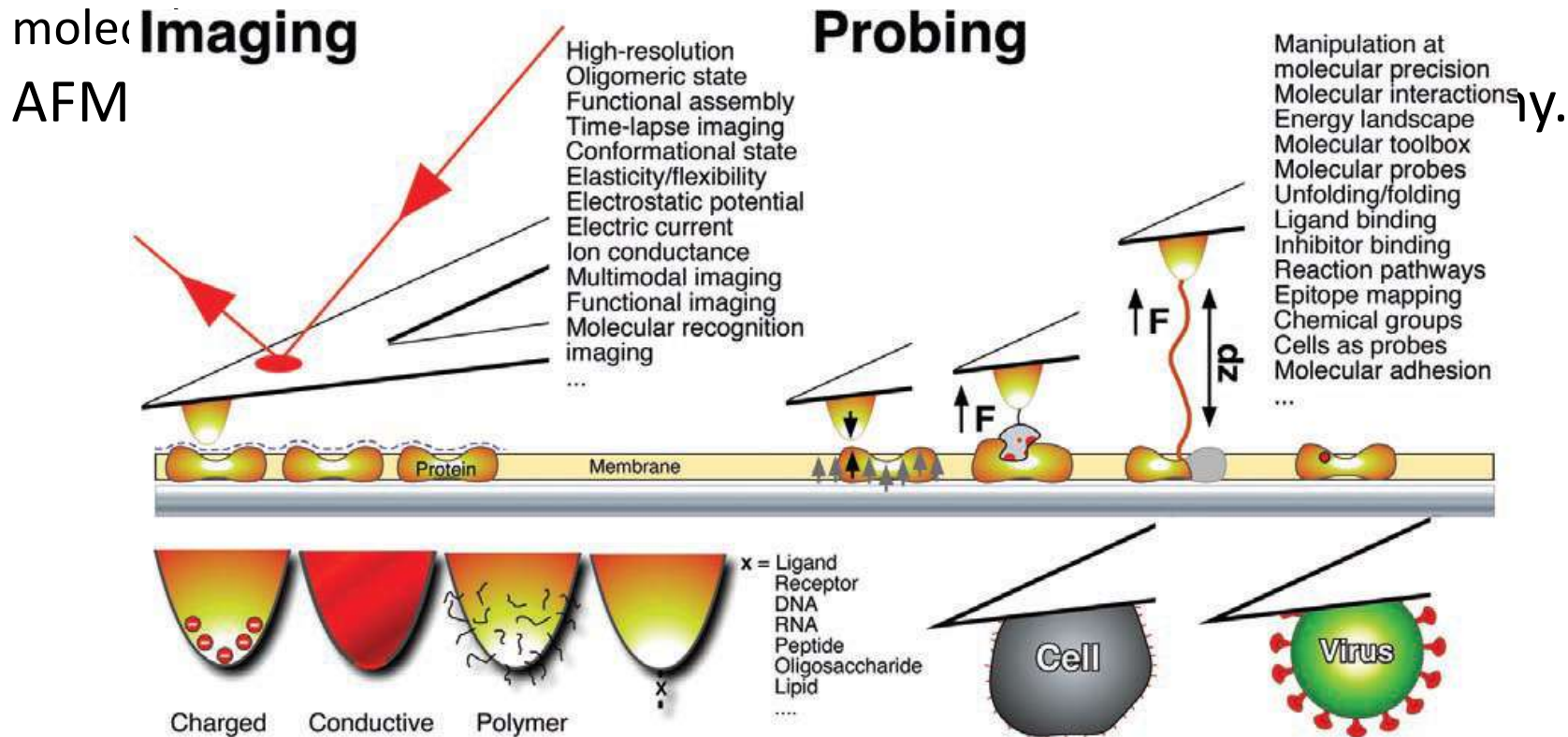
Phospholipids represent ~ 40% of PM lipids. their head-group comports two negative charges which makes them particularly hydrophilic. Fluorescence studies have demonstrated that phospholipids **are located mainly in PM cytoplasmic leaflet inter-trimer space**.

Glycolipids represent ~ 30% of PM lipids. Unlike phospholipids, glycolipids show clear patterns in PM diffraction experiments suggesting that they are **specifically and tightly bound to bR**.

Local probe techniques have also been used to study purple membrane (Tamayo et al. 1995) and bR was **the first membrane protein extensively studied by atomic force microscopy and force spectroscopy**.

HR-AFM in membrane biology

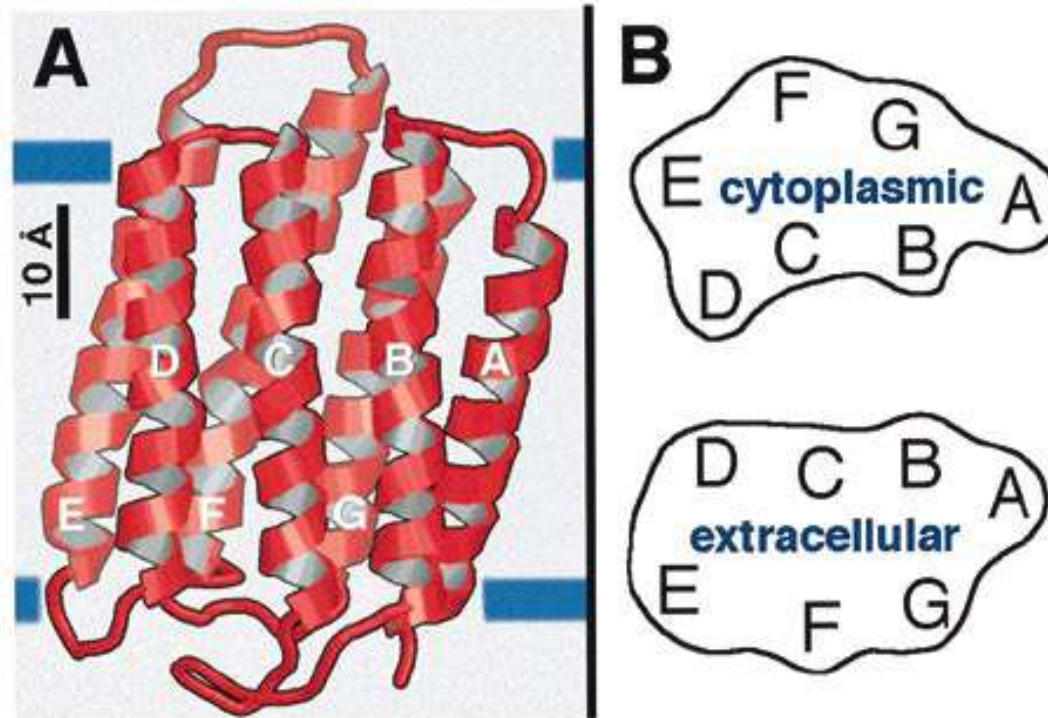
High-resolution AFM has been applied to the imaging of bacterial membrane proteins, deriving the free energy landscape for domains within single protein molecules.



Imaging resolution in cell membranes: 10 nm

Imaging resolution in supported cell membranes: better than 1 nm (no fixing, labeling, Staining, room T, buffer solution)

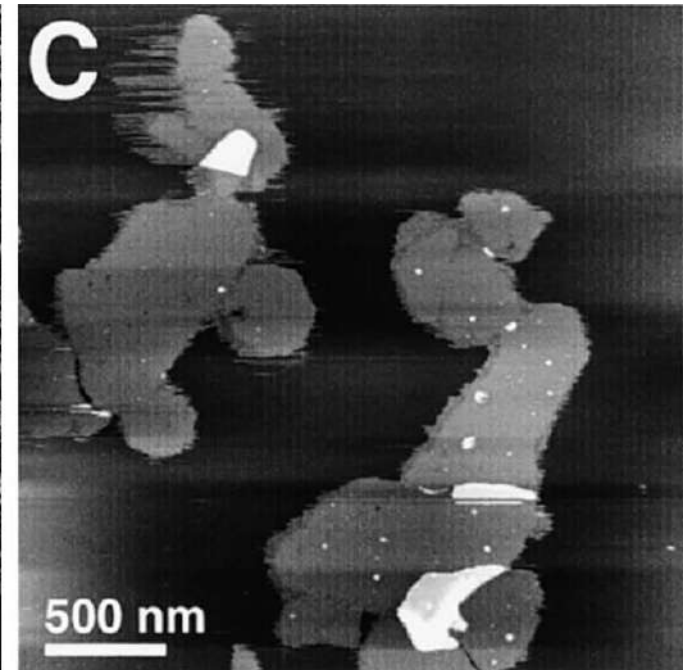
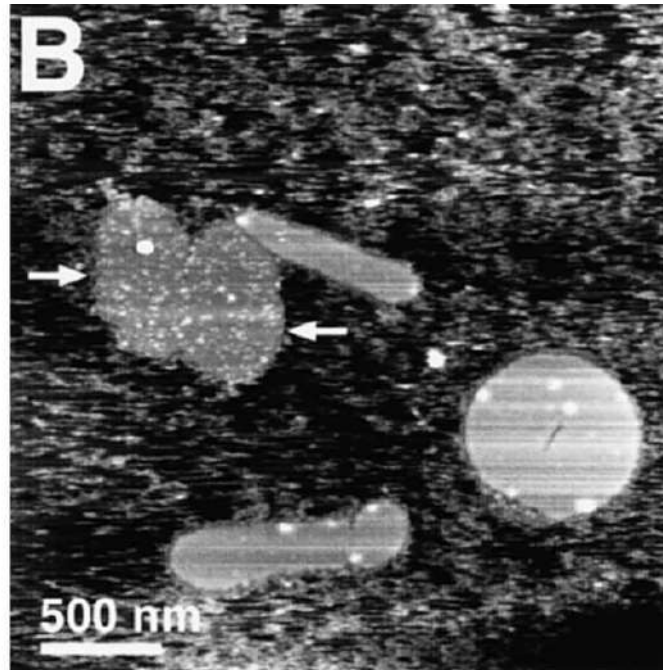
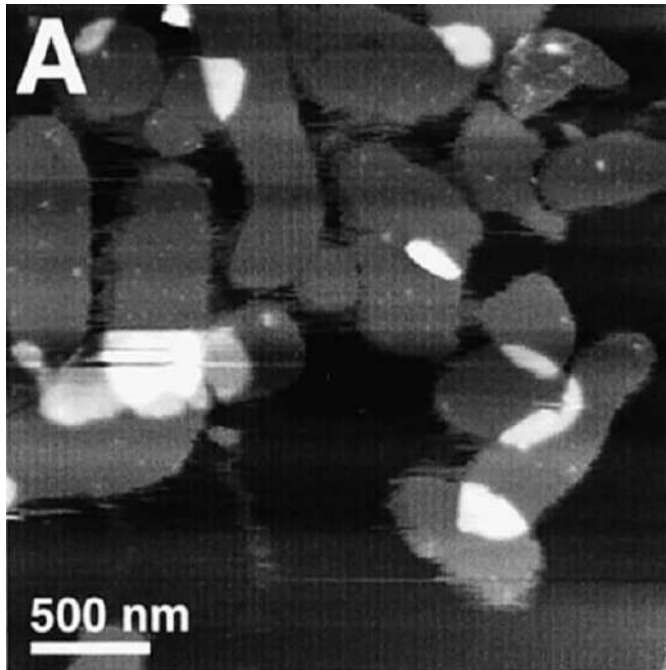
S. Scheuring, D. Muller, H. Stalberg, H.-A. Engel, A. Engel, *Eur. Biophys. J.* **31**, 172 (2002)



Structure of bacteriorhodopsin. (a) Ribbon representation as revealed by electron crystallography (Grigorieff et al., 1996). Because of their disordering, the N terminus of helix A and the C terminus of helix G were not resolved and the B-C loop was only partly resolved. Blue lines indicate the cytoplasmic and extracellular surfaces determined by Kimura et al. (1997).

(b) Outlines of 10 Å thick slices of the cytoplasmic and the extracellular BR surface.

PM reconstructed membrane on mica. Cytoplasmic vs. extracellular side

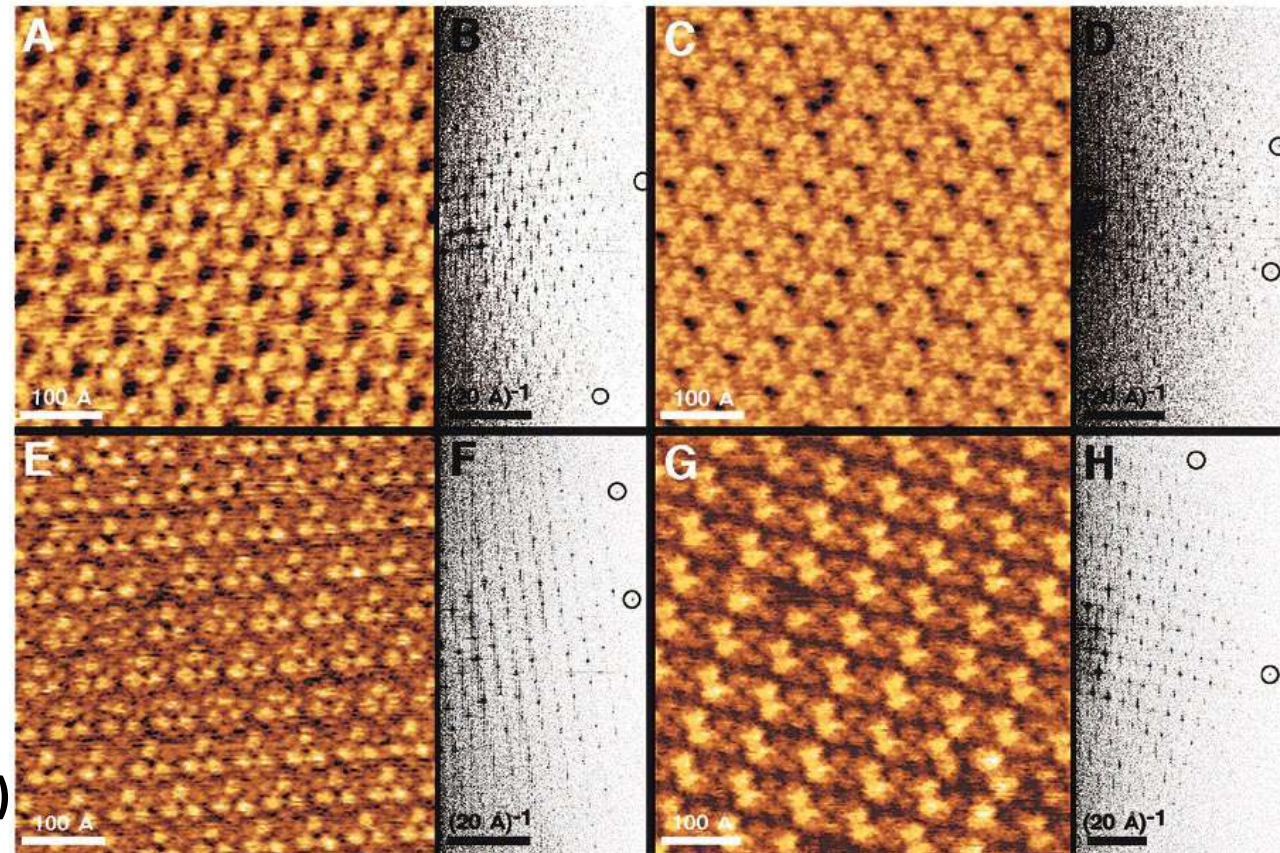


8.3(\pm 1.9) Å (n . 398)

6.4(\pm 1.2) Å (n . 398)

$a=b=6.2 \pm 0.2$ nm

The loops connecting the **alpha** - helices appeared to be disordered as they could not be resolved reliably.



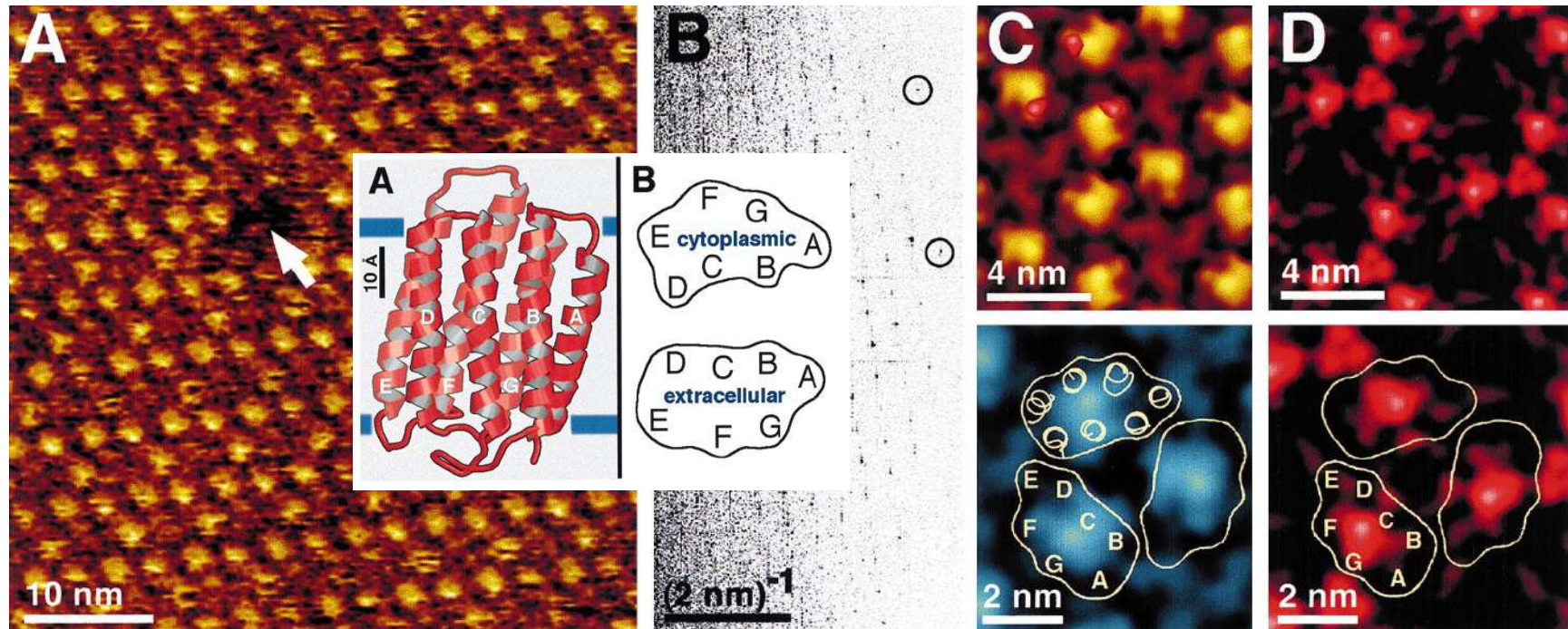
5.3(\pm 0.7) Å (n . 320)

in A protrusion arises from the loop connecting transmembrane α -helices E and F

- (a) Native cytoplasmic surface recorded at 100 pN. (b) Power spectrum of (a).
- (c) Cytoplasmic surface recorded at 200 pN. (d). Power spectrum of (c).
- (e) Native extracellular surface recorded at 100 pN. (f) Power spectrum of (e).
- (g) Orthorhombic crystal of BR recorded at 100 pN. In this crystal form (p22121) the rows of BR dimers alternate, to expose either their cytoplasmic or their extracellular surfaces to the aqueous solution. (h) Power spectrum of (g).

N.B.: For the achievement of high resolution imaging a specific ionic concentration was required in order to balance van der Waals attractive forces with Electrostatic Double Layer repulsive forces (Muller & Engel 1997; Muller et al. 1999a).

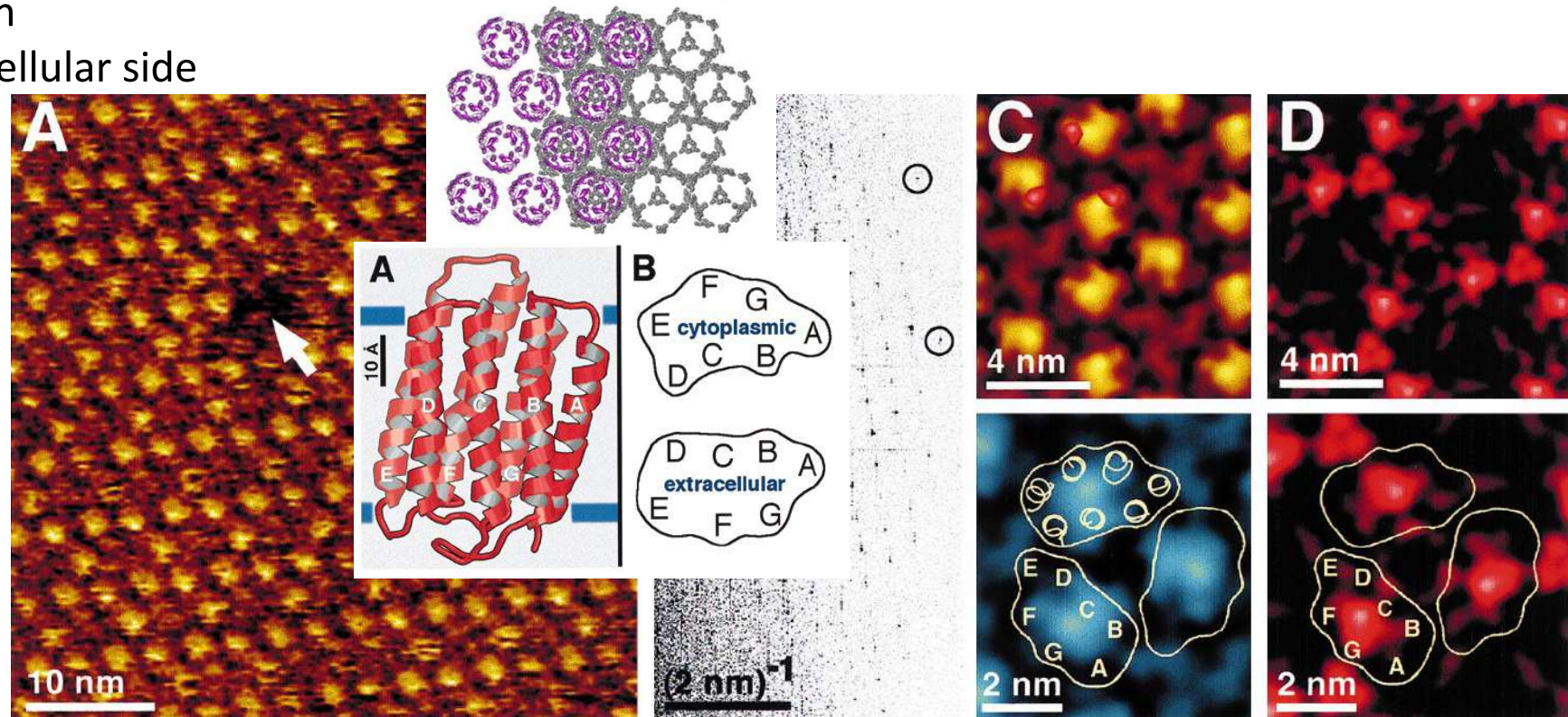
Imaging of a statistically significant number of single proteins by AFM allows structural variability assessment and multivariate statistical classification to unravel the principal modes of the protein motion. arrangement of tripartite protrusions on a trigonal lattice (a = b = 6.2 ± 0.2 nm) exhibiting a maximum height difference to the lipid membrane of 0.53 ± 0.07 nm.



Extracellular purple membrane surface recorded in buffer solution (A). The PM surface exhibits a defect of the size of a BR trimer (arrow). (B) The power spectrum of A extends to the 11th order indicating a lateral resolution of 0.49 nm. (C) Averaged extracellular surface of the BR trimer (average of 320 unit cells). The correlation average is displayed in perspective view (top, shaded in yellow brown) and in top view (bottom, in blue) with a vertical brightness range of 1 nm and exhibited a 6.1% root-mean-square (RMS) deviation from three-fold symmetry.

Imaging of a statistically significant number of single proteins by AFM allows structural variability assessment and multivariate statistical classification to unravel the principal modes of the protein motion

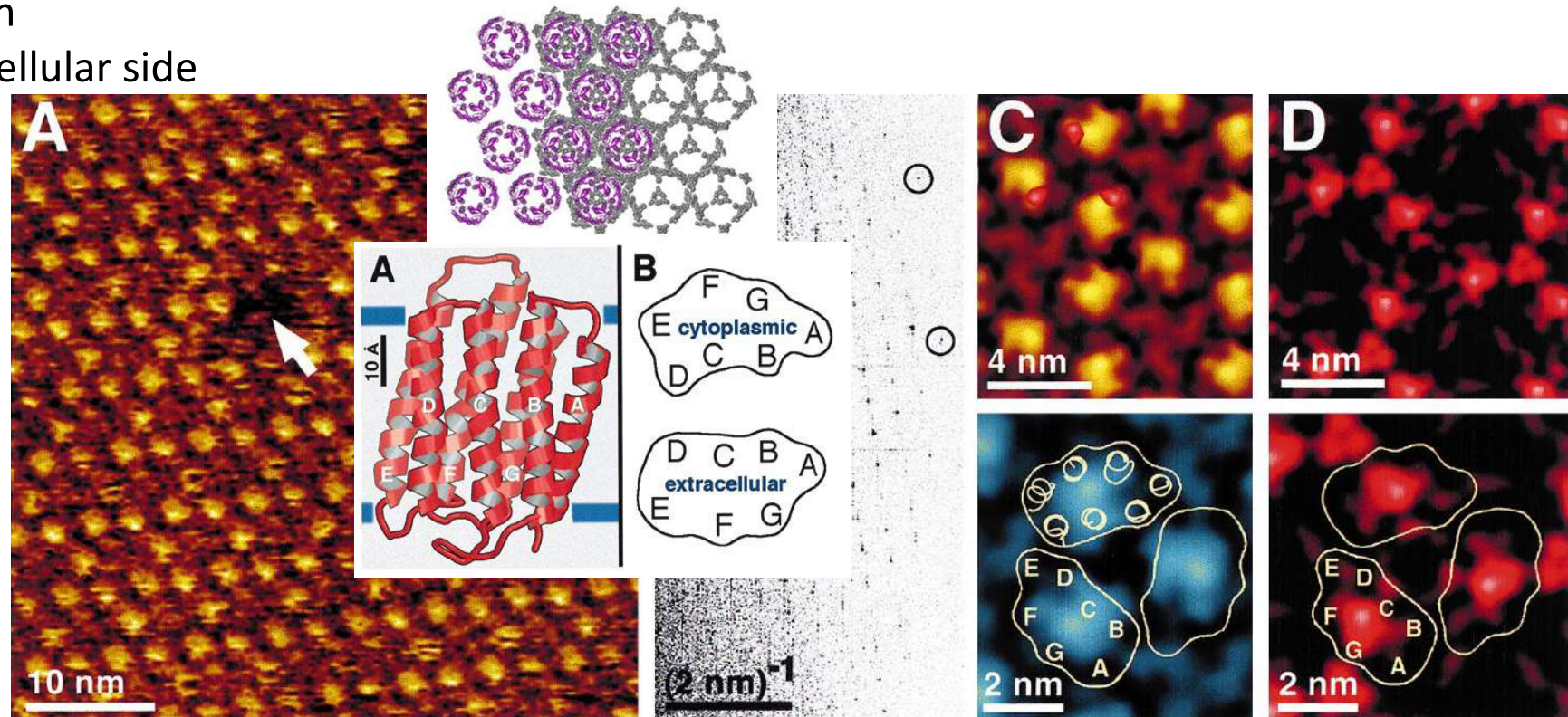
Extracellular side



To assess the flexibility of the different structures, **standard deviation (S.D.) maps are calculated** (D) and had a range from 0.07 (lipid) to 0.12 nm (region of the FG loop). Surface regions exhibiting an S.D. above 0.1 nm are superimposed in red-to-white shades in top of C. The topograph was recorded in buffer solution (100 mM KCl, 10 mM Tris[^] HCl, pH 7.8) at a loading force of 100 pN. The outlined BR trimer representing sections close to the extracellular surface of the lipid membrane was obtained after merging five atomic models of BR derived from electron and X-ray crystallography.

Imaging of a statistically significant number of single proteins by AFM allows structural variability assessment and multivariate statistical classification to unravel the principal modes of the protein motion

Extracellular side



The most prominent protrusion is the L-hairpin in the BC loop connecting the transmembrane K-helices B and C. In the topograph, this protrusion is located between helices C and G. The shoulder near helix A is likely the N-terminus. Loop FG may contribute to the major protrusion, although it does not extend much above the lipid headgroups in the atomic models.

However, this area exhibits an enhanced standard deviation (S.D.) of 0.12 nm compared to the background (0.07 nm; Fig. 2D) indicating an increased structural variability and alternative conformations not reflected in the atomic models derived from electron and X-ray crystallography.

D.J. Muller et al. *J. Mol. Biol.* (1999) 285, 1903-1909 / *Bioch. et Bioph. Acta* 1460 (2000) 27-38

Pronounced protrusion extending 0.83 ± 0.19 nm above the lipid surface. This protrusion is associated with the loop connecting helices E and F

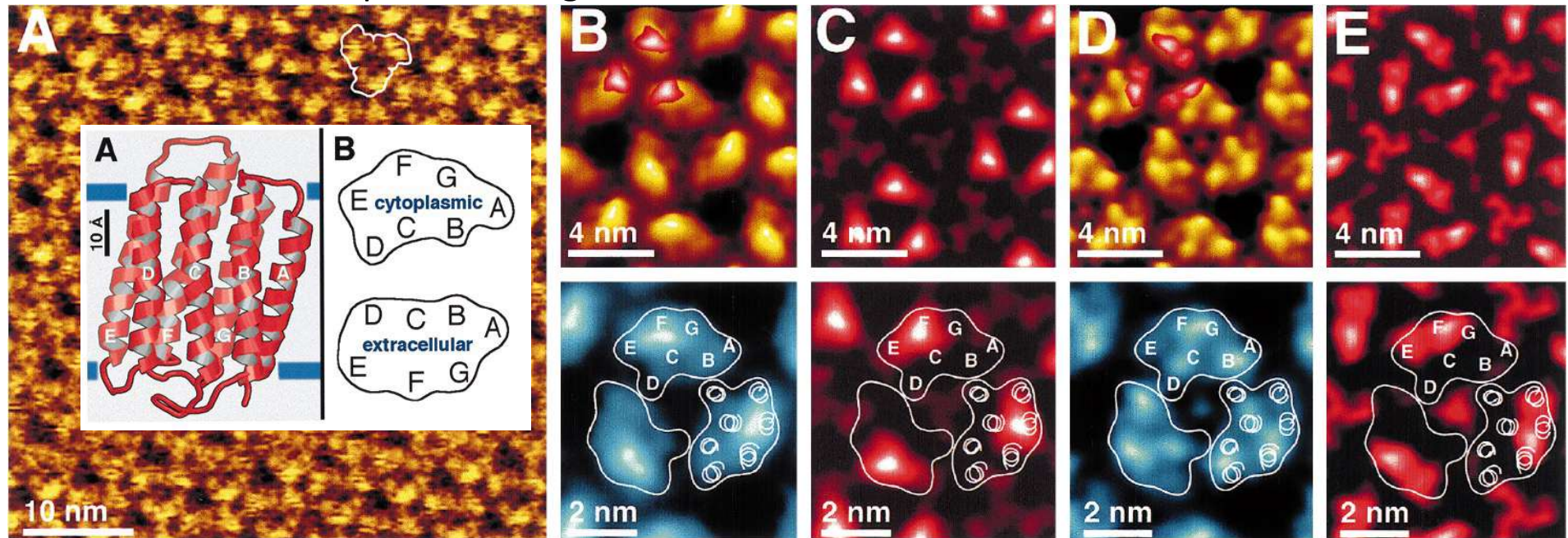


Fig. 3. Force-dependent surface topography of the **native cytoplasmic purple membrane surface**. (A) At the top of the image, the force applied to the AFM stylus was 100 pN. While scanning the surface line by line, the force was increased until it reached 150 pN at the bottom of the image. This force-induced conformational change of BR was fully reversible. Correlation averages of the cytoplasmic surface recorded at 100 pN (B) and at 200 pN (D). The correlation averages are displayed in perspective view (top, shaded in yellow brown) and in top view (bottom, in blue) with a vertical brightness range of 1 nm and exhibited 9.2% (B) and 14.1% (D) RMS deviations from three-fold symmetry. Structural flexibilities were accessed by S.D. maps (C and E corresponding to B and D, respectively) which had a range from 0.08 (lipid) to 0.19 nm (EF loop region). Surface regions exhibiting an S.D. above 0.12 nm are superimposed in red-to-white shades in the top of B and D. The topograph was recorded in buffer solution (100 mM KCl, 10 mM Tris[^]HCl, pH 7.8). The outlined BR trimer representing sections close to the cytoplasmic surface of the lipid membrane was obtained after merging six atomic models of BR.

At 200 pN AFM topographs changed: prominent EF loops (S.D. of 0.19 nm) bent away; shorter loops of the BR monomers were visualized. conformational change fully reversible suggesting that loop EF is flexible

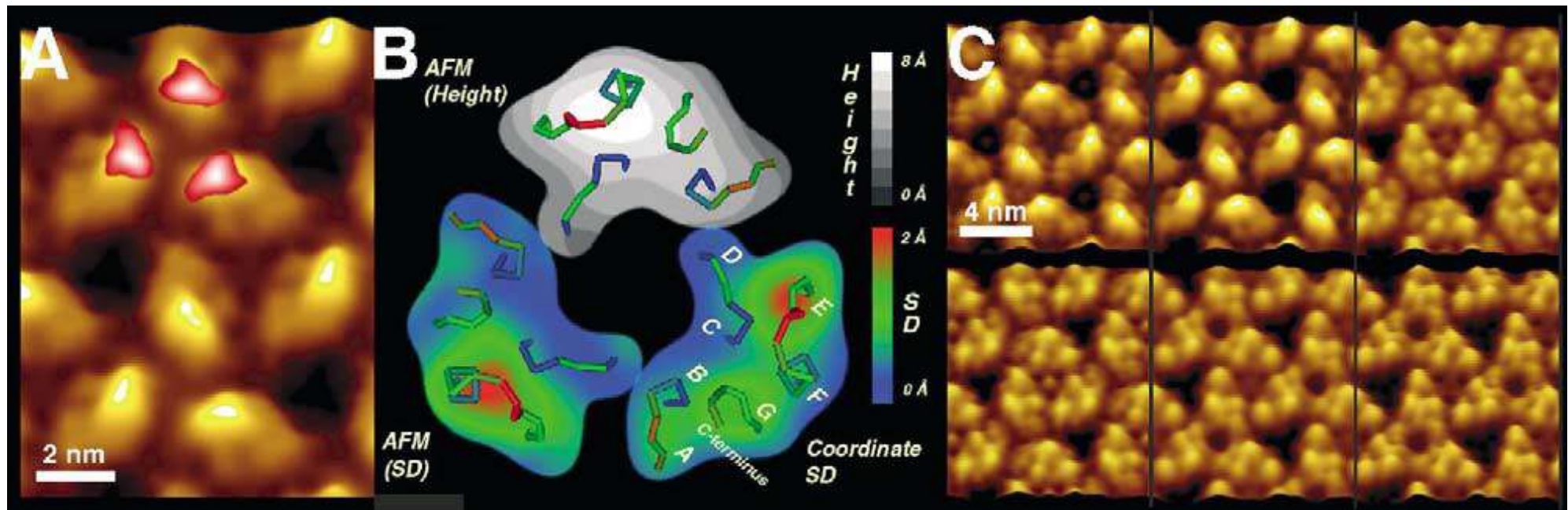
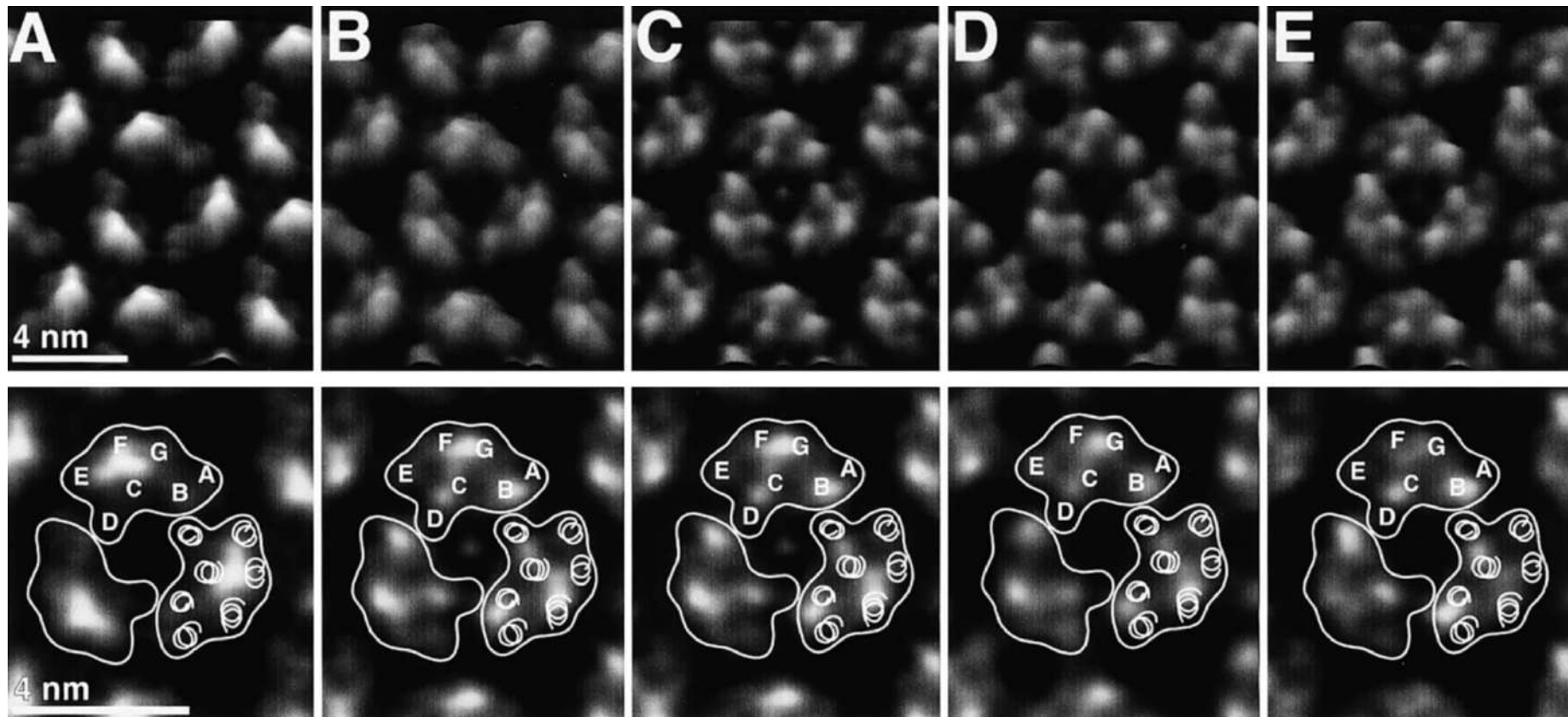
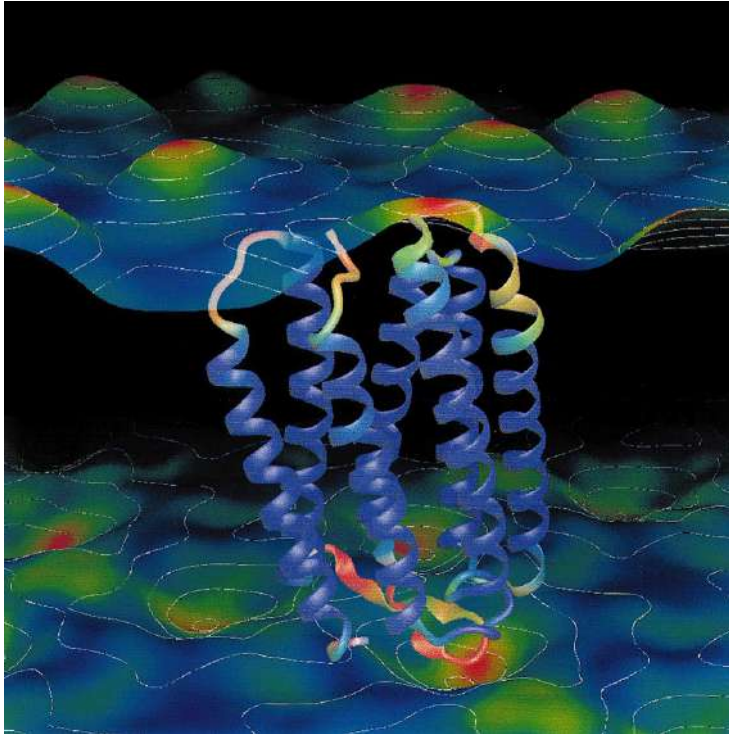


Fig. 16. Quantitative analysis of the native cytoplasmic purple membrane surface. (A) Correlation average of the AFM topograph recorded at an applied force of 100 pN (Müller et al., 1999b). Regions with enhanced flexibility are derived from SD maps and superimposed in red to white shades. (B) Different surface properties of bacteriorhodopsin. The surface loops are shown as backbone tracings colored according to the backbone coordinate root-mean-square deviation (SD) calculated after merging five different atomic models of bacteriorhodopsin (Heymann et al., 1999). The gray scale image shows the height map determined by AFM (A) with the prominent protrusion representing the EF loop. The colored monomers represent the SD between the atomic models, and of the height measured by AFM. (C) Unraveling the force induced structural changes of the cytoplasmic surface by multivariate statistical analysis. Top left: purple membrane imaged at 80 pN. Top center: same membrane imaged at approximately 100 pN. Top right: at about 150 pN the EF loop is bent away while the shorter polypeptide loops of the cytoplasmic surface become visible. Bottom row: three conformations differing in their central protrusion are observed at approximately 180 pN. Topographs exhibit a vertical range of 1 nm and are displayed as relief tilted by 5°.



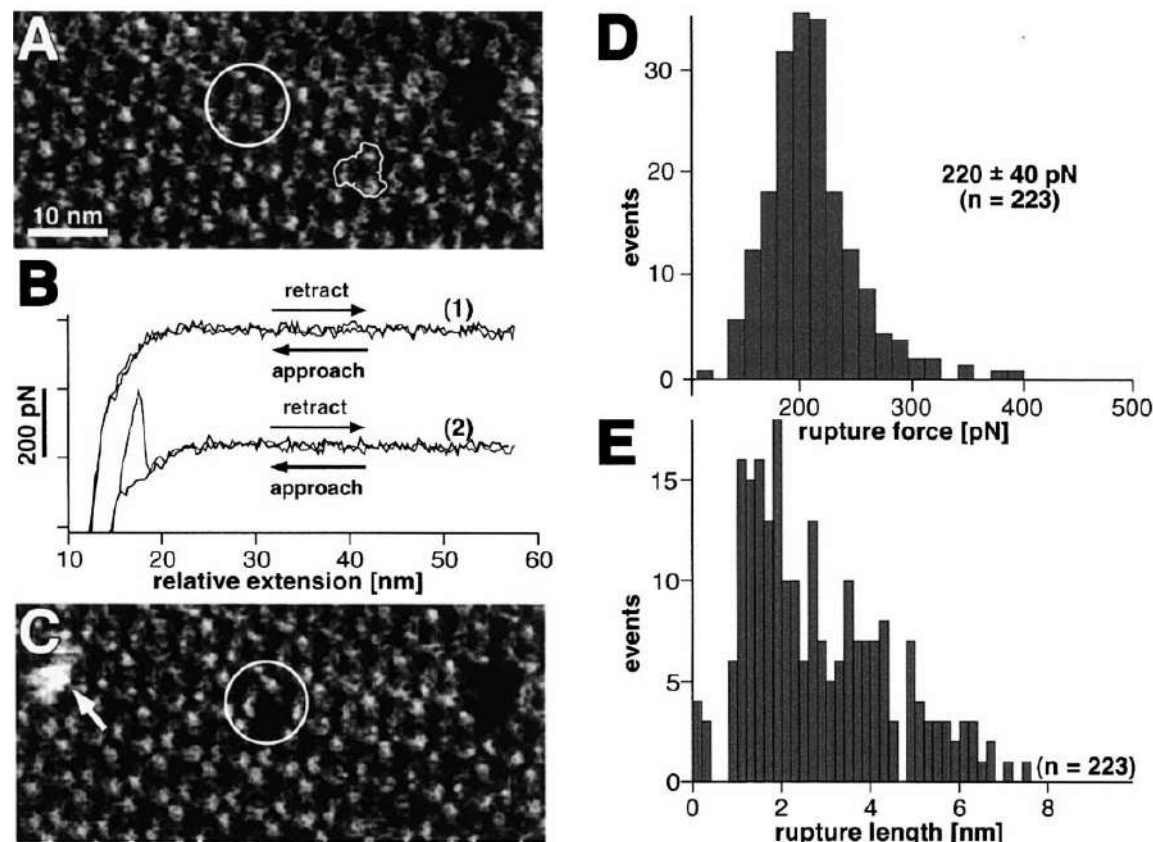
Structural variability of the native cytoplasmic purple membrane surface. The three-fold symmetrized averages were calculated from unit cells classified by multivariate statistical analysis using the algorithm kindly provided by J.-P. Breaudiere. (A) PM imaged at slightly enhanced forces of 120 pN (compare to Fig. 3B). Same membrane imaged at an applied force of approximately 150 pN (B). In C, D and E, three conformations of the membrane are imaged at approximately 180 pN. The last three averages differ in their central protrusion. The correlation averages are displayed in perspective view (top) and in top view (bottom) with a vertical brightness range of 1 nm.



Information about the surfaces of BR have been derived from electron crystallography and Xray diffraction at high resolution, and AFM at medium resolution. This provided an excellent opportunity to assess the quality of the AFM topographs of the PM, and **to understand the implications of combining AFM data with the other structure determination methods.**

Six BR atomic models were combined and compared with the AFM data to determine the value and reliability of each source of information.

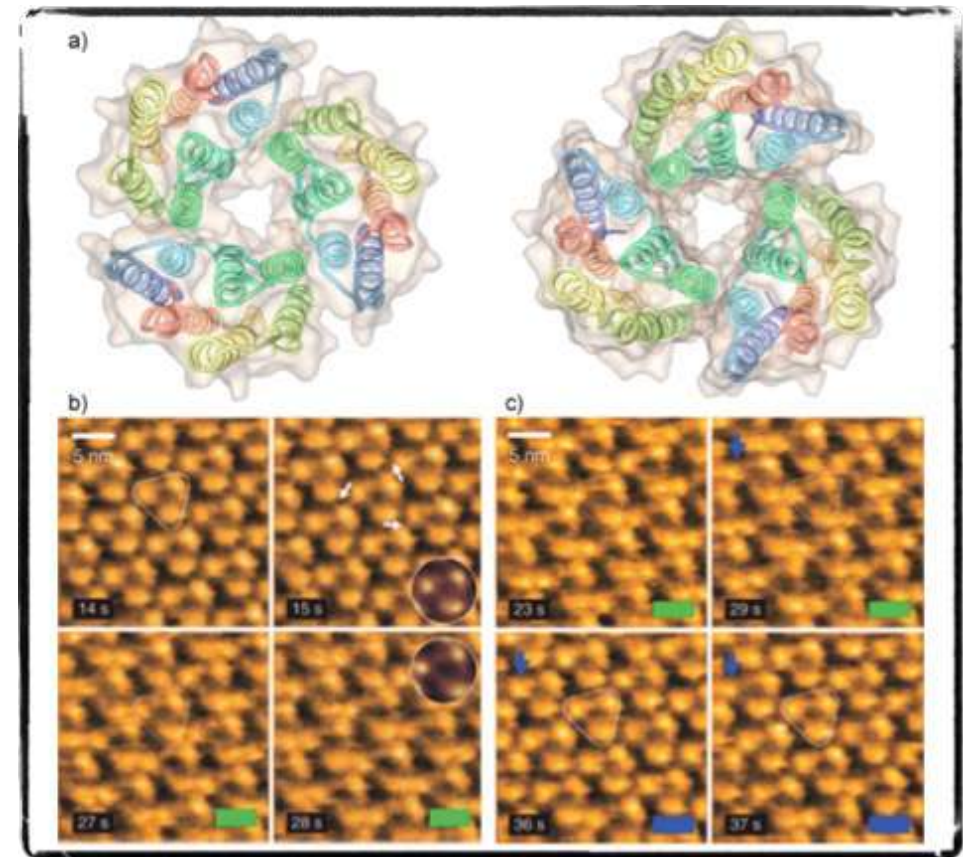
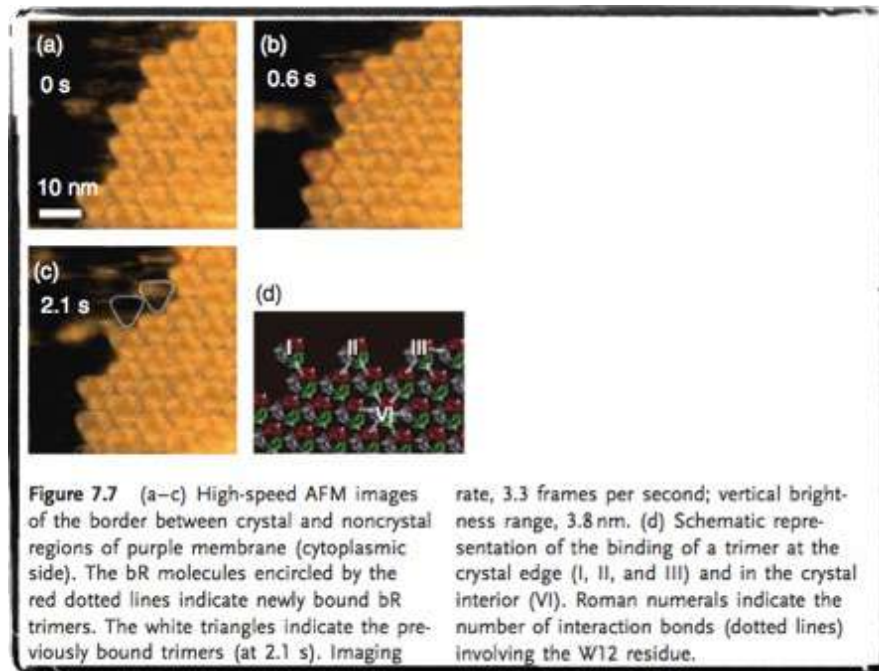
Fig. 6 shows one atomic model suspended within an envelope of the PM reconstructed from the AFM data. The ribbon diagram is color coded according to the coordinate variance between the different atomic models, while the surfaces are mapped with the AFM S.D. images. There is an excellent correspondence between the surface loops of the BR model and the AFM envelope.



Extracting individual bacteriorhodopsins from native purple membrane. (A) AFM topograph of the cytoplasmic surface of PM recorded in buffer solution. The BR molecules forming trimers (outlined trimer) are clearly visible. (B) Most of the extension curves recorded on the cytoplasmic surface were unspectacular (1). However, 10% of the other extension curves showed one adhesion peak at a separation of several nm from the PM surface (2). The adhesion force of the peak shown in (2) was about 220 pN. (C) The topograph of the same surface imaged after recording the adhesive force peak showed one BR monomer missing (outlined circle). After extraction of the BR from the PM, a protrusion of about the size of an individual BR molecule was observed to be adsorbed onto the membrane surface (arrow). The missing trimer at the upper right was taken to align the topographs. Full gray level range of topographs, 1.5 nm. (D) Histogram of the rupture forces required to pull an individual BR from the PM. The average adhesion force was 220 ± 40 pN ($n = 223$). (E) Histogram of the pulling lengths until the BR molecules were extracted from the membrane.

Dynamics of bR on purple membranes

Ando's group, Angew Chem Int Ed, 2011



bR molecules with two binding partners associated for longer time periods to the array than proteins that had only one neighbor. Statistical assessment of the dissociation frequencies allowed the calculation of the **strength of a single bR–bR interaction of 1.5kBT (0.9 kcal/mol), resulting in a stability of about 5.4 kcal/ mol for the purple membrane arrays**, in good agreement with ensemble measurements by calorimetry

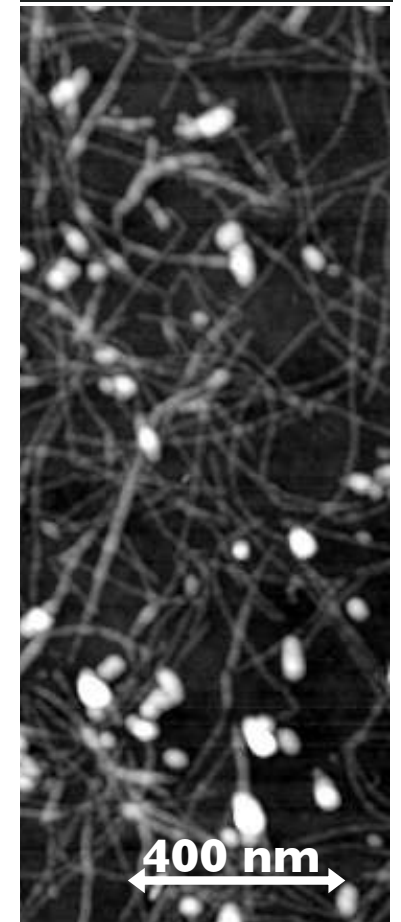
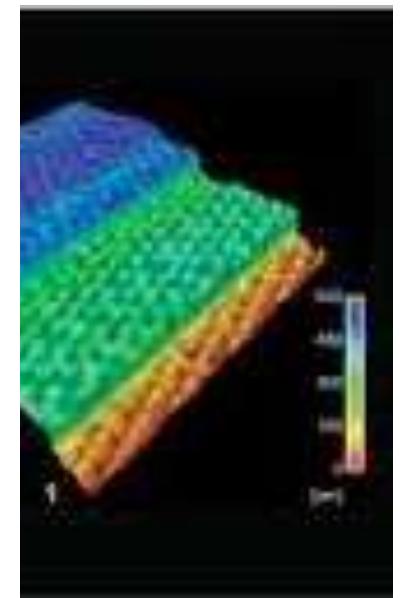
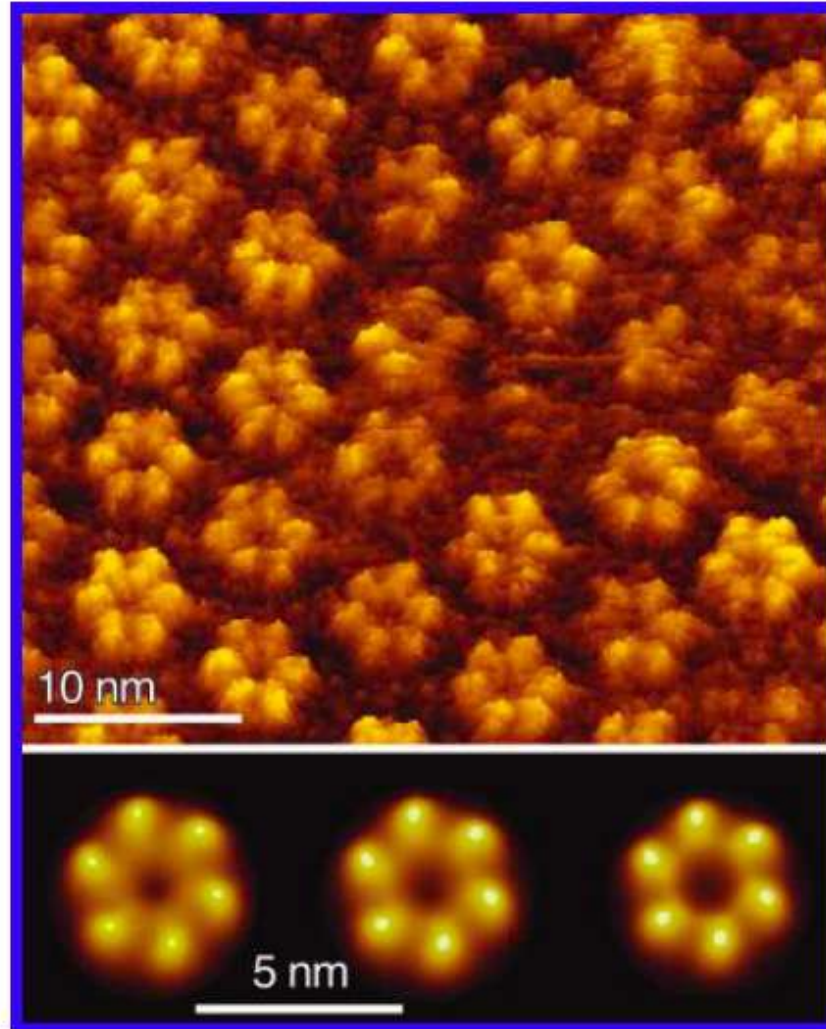
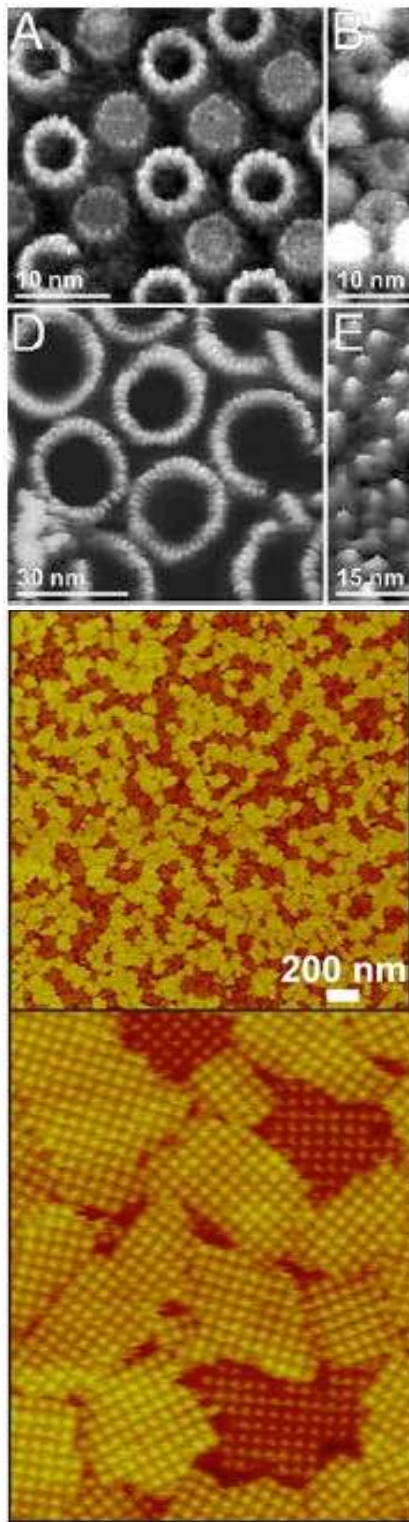
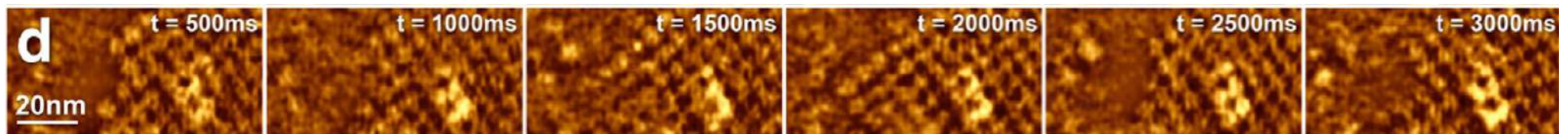


FIGURE 4: Watching communication channels at work. High-resolution AFM topograph showing the extracellular surface of Cx26 gap junction hemichannels. The gap junction membranes have been dissected with the AFM probe to expose their extracellular surface (27). The bottom row shows the conformational change of hemichannels in response to Ca^{2+} . The closed channels (left) switch, via an intermediate conformation (middle), to the open state (right) in the presence of 0.5 mM Ca^{2+} . Hemichannels in the bottom row represent correlation averages.



Using HS-AFM in contact mode, applying additional force s the junctional microdomains were dissected, revealing that the adhesion function of the proteins was cooperative: the entire membrane patches dissociated at once. From high spatial and temporal res. Assembly/dissassembly of auqaporin-0 and connexons to/from functional microdomains, with interaction strenght of $-2.7 K_B T$

HS-AFM on life cell

2.7 s/frame, with bright-field illumination

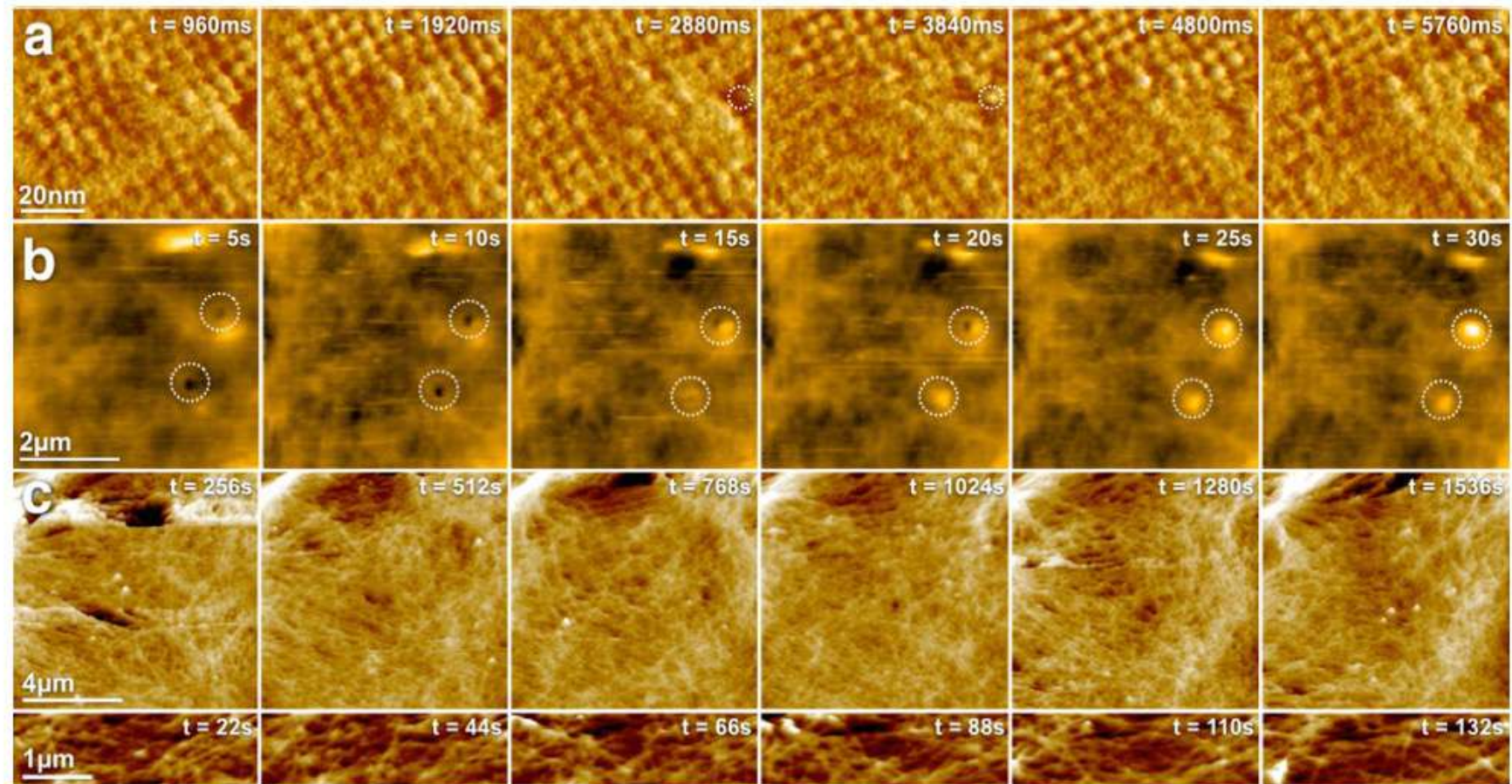


Fig. 2. HS-AFM applications on life cells. (a) High-resolution HS-AFM imaging of AQP0 in junctional microdomains in native eye lens cells. The dynamic association of individual AQP0 could be observed (outline). (b) Endocytosis events observed by HS-AFM on HeLa cells. (c) Dynamic PeakForce tapping imaging of the membrane cortex underneath the plasma membrane of 3T3 fibroblasts.

Colom, A., Casuso, I., Rico, F. and Scheuring, S. (2013) A hybrid high-speed atomic force–optical microscope for visualizing single membrane proteins on eukaryotic cells. *Nat. Commun.* 4.

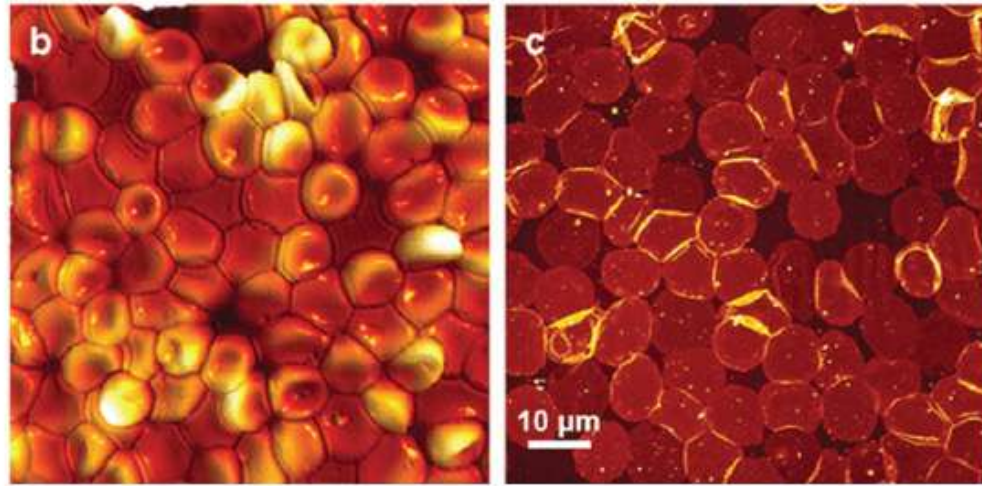
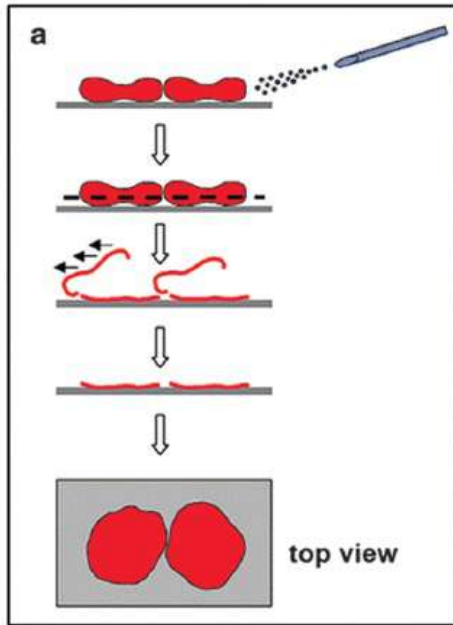


Fig. 11 Membrane preparation scheme. (a) RBCs are exposed to fluid flow-imposed shear stress to open the cells. (b) AFM images of RBCs attached to poly-L-lysine-coated glass. (c) Inside-out RBC membranes spread on the glass surface after shear stress. Adapted from ref. 91, Figure 1 with permission.

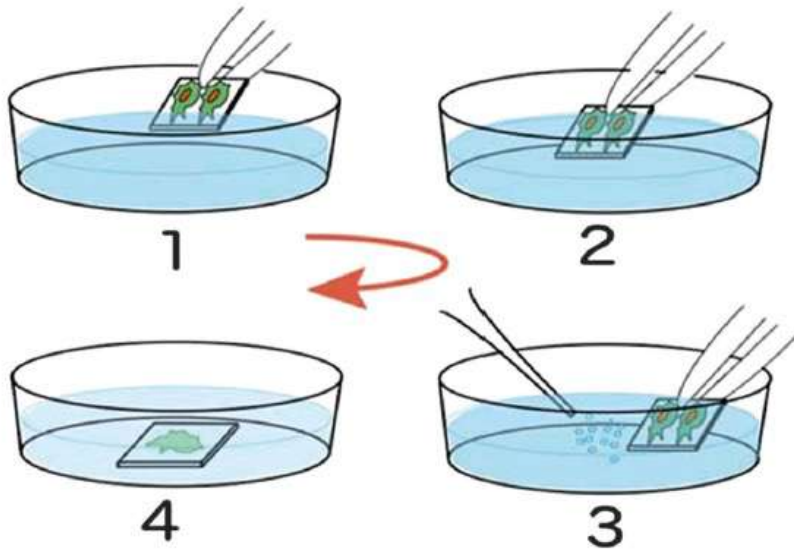


Fig. 12 Scheme for unroofing cells. The cells are washed three times in hypotonic HEPES-based mammalian Ringer's solution and subsequently unroofed by ultrasonic stimulation, which removes the apical cell membrane and the cytoplasm. Adapted from ref. 95, Figure 1 with permission.

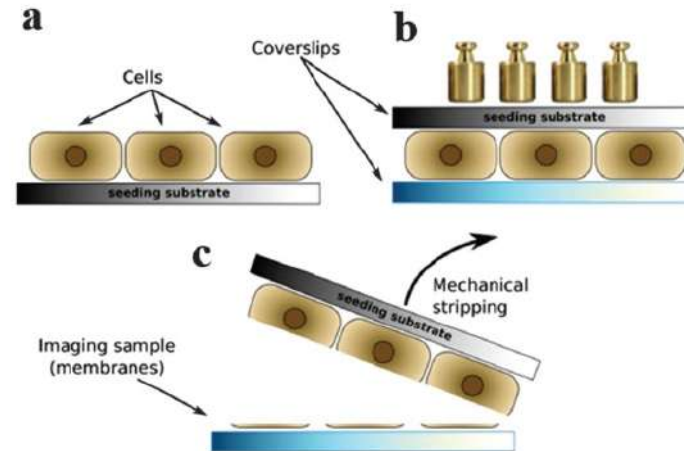
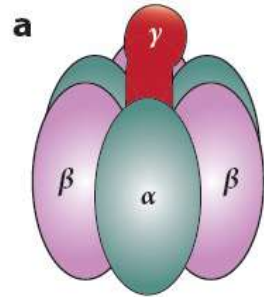
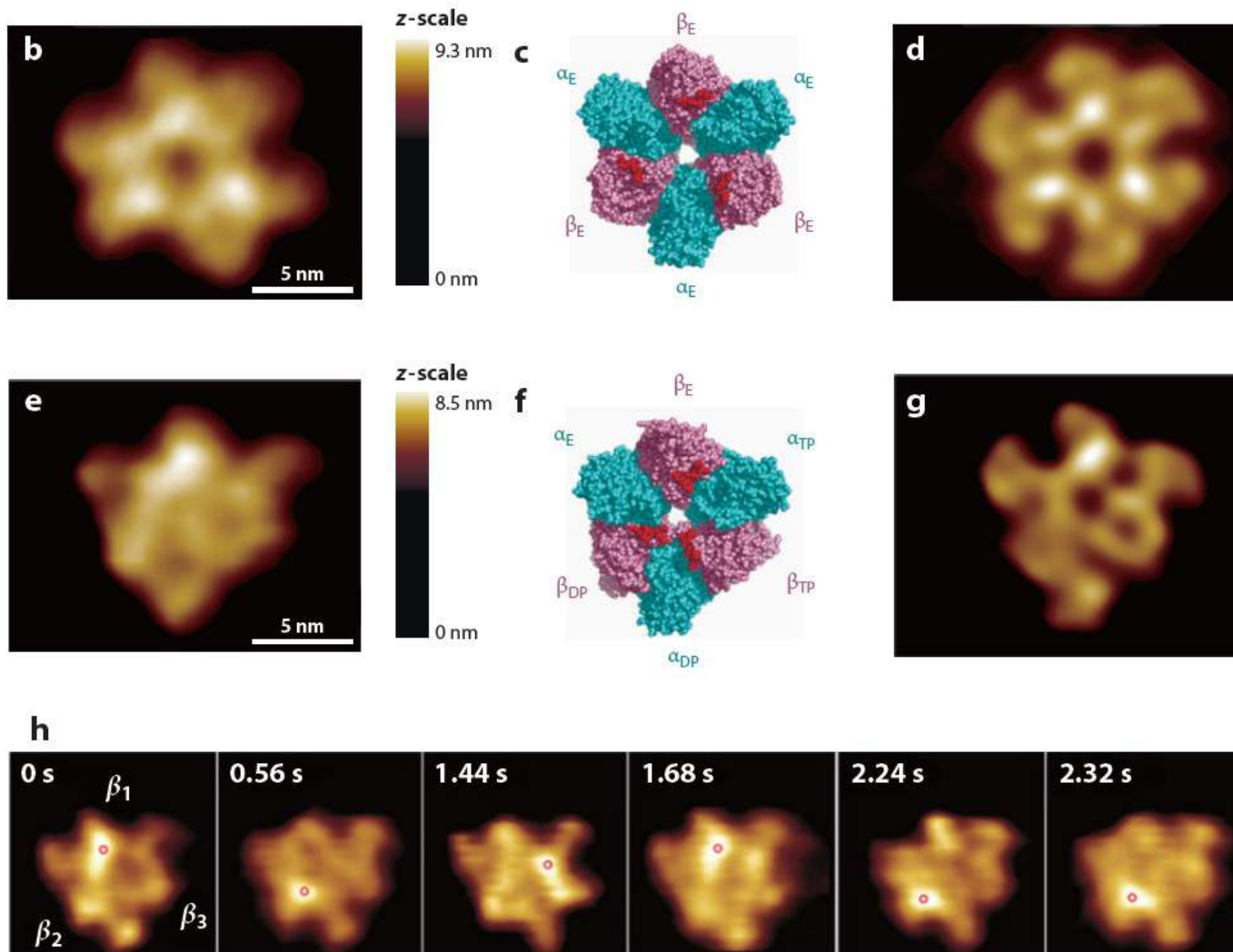


Fig. 13 Scheme of the preparation of the apical cytoplasmic side of membranes. (a) Cells are cultured on a seeding substrate. (b) A coverslip covers another side of the cells, and weights are placed on the seeding substrate. (c) Stripping the seeding substrate to leave the apical membranes for imaging. Adapted from ref. 97, Figure 1 with permission.



The $\alpha_3\beta_3\gamma$ subcomplex of F_1 -ATPase (a part of ATP synthase) is the minimum complex for the full ATPase activity. About half the length of the long γ subunit is inserted into the central cavity formed by a ring-shaped $\alpha_3\beta_3$ where three α subunits and three β subunits are arranged alternately (1). Three ATP binding sites locate at the α - β interfaces, mainly in the β subunits. The $\alpha_3\beta_3\gamma$ subcomplex is a rotary motor (34, 48, 68, 115) (Figure 5a). The γ subunit rotates in the stator $\alpha_3\beta_3$ ring driven by rotary hydrolysis of ATP at the three β subunits. The rotation occurs in the counterclockwise direction as viewed from the exposed side of the γ subunit (or from C-terminal side of $\alpha_3\beta_3$). In the ATPase cycle, three β subunits take different chemical states: ATP-bound, ADP-bound, and nucleotide-free (empty) states (1, 34). Each chemical state cyclically propagates over the three β subunits. Thus, there is strong cooperativity between β subunits.



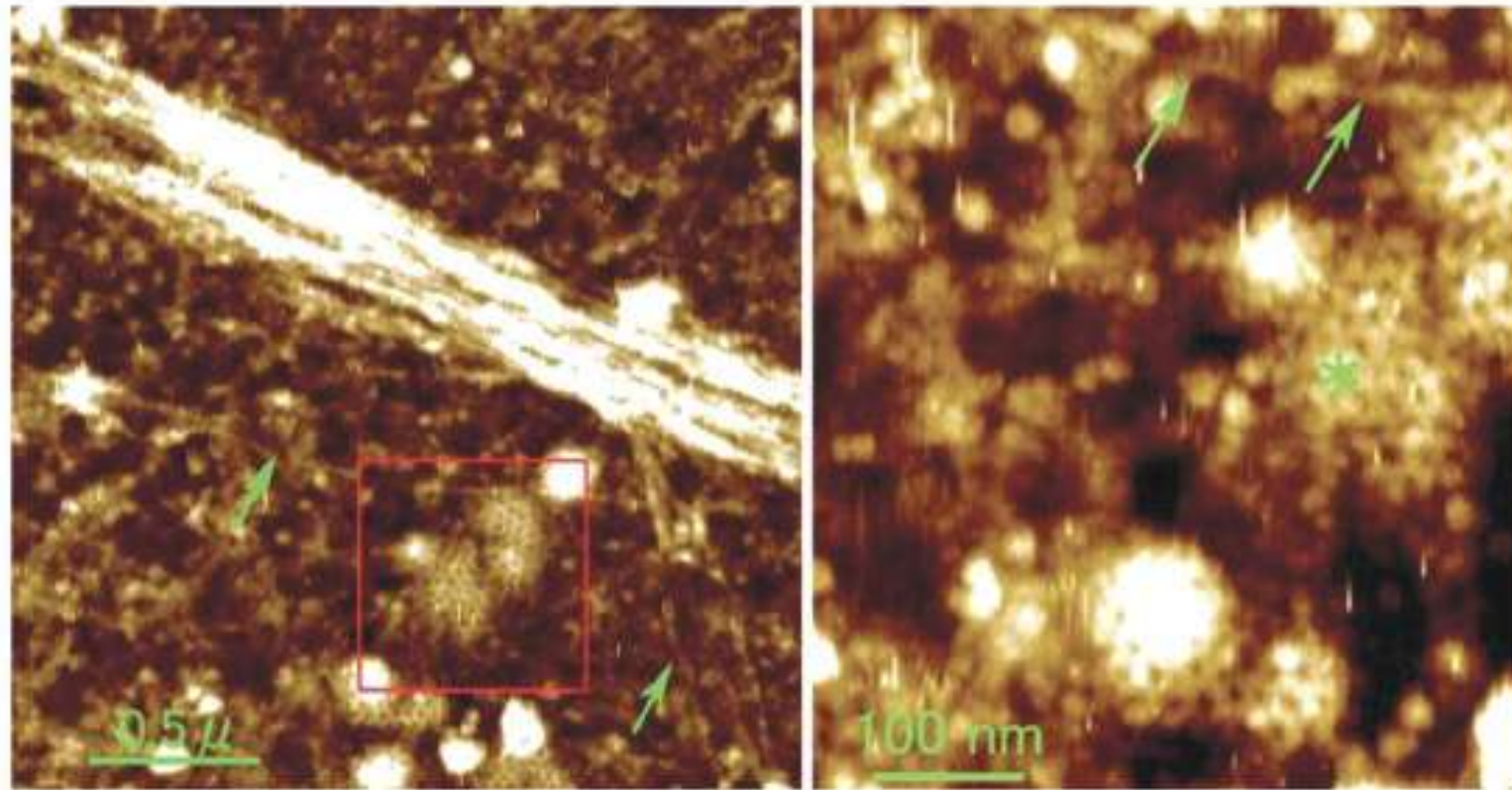


Fig. 18 AFM image of clathrin coats and actin filaments at the cytoplasmic surface of the plasma membrane. The right figure shows an enlarged view of the boxed area in the left figure. Clathrin-coated pits are clearly observed in the boxed area. Arrows indicate actin filaments. From ref. 95, Figure 6 with permission.

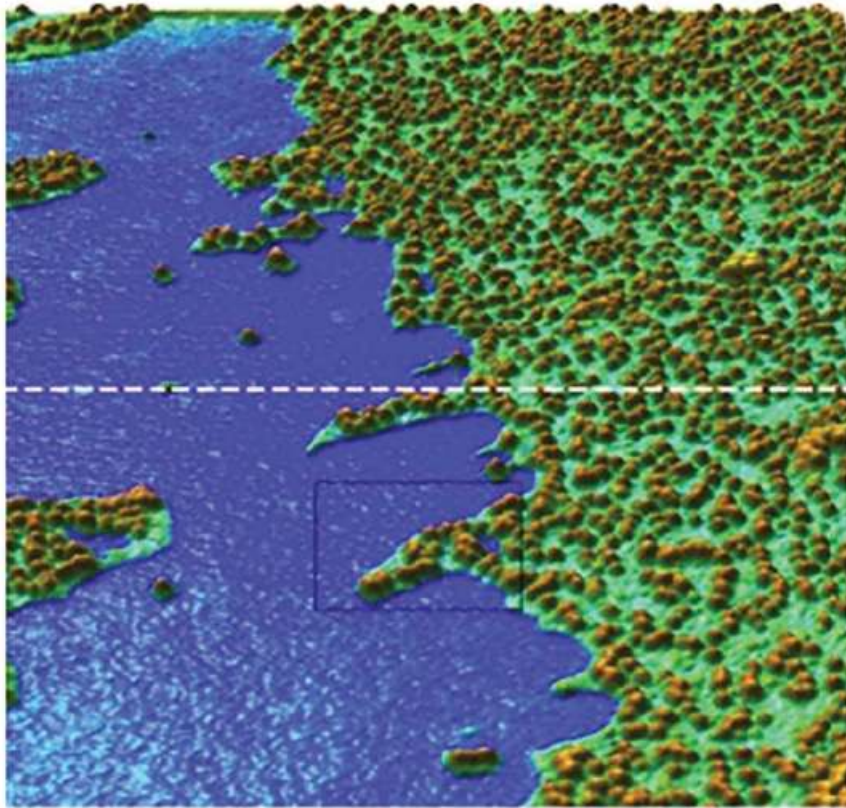
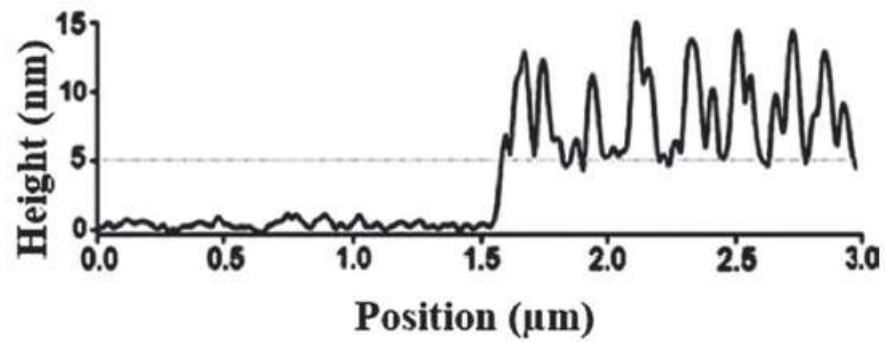
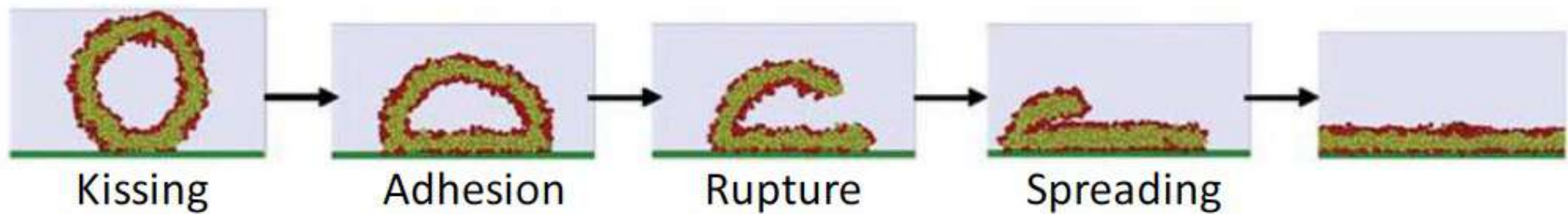
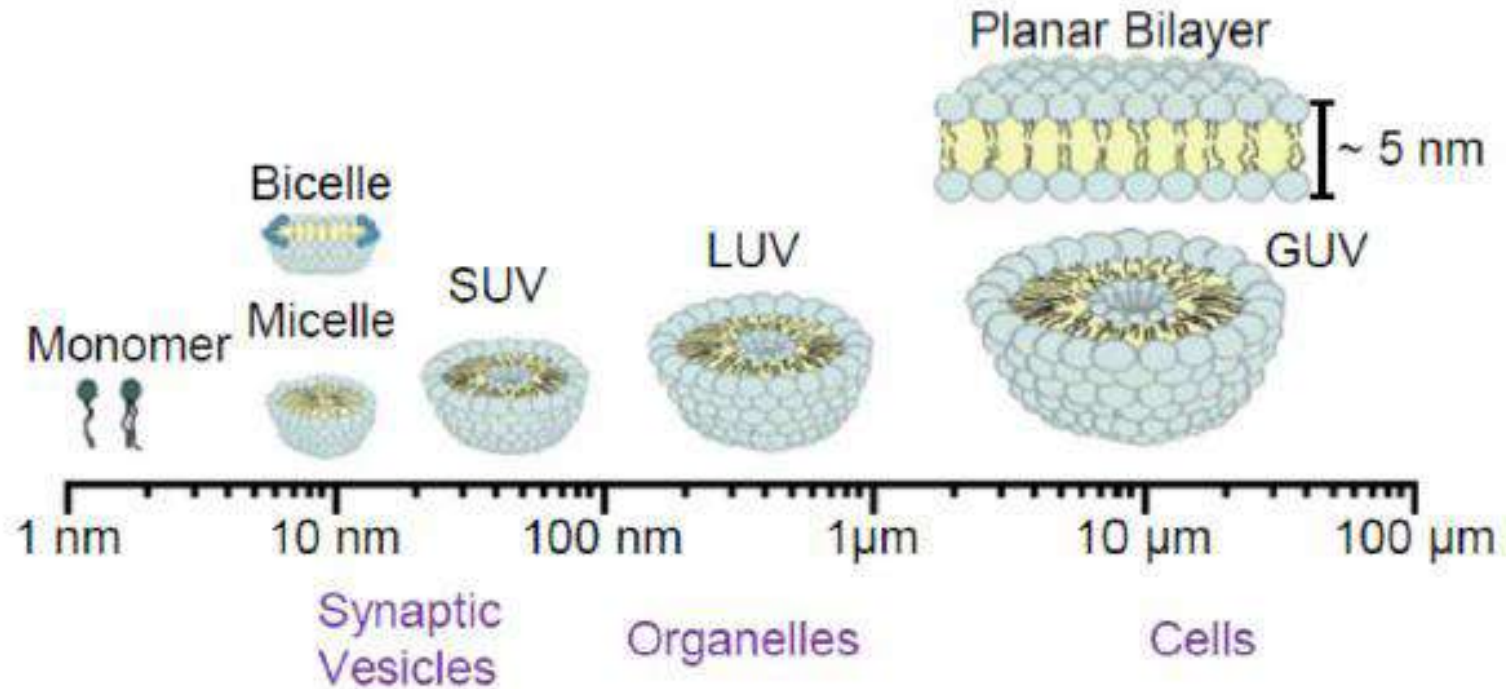


Fig. 17 AFM image of South African frog oocyte membranes (cytosolic side). Poly-L-lysine-coated glass (blue), the lipid bilayer membrane (turquoise), and the membrane proteins (brown). The height profile along the broken line is presented at the bottom. From ref. 91, Figure 6 with permission.



Model membranes



Cell membrane: an optimized 2D fluid system

Membrane fluidity depends on the type of lipid:

Saturated lipid are more ordered, therefore more rigid than the **unsaturated** ones

Cholesterol is hydrophobic, but reacts with a OH^- group with the hydrophilic heads of neighbor phospholipids

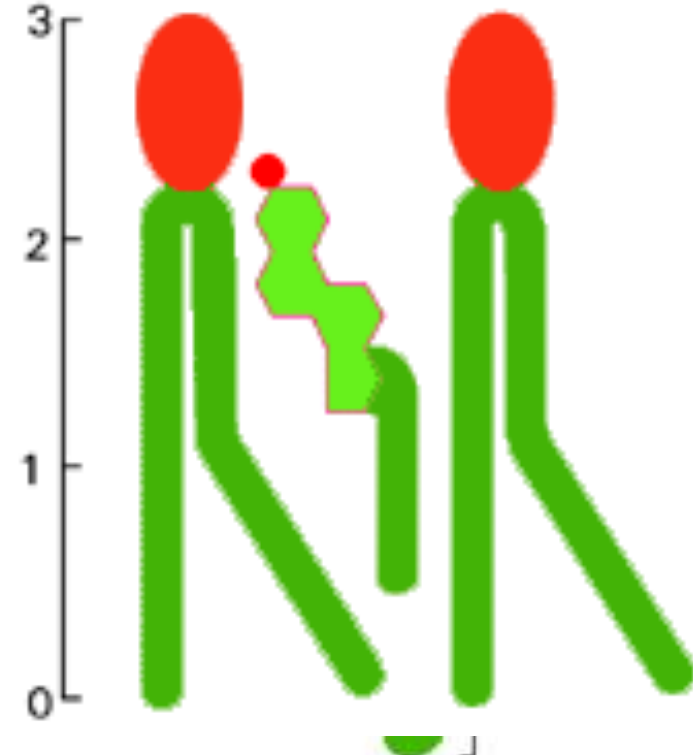
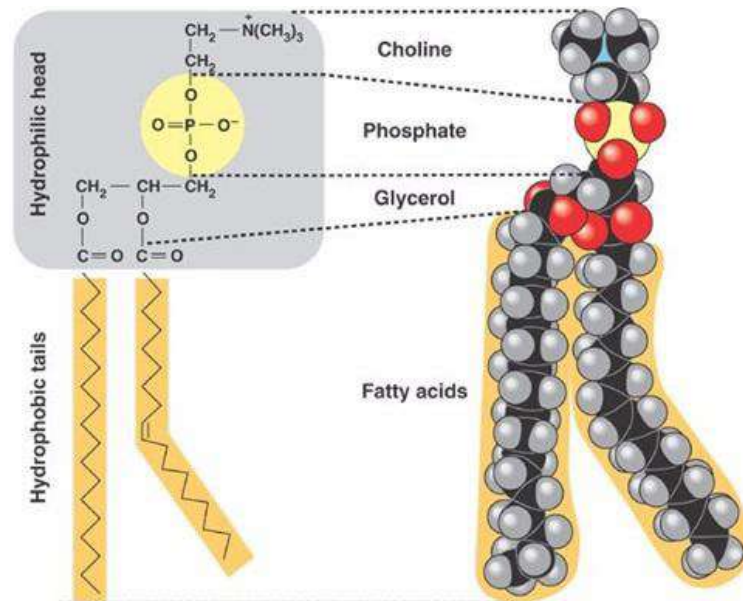
Low T: chol is a spacer, fluidity high

High T: chol stabilizes the membrane (sealing)

Stearic acid - saturated

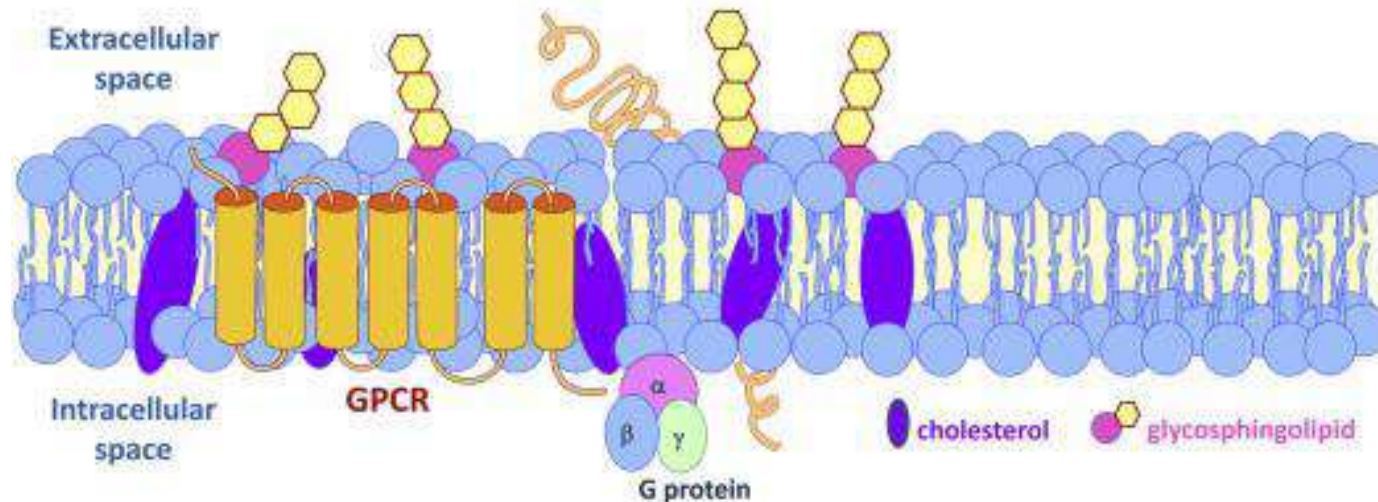
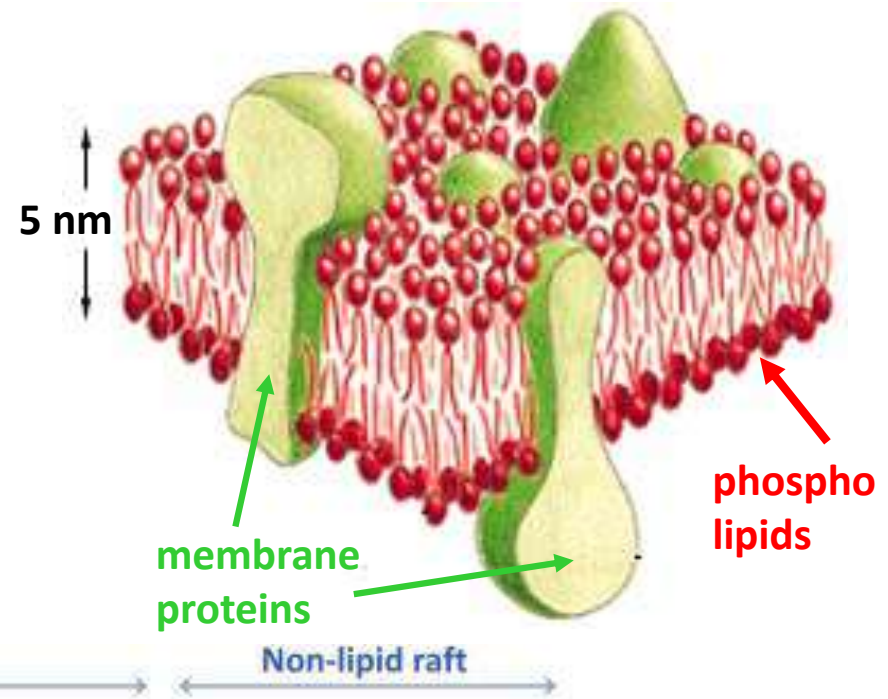


Oleic acid - unsaturated

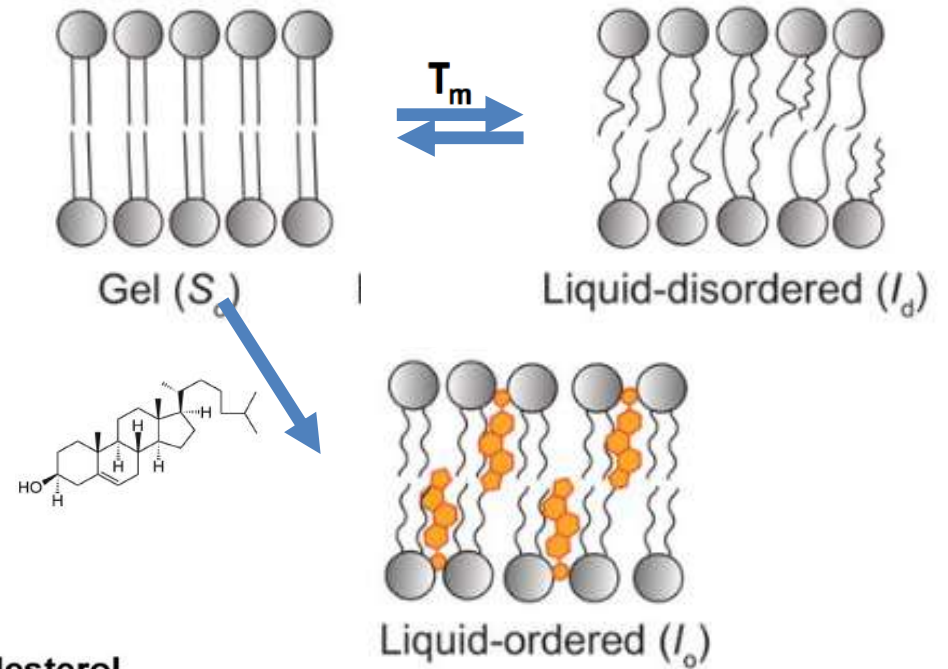
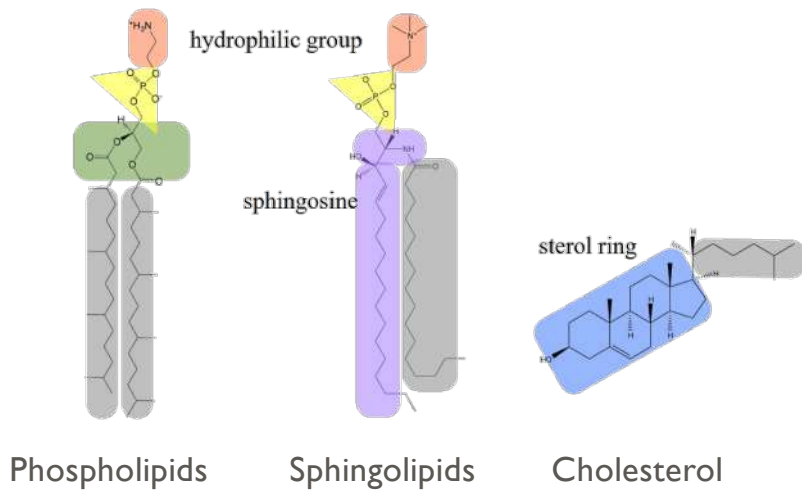


Cell membranes-rafts

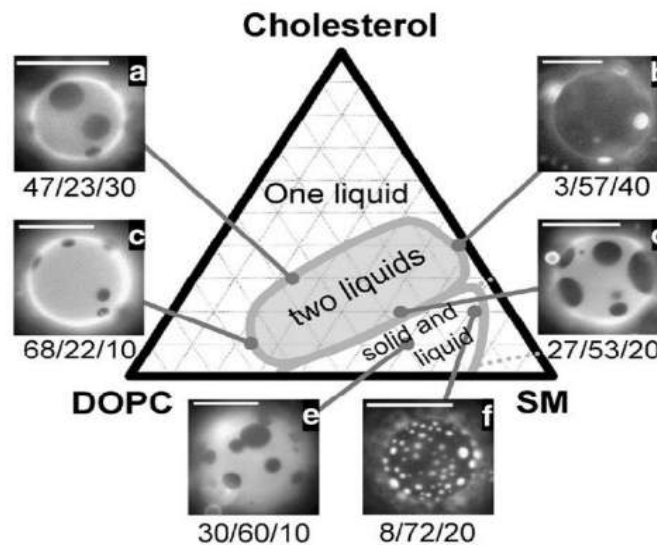
Tasks such as energy transduction and chemical communication between the inside and the outside of the cell are achieved by membrane proteins. However, molecular level understanding of membrane proteins function is largely hindered by the lack of structural information available, especially in biologically relevant environments



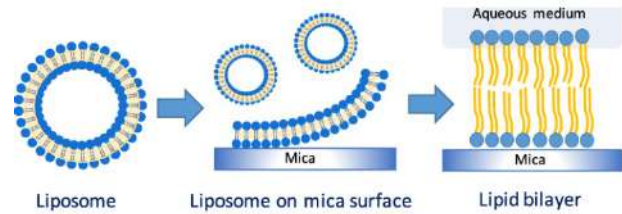
Supported lipid bilayer



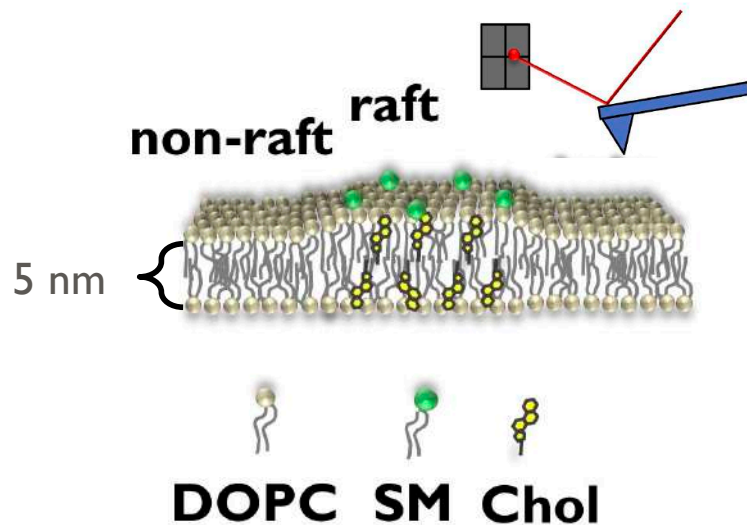
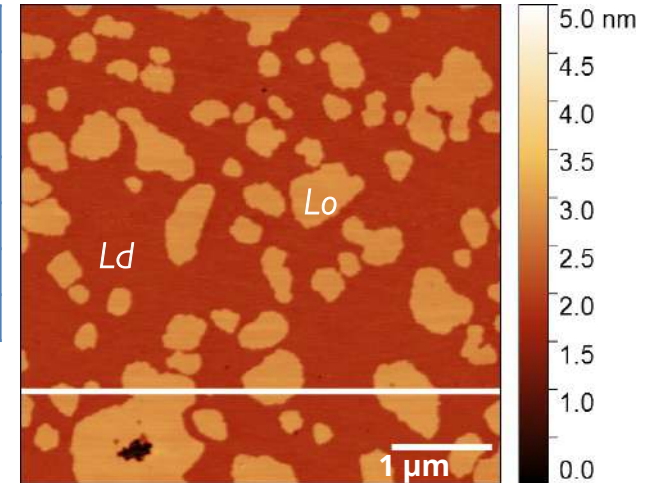
	DOPC	SM	DPPC
T_m (°C)	-17	38	41



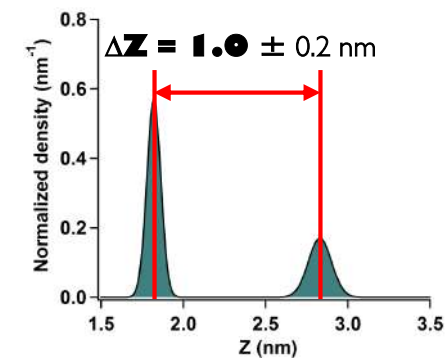
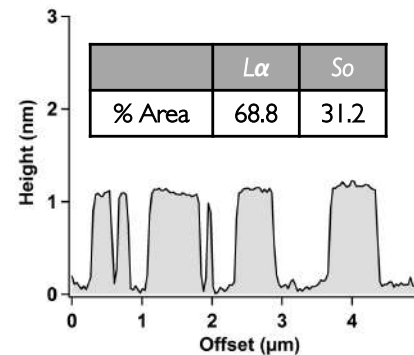
Supported lipid bilayers: AFM



DOPC
1,2-dioleoyl-sn-glycero-3-phosphocholine
SM
Sphingomyelin
Chol
Cholesterol



AFM imaging in dynamic AC-mode in liquid environment



surface roughness: $L\alpha=0.16 \pm 0.01$ nm, $L_0=0.14 \pm 0.01$ nm

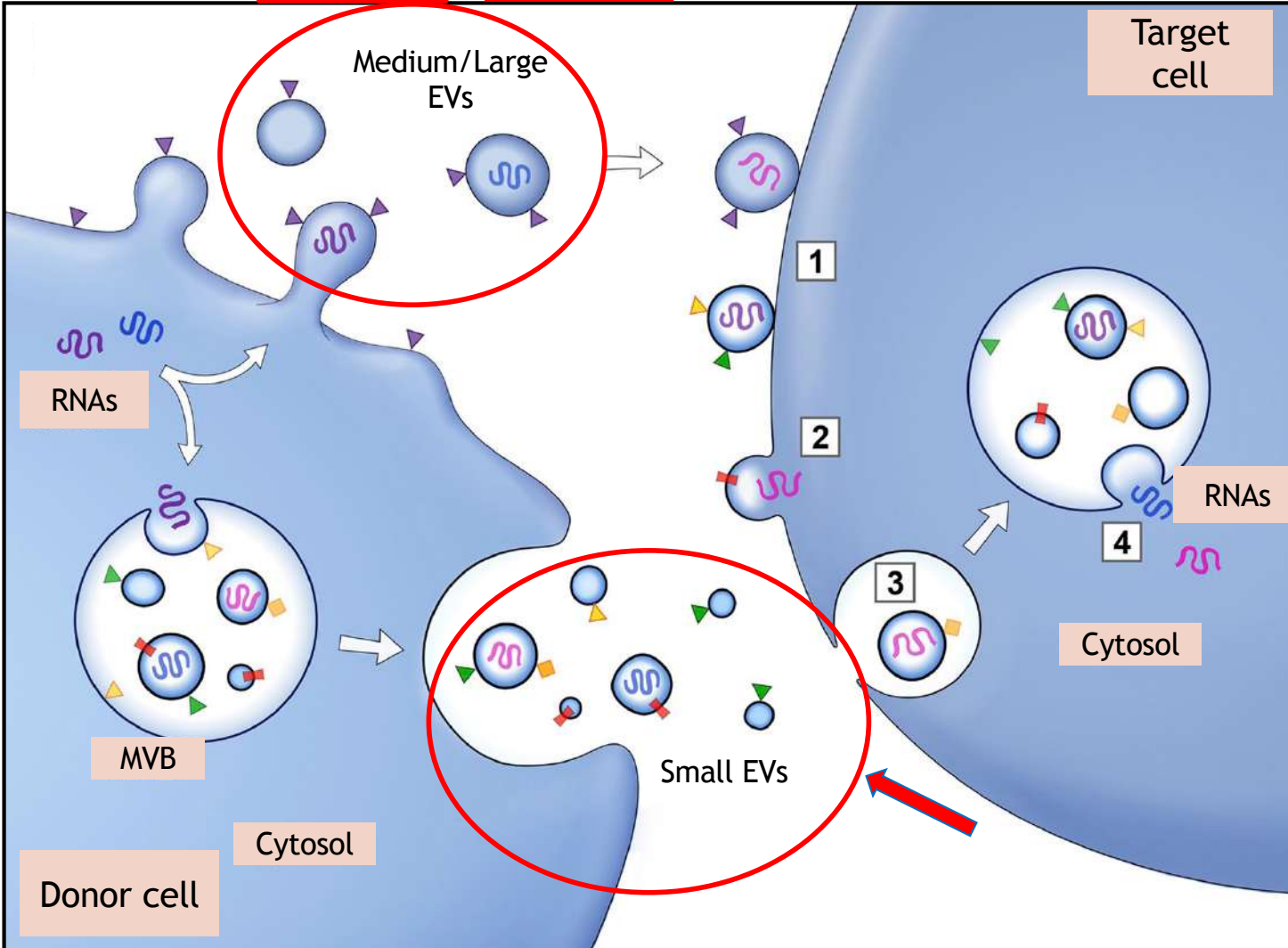
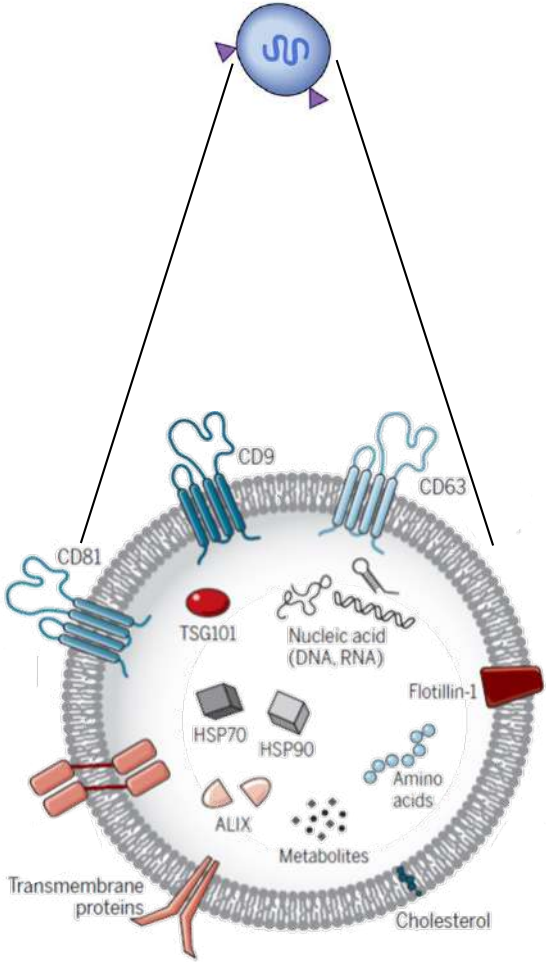
Lipid collective behaviour influences **membrane fluidity**, lipid packing, bilayer thickness, elastic moduli, and surface charge density, and in turn protein interactions, dynamics, and functions. **Lipid raft** are fundamental players in regulating **cell proliferation, adhesion, and invasion**

Extracellular Vesicles (EVs)

ROLE

Transport of macromolecules throughout the body.
Impact recipient cells fate.

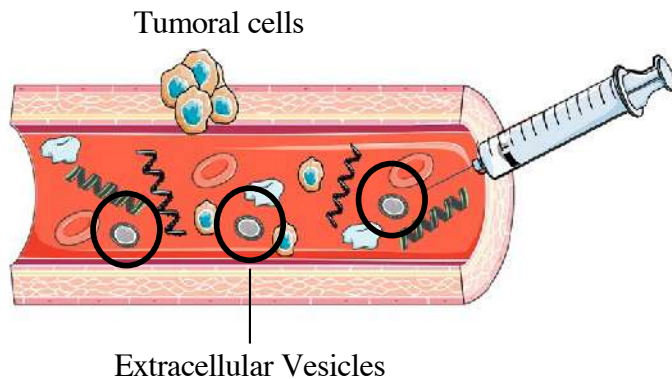
	m/l-EVs	s-EVs
Size (nm)	1000 ÷ 200	200 ÷ 30



Modified from Raposo et al. 2013, J Cell Biol.

sEVs mediator of cell-cell communication

Diagnostics



Specific signatures
from originating cells

↳ Biomarkers

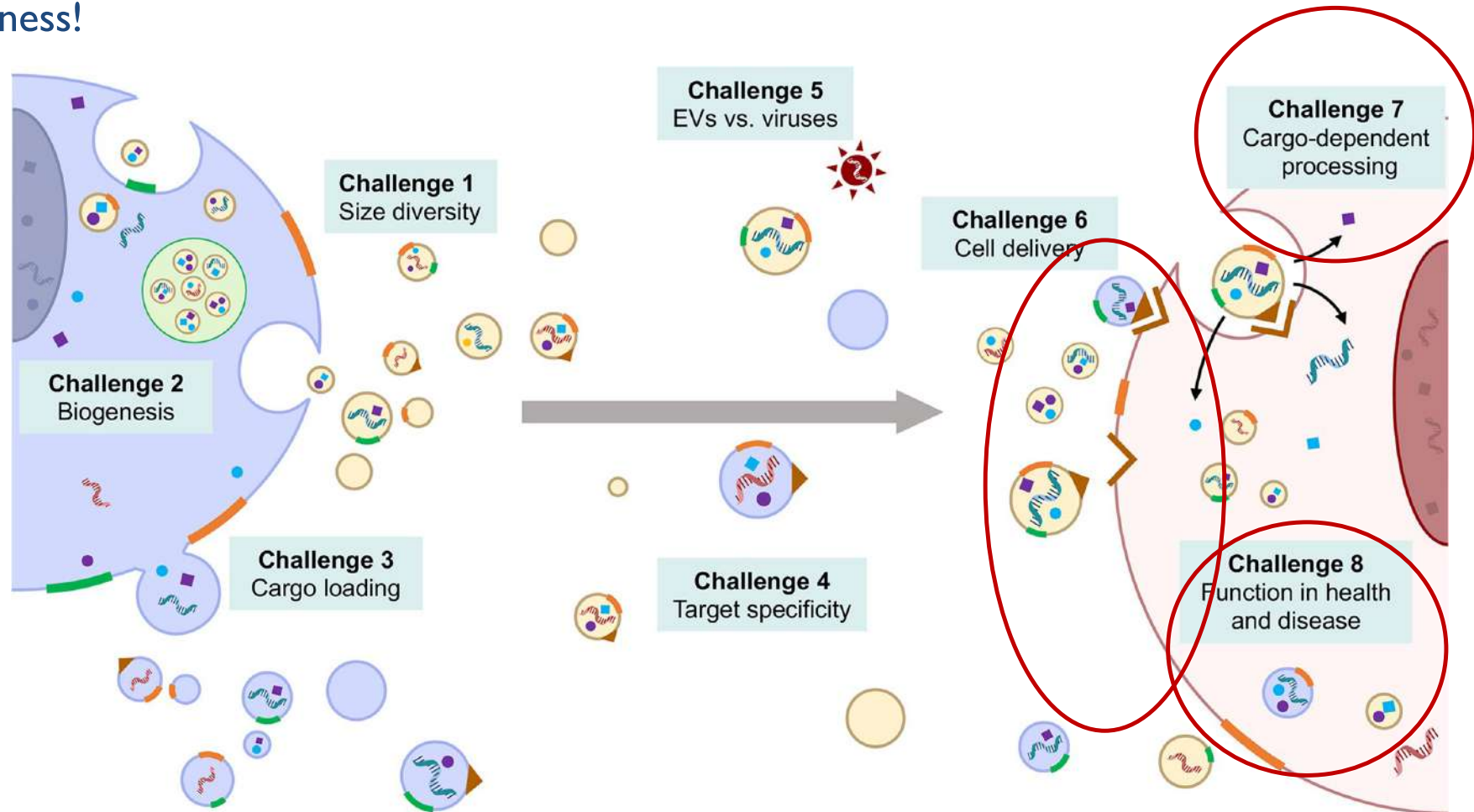
Therapy



Influence on the fate of recipient cells
Analogies with enveloped single-stranded RNA viruses (glycoproteins as ligand to target receptors and **promote fusion**),
↳ Involved in disease spreading;
↳ Therapeutic agents (regenerative medicine, drug delivery, ...)

sEVs: the many challenges

Lightness!



Margolis & Sadovsky, PLOS biology 2019: The known unknown

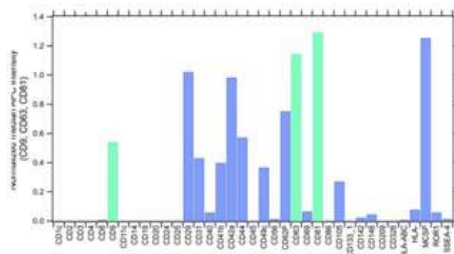
How is EVs uptake and cargo release regulated?

Challenge I: sEV characterization

Consistency! Exactitude!

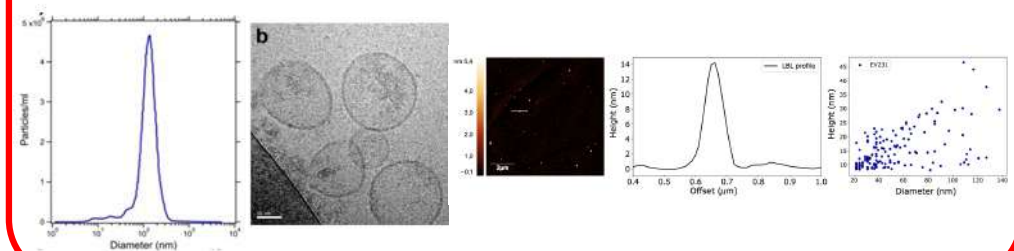
Surface markers

tl sEV/exosome markers (tetraspanins CD9, CD63 and CD81)



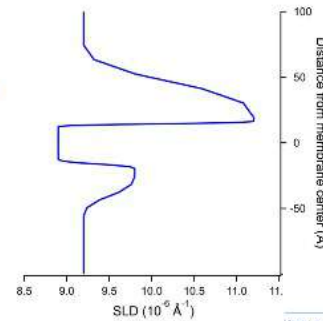
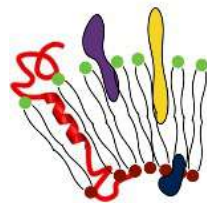
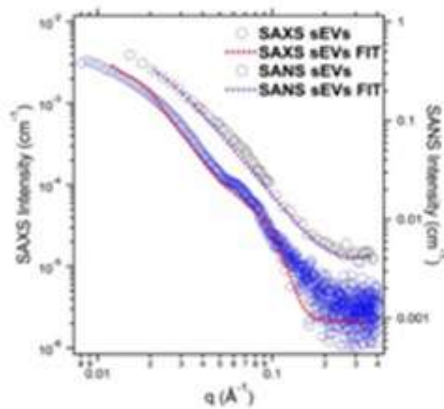
DLS, NTA, CryoEM, AFM

particles sized less than 50 nm + sEVs sized ~ 100 nm

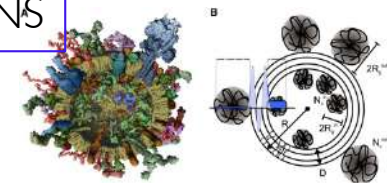


10^{10} - 10^{11} particles/mL 60-160 nm dia

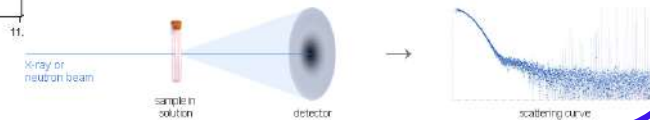
3-layered membrane model
accounting for the proteomic component extending in the extra-vesicular solution.



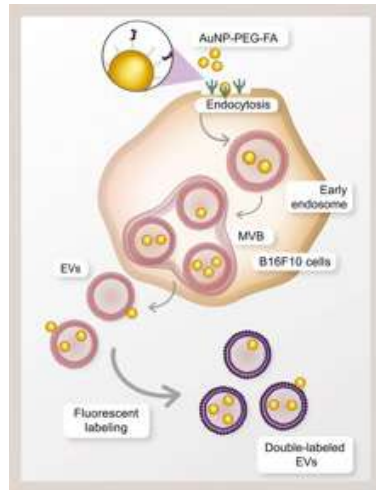
SAXS
SANS



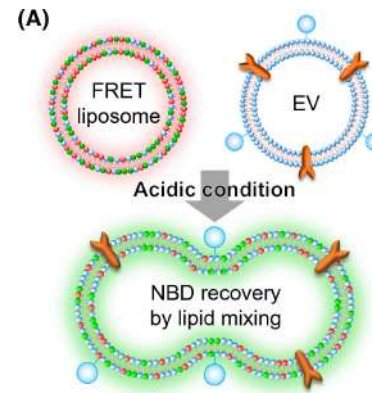
Castorph et al. Biophysical Journal (2010)
(Synaptic vesicles)



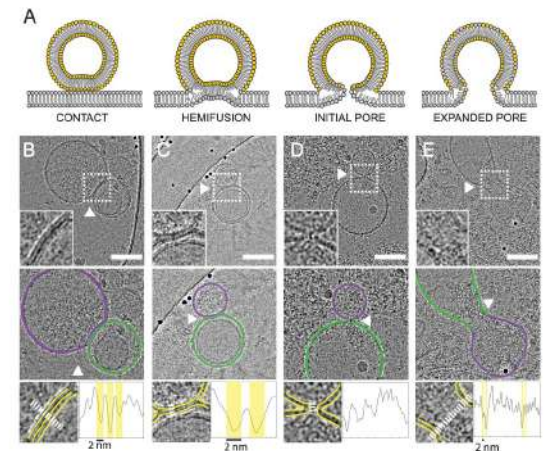
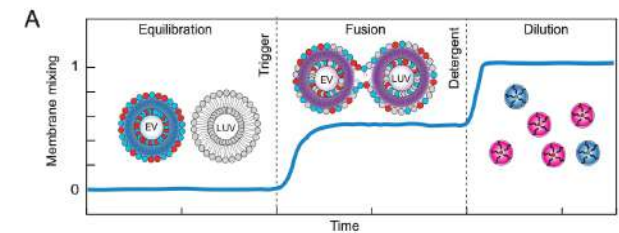
sEVs uptake and fusion assay



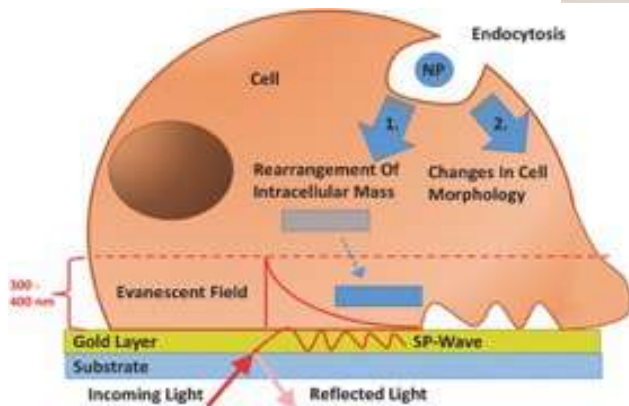
Lara et al., *J Nanobiotechnol* 2020



FEBS Open Bio, 2022

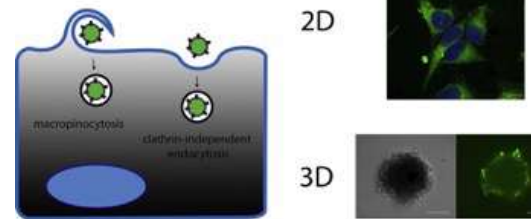


Morandi et al, *PNAS* 2022



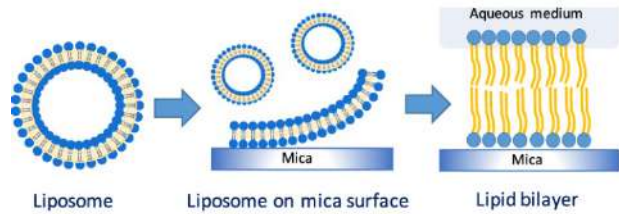
Koponen et al., *Biosens. Bioelectronics*, 2020
Suutari et al., *Small*, 2016

Extracellular vesicle uptake

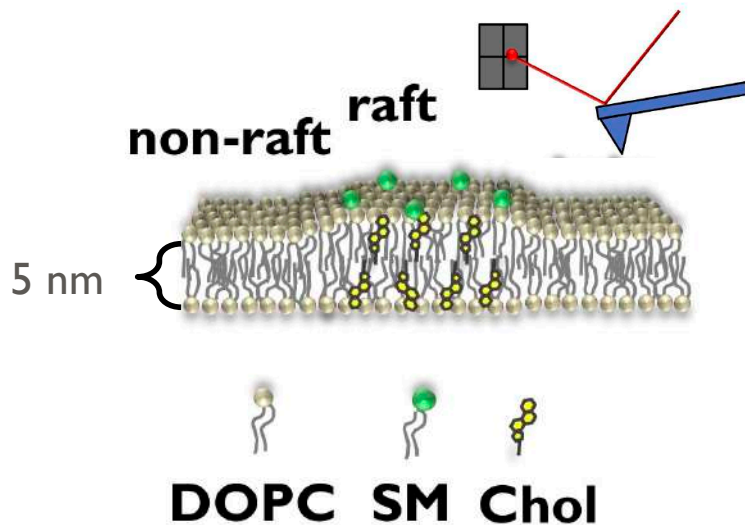
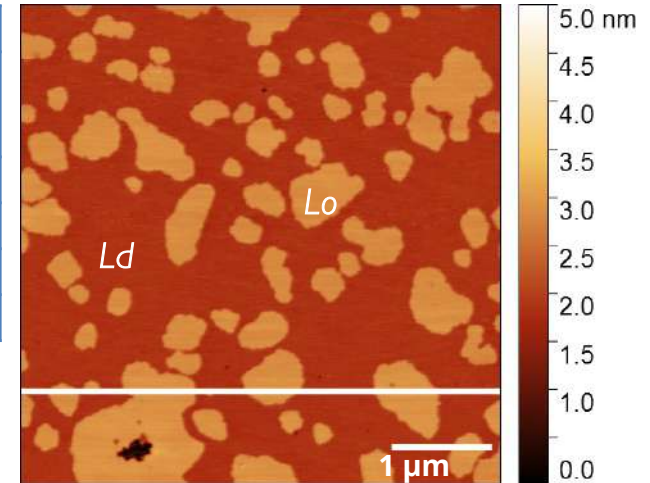


Verdera et al., *Journal of Controlled Release*, 2017

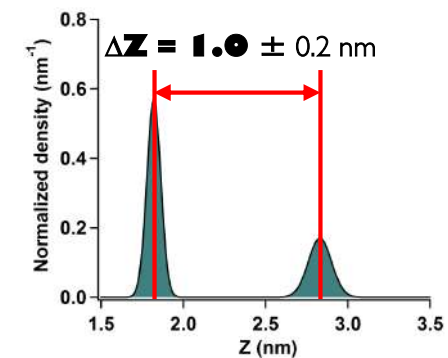
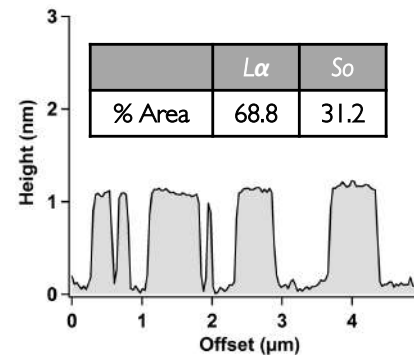
Our assay: Supported lipid bilayers



DOPC
1,2-dioleoyl-sn-glycero-3-phosphocholine
SM
Sphingomyelin
Chol
Cholesterol



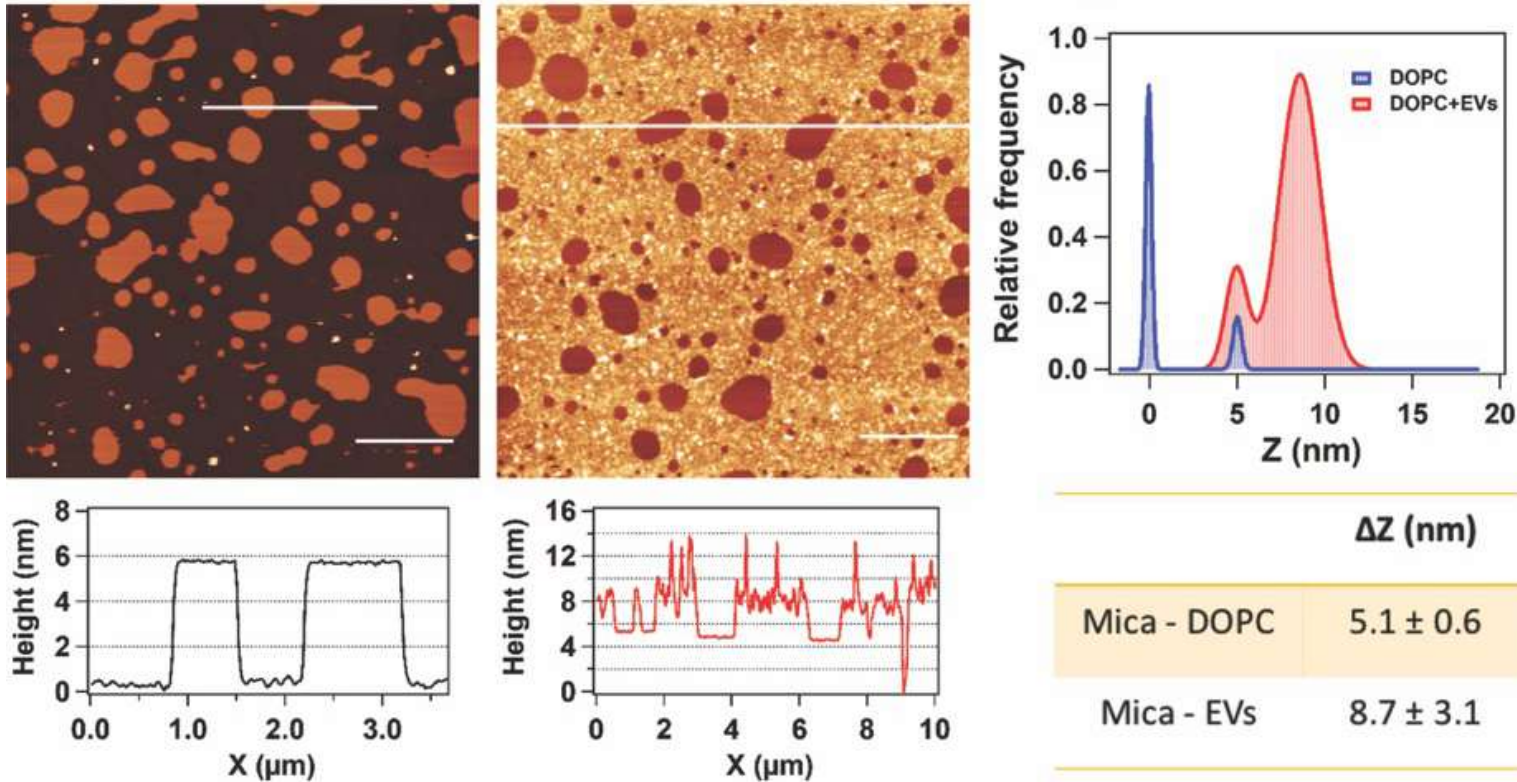
AFM imaging in dynamic AC-mode in liquid environment



surface roughness: $L\alpha = 0.16 \pm 0.01 \text{ nm}$, $L_0 = 0.14 \pm 0.01 \text{ nm}$

Lipid collective behaviour influences **membrane fluidity**, lipid packing, bilayer thickness, elastic moduli, and surface charge density, and in turn protein interactions, dynamics, and functions. **Lipid raft** are fundamental players in regulating **cell proliferation, adhesion, and invasion**

UC-MSC sEVs + SLB



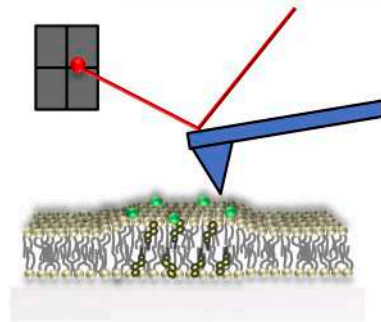
Partially formed SLB

UC-MSC sEVs + SLB

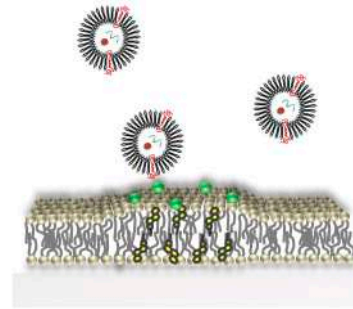
DOPC:SM:Chol (2:1:0.15)
vesicles fusion



characterization



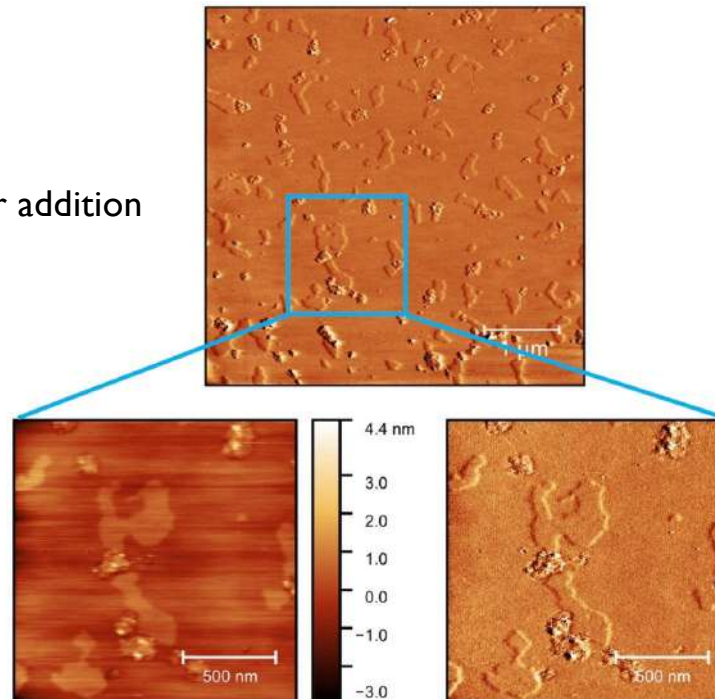
sEVs
injection from bulk water



mixed system
characterization

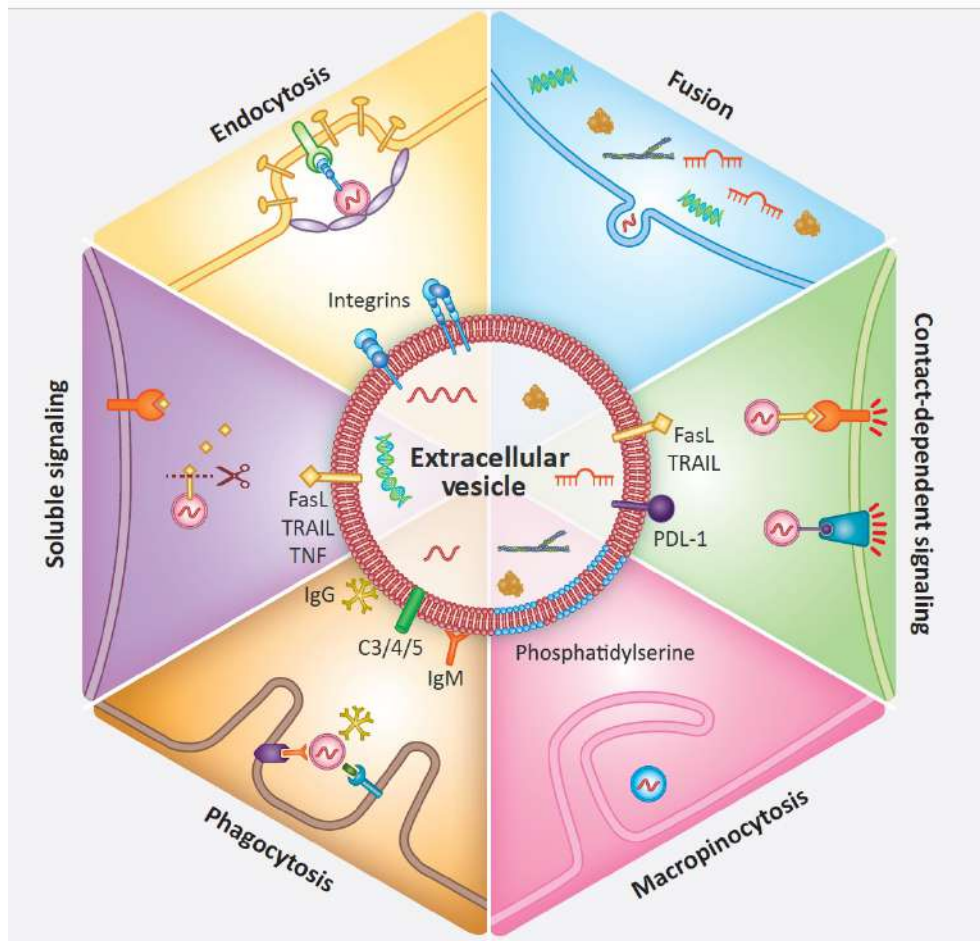
- I. Wash and measure
- II. Time lapse measurements

SLB (5% chol) 5 minutes after addition
of sEVs

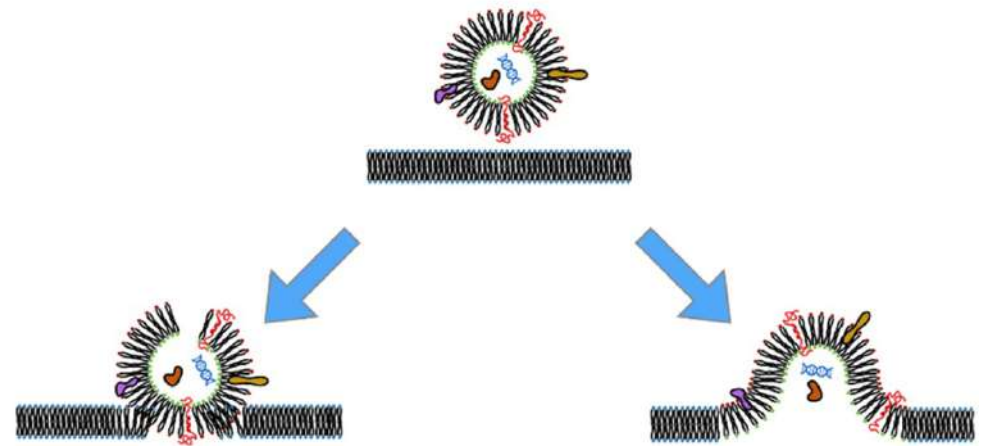


sEVs preferentially dock and break
at phases borders: at thickness
mismatches the free energy
minimum enables favourable
interactions without the need of
large curvature deformations.

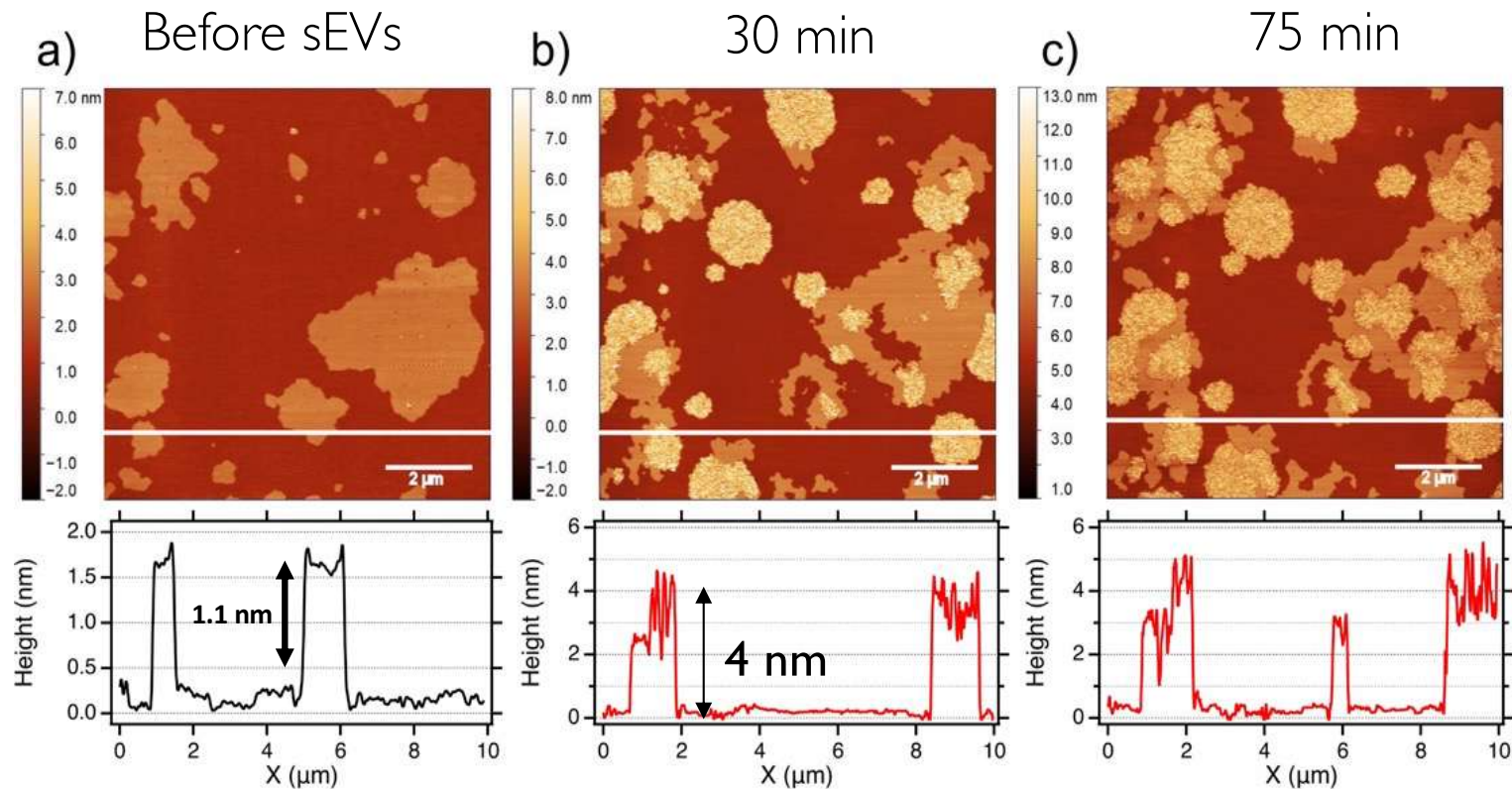
sEVs-uptake mechanism?



Cargo release may be favoured or prevented



Morphology changes vs. time: L_d expansion

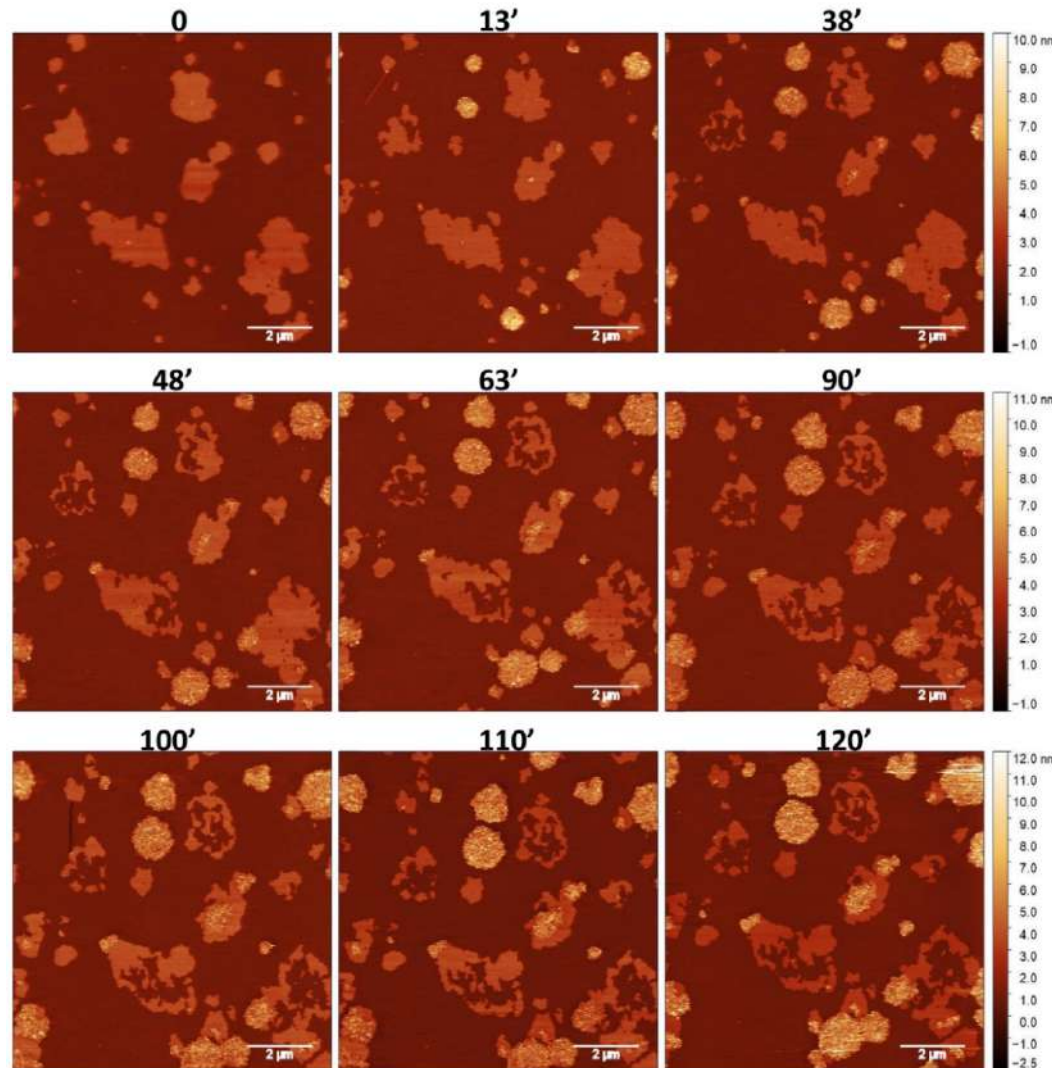


Patches protruding 3-4 nm above SLB tend to **expand in a more favourable fashion in L_d phase**

initial nucleation seeds which act as docking sites for other EVs from solution

L_o phase reshaping

L_o phase re-shaping, borders granularity



L_o granularity from literature:
-> cholesterol depletion
-> components redistribution

Distinct processes occur:

1. Fast diffusion of lighter elements
laterally migrating along phase
boundaries

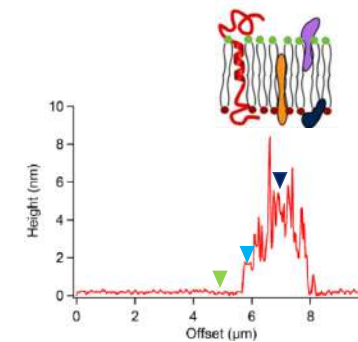
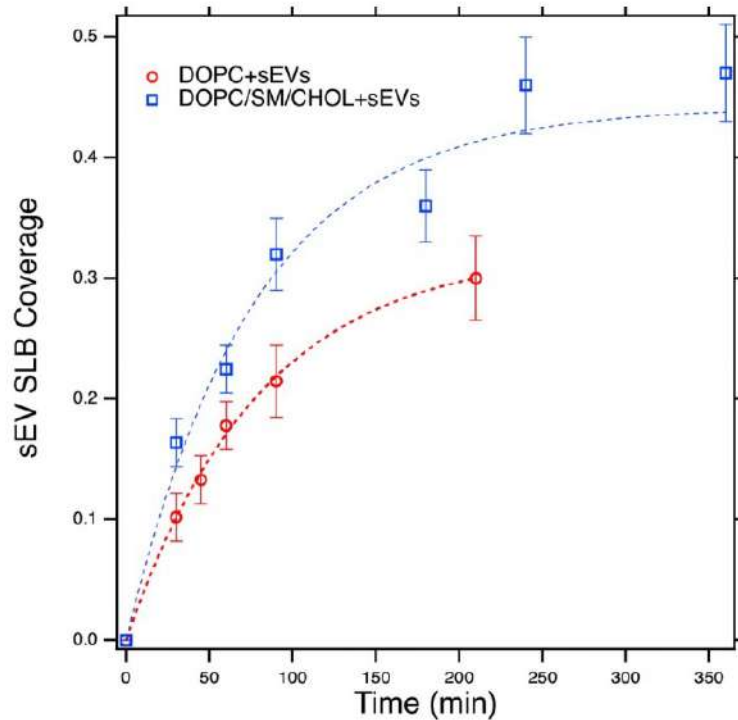
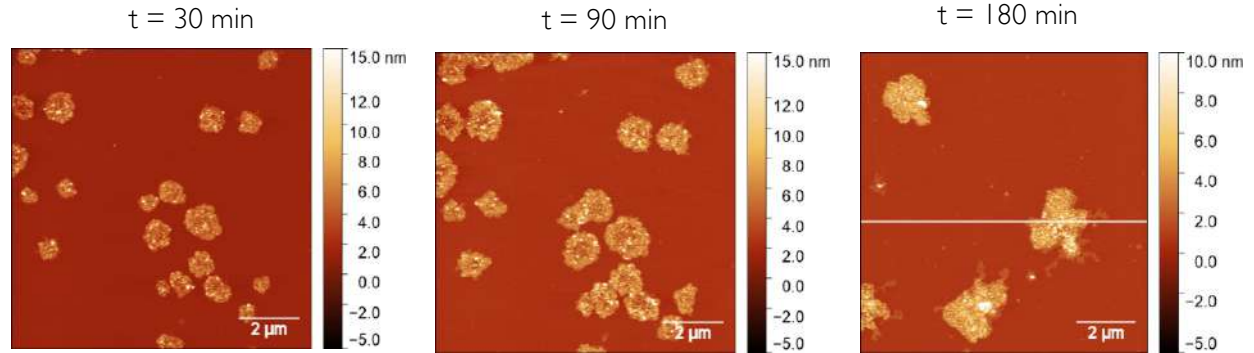
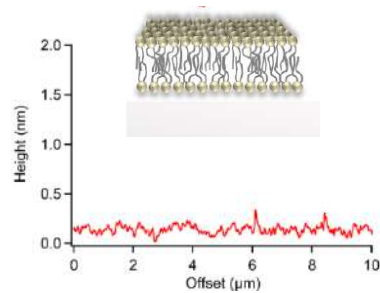
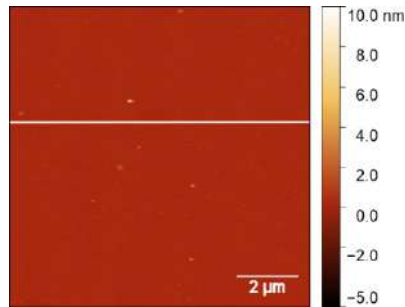
2. Diffusion of bulkier sEVs
components mixing with target
membrane

Different sEVs components spread with different kinetics!

sEVs+single component membrane (PC)

DOPC

+ sEVs

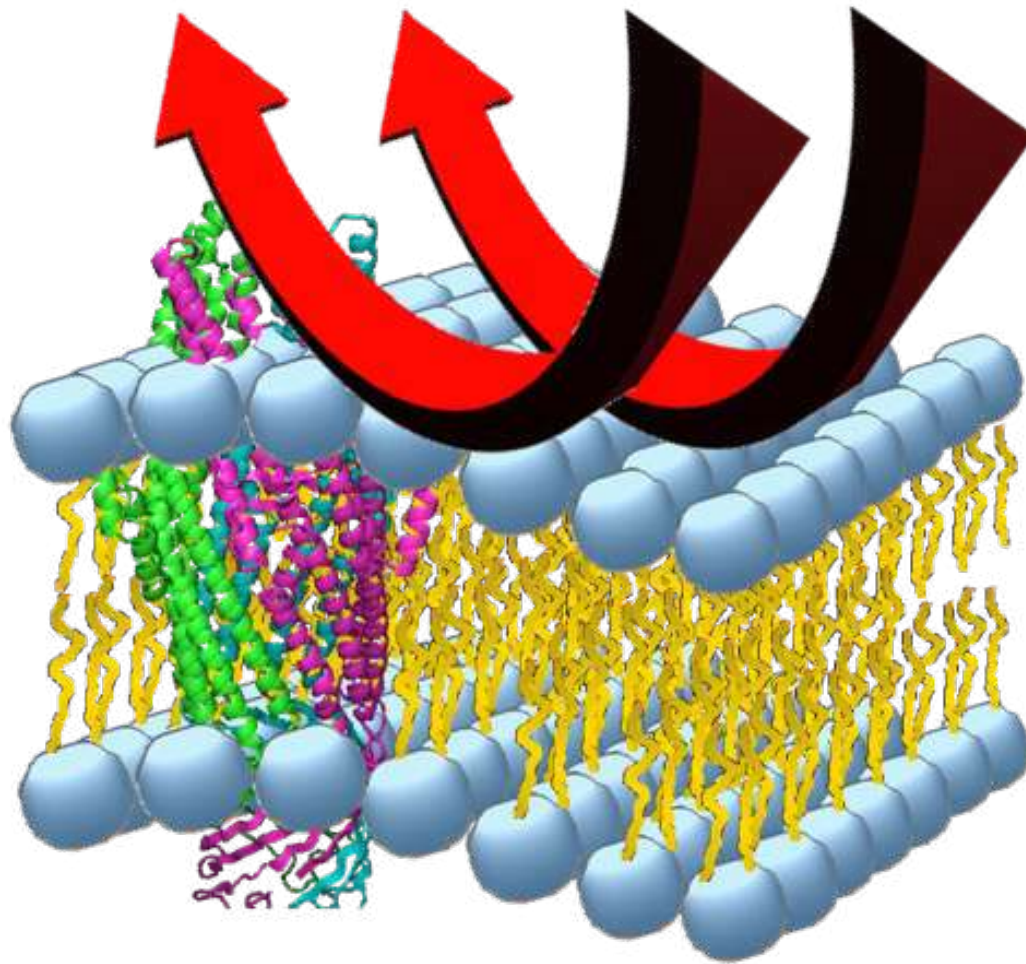


Protrusion of patches 3.4± 0.7 nm

mesoscale heterogeneity due to the presence of EVs membrane proteins as well as cargo macromolecules released from the opened EVs

Single sEV-related bilayer with a (partial) mixing of the vesicles with the SLB: step towards complete fusion sEVs-SLB

Neutron Reflectometry



See Giovanna Fragneto file

Neutron Reflectometry

Why Neutron Reflectometry?

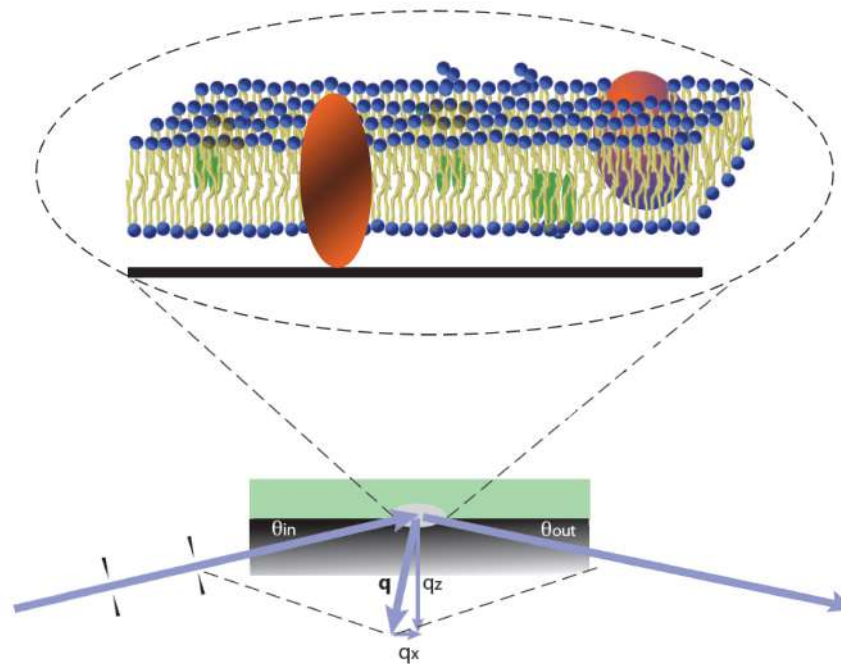
Probe relevant lengths (\AA to μm)

Sensitive to light elements (H, C, O, N)

Buried systems and complex sample environment

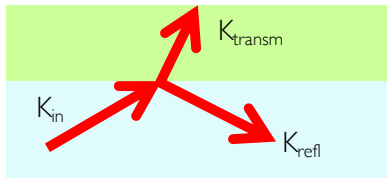
Possibility of isotopic labelling

Non-destructive



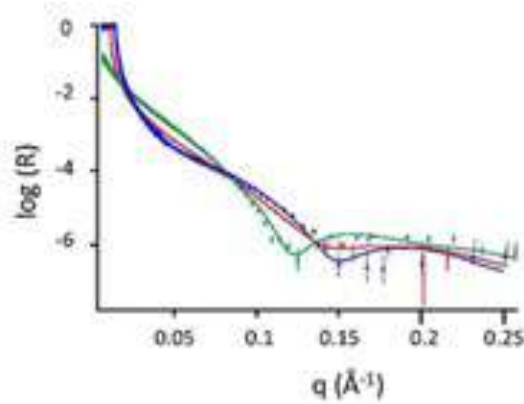
Neutron Reflectometry

Valeria Rondelli



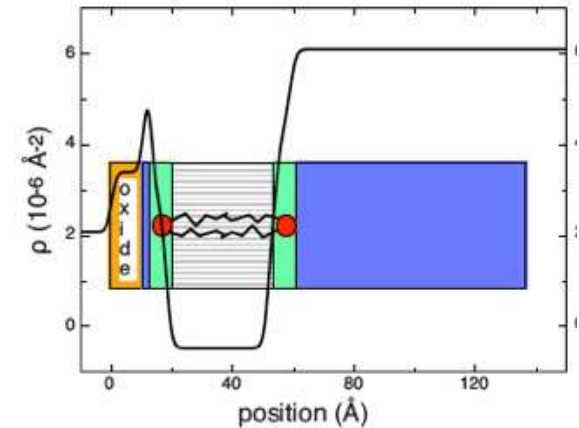
The Reflectivity spectrum obtained is given by the interference of the waves reflected from the top and bottom of each layer.
 q_z is the momentum transfer vector

$$R \approx \left(\frac{16\pi^2}{q^4} N_b^2 \right) e^{-q_z^2 \sigma^2}$$

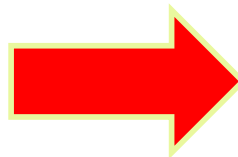


Scattering length density (SLD, or N_b) profile extracted from data analysis

Sensitive to light elements (H,O,N,C..)



SAMPLE CROSS PROFILE



Information about the transverse structure of the sample, layer by layer: thickness, composition, compactness, roughness

Neutron Reflectometry

V represents the net effect of the interactions between the neutron and the scatterers in the medium through which it moves.










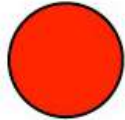

$$V = \frac{h^2}{2\pi m_n} N_b$$

$$N_b = \frac{\sum_j b_j n_j}{Vol}$$

scattering length density

Neutron Reflectometry

Coherent neutron scattering lengths [fm]

	p	d	C	N	O	P	S
average	 -3.74	 6.67	 6.65	 9.36	 5.81	 5.13	 2.85
spin up	 10.82	 9.4					
spin down	 -18.3	 3.8					

$$N_{b_{H_2O}} = \frac{2b_H + b_O}{V_{H_2O}} = \frac{(5.81 - 3.74 \cdot 2) \text{ fm}}{30 \text{ \AA}^3}$$

$$N_{b_{H_2O}} = -0.56 \cdot 10^{10} \text{ cm}^{-2}$$

$$V_{H_2O} = \frac{M_{H_2O} \bar{V}_{H_2O}}{N_A}$$

Calculation of the scattering length density

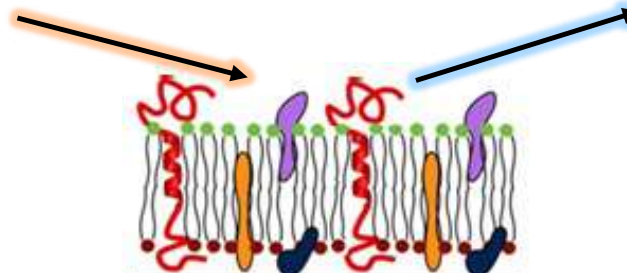
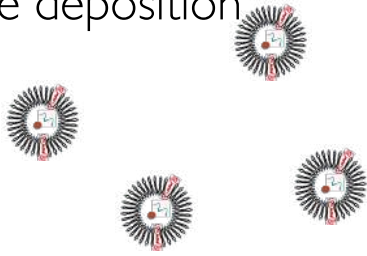
Spin-dependent scattering lengths

neutrons deflected from hydrogen are 180° out of phase relative to those deflected by the other elements

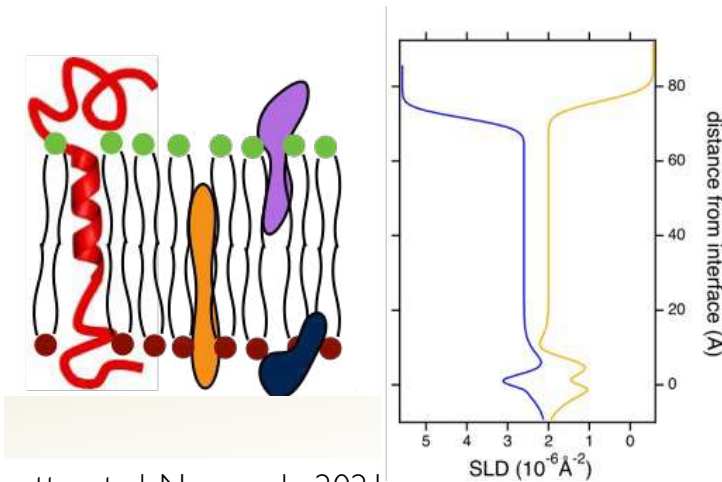
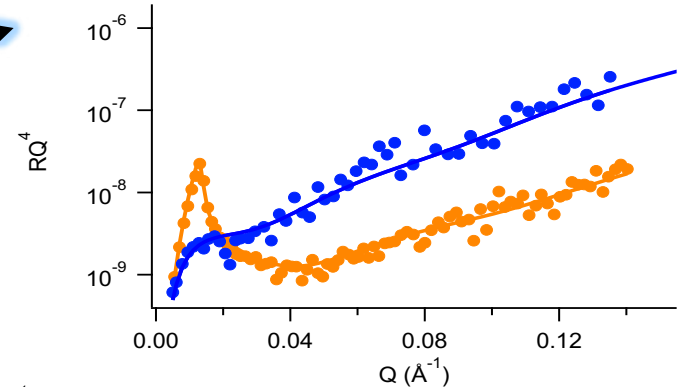
sEVs-derived bilayer

Neutron Reflectometry

Vesicle deposition



0.5 nm water between membrane and silicon support



6.9 ± 0.2 nm thickness

single bilayer containing molecules other than lipids, as large proteins

Perissinotto et al. Nanoscale 2021

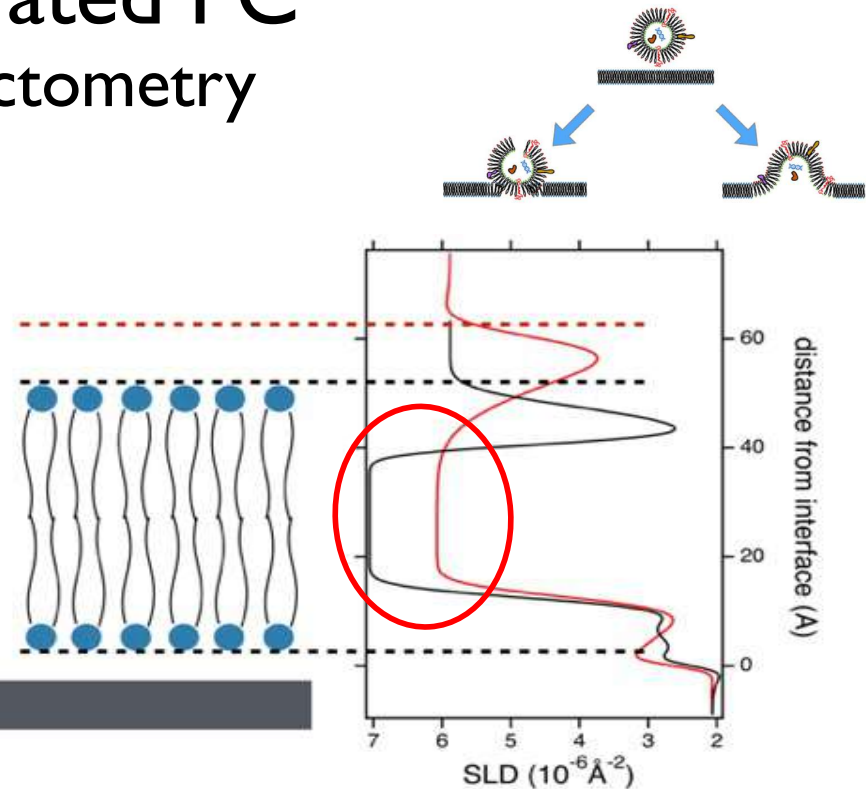
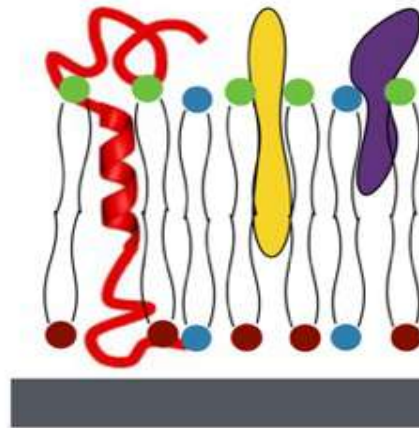
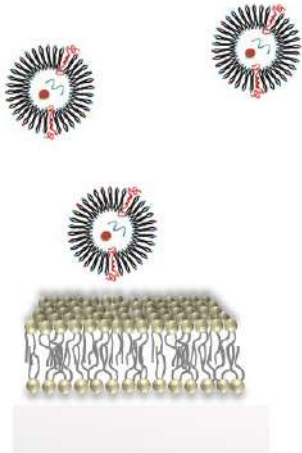
$$R \approx \left(\frac{16\pi^2}{q^4} N_b^2 \right) e^{-q_z^2 \sigma^2}$$

SLD of 2 ± 0.2 × 10⁻⁶ Å⁻²

lipid to non-lipid ratio 22:78 (by volume)

sEVs+deuterated PC Neutron reflectometry

$$R \approx \left(\frac{16\pi^2}{q^4} N_b^2 \right) e^{-q_z^2 \sigma^2}$$

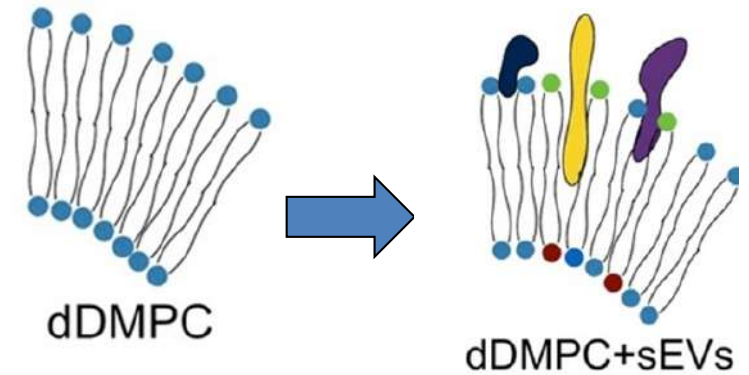
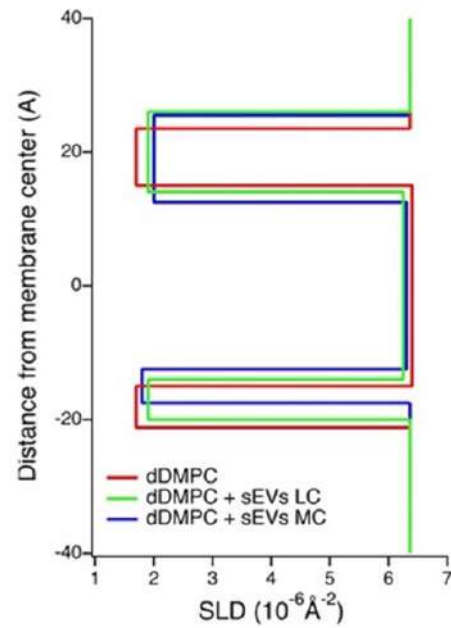
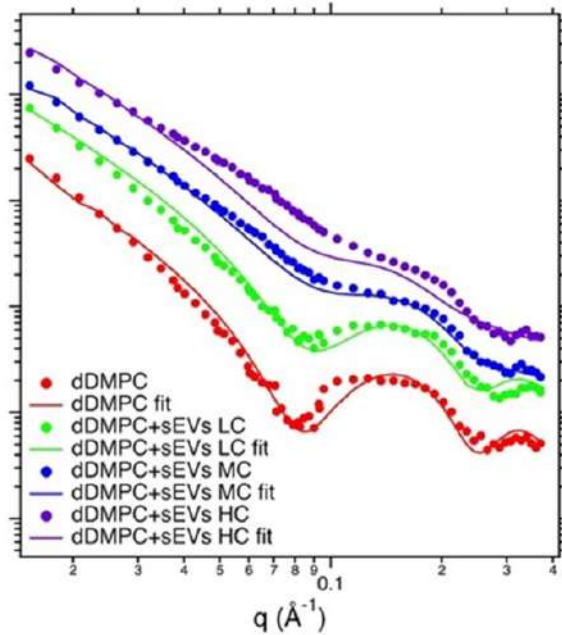
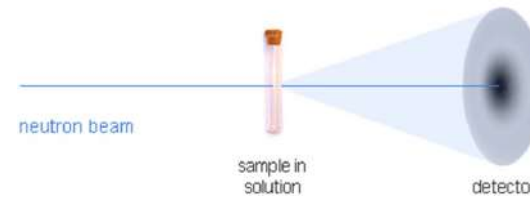
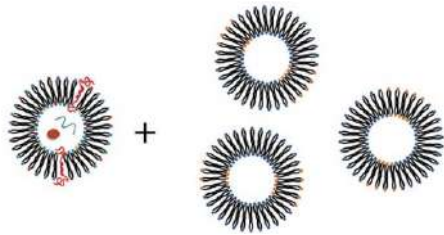


Playing with selective deuteration: [protiated molecules in a ghost phospholipid matrix](#)

- 20% volume penetration
- Change in contrast spans whole membrane thickness
- Asymmetry

	AFM ΔZ (nm)	NR h (nm)
PC	5.1 ± 0.6	4.2 ± 0.3
PC+EVs	6 ± 2	5.4 ± 0.3

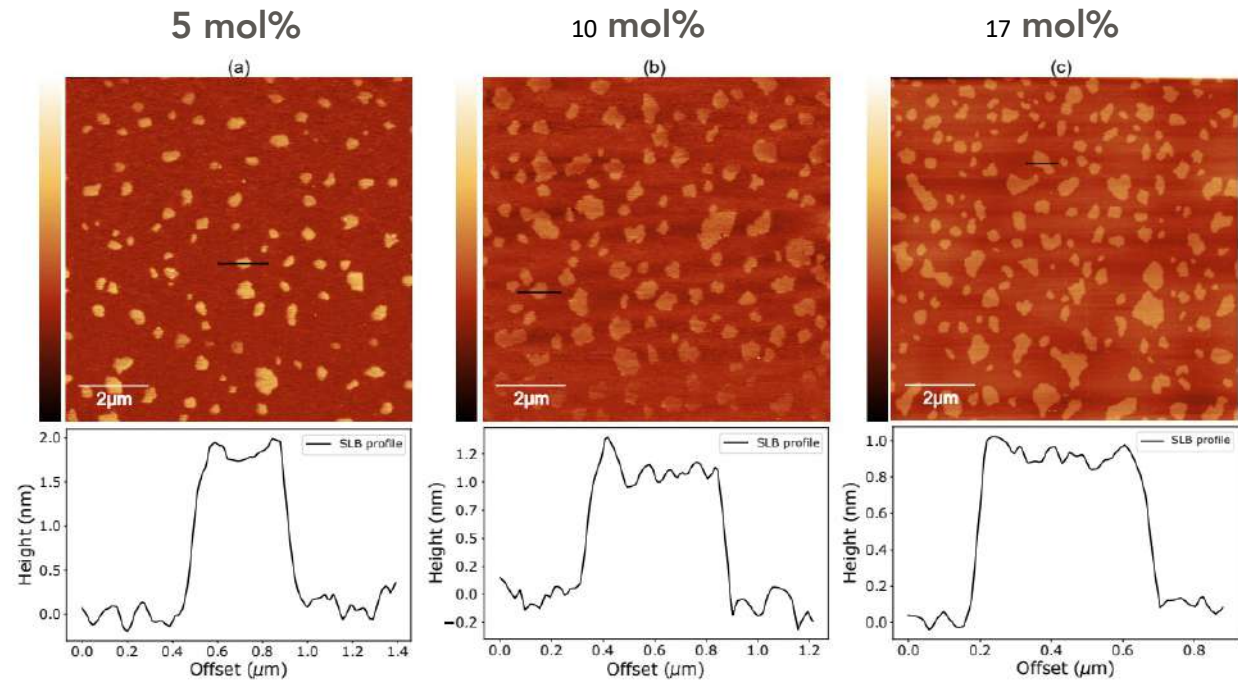
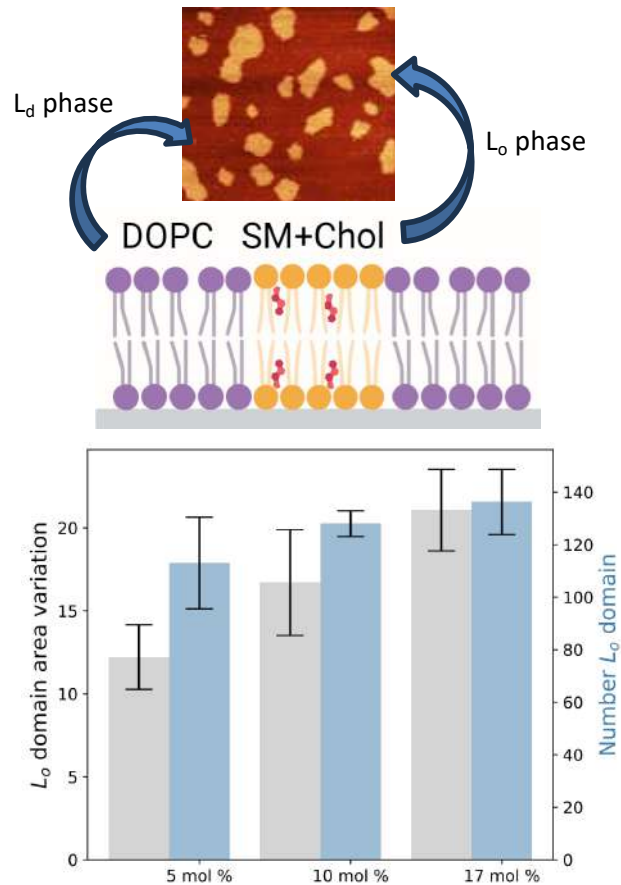
sEVs+deuterated PC SANS



sEVs : dDMPCVs
 1:15000
 1:3000
 1:2700

- Change in contrast spans whole membrane thickness
- Asymmetry

What about cholesterol ?



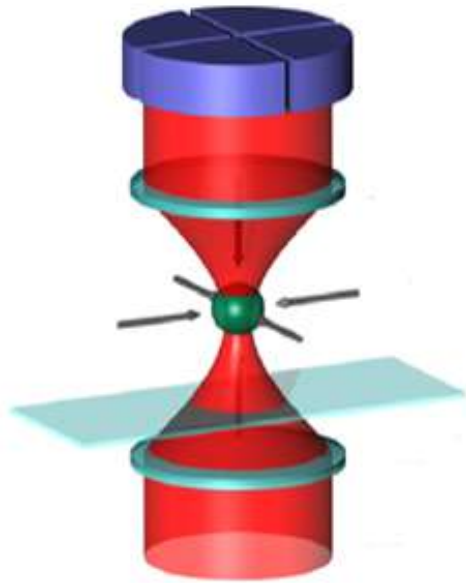
Rafts-covered area scales with chol. Height difference decreases.
Both preferred co-localization with SM and chol-condensing effect on L_d phase

Paba, et al. JCIS, 2023

‘cholesterol-condensing effect’ on phospholipids thickening of the L_d phase and a reduced height difference with the L_o domains

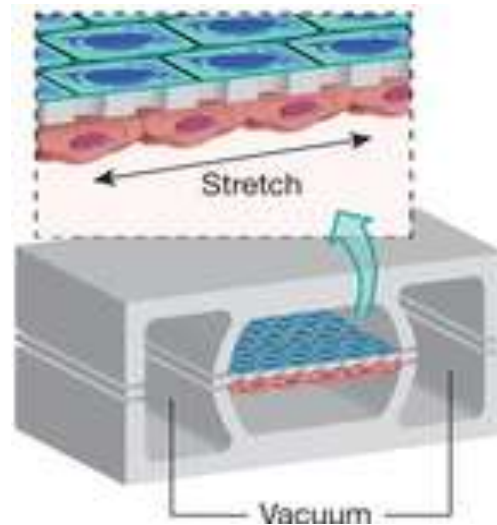
Atomic Force Spectroscopy

How to study cell mechanics



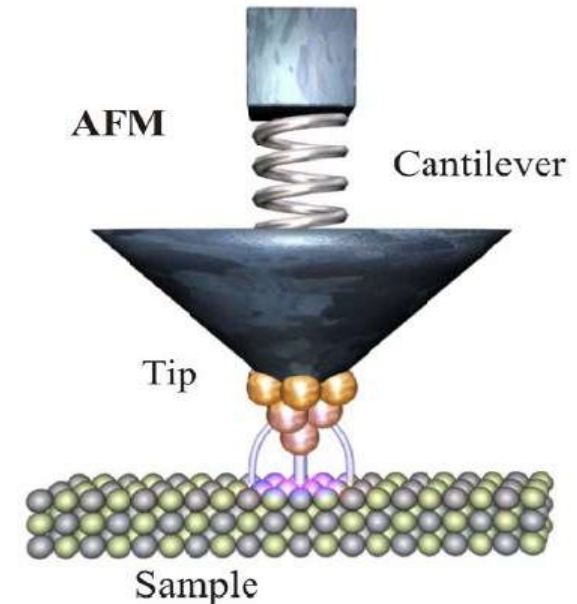
OPTICAL TWEEZER

- Two lasers in order to trap a bead
- The bead displacement converted to force by the software
- Force applied from 0.1 to 100 pN



STRETCHING IN MICROFLUIDIC CHANNELS

PDMS soft lithography



ATOMIC FORCE MICROSCOPY

- Tip mounted on a flexible cantilever
- Tip/sample interaction monitored by a laser
- Force applied from 10 pN to 100 nN

AFM and cell mechanics

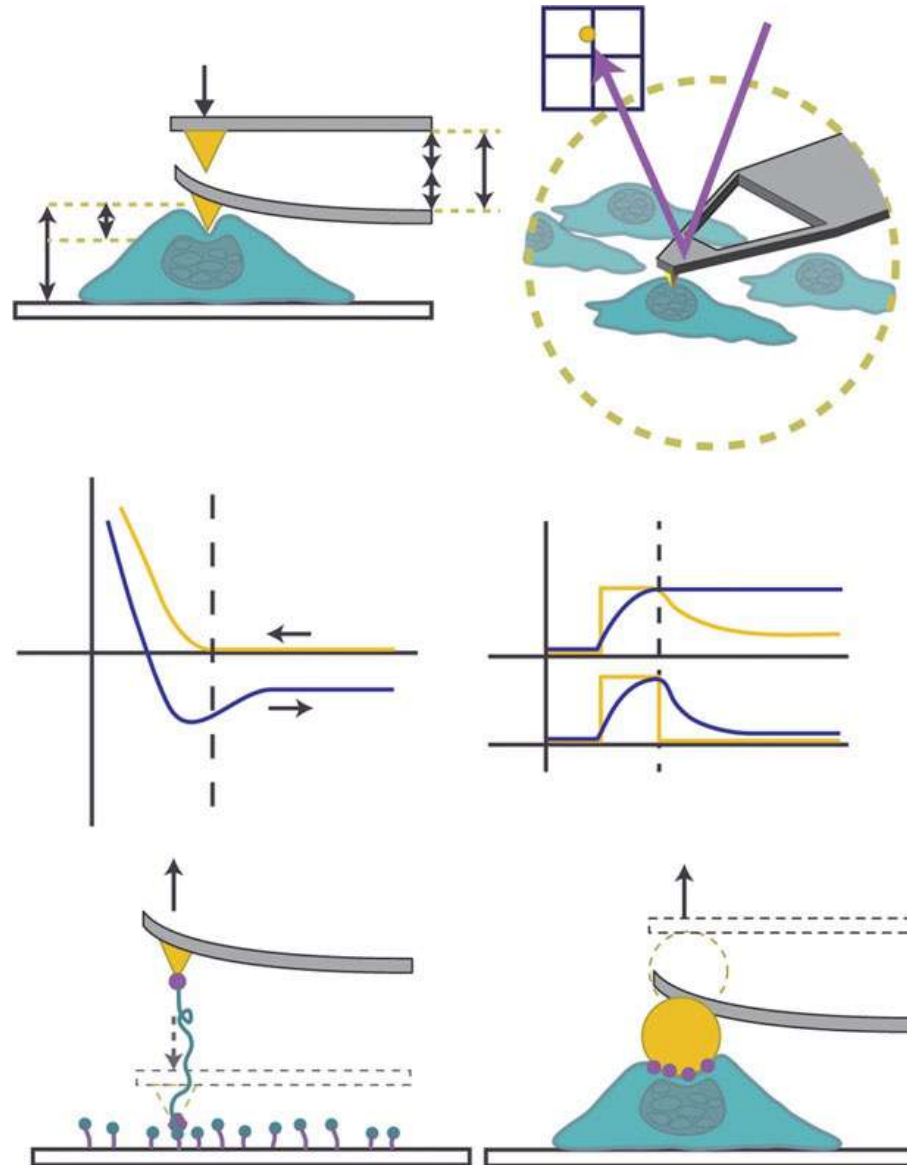
AFM has been used to measure both **elastic** and **viscous** cellular responses

AFM can be used to **directly apply and simultaneously measure cellular forces**.

Its advantage is its **versatility**, as AFM can be used for imaging as well as force transmission and measurement.

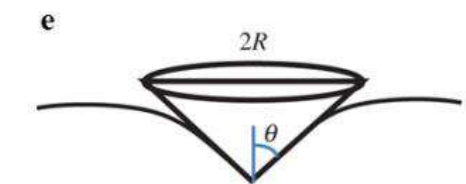
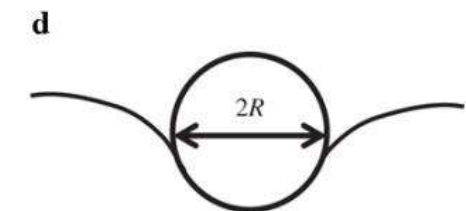
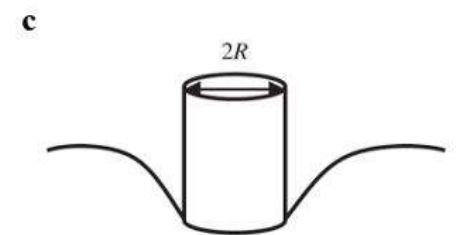
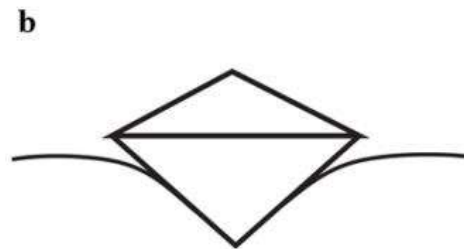
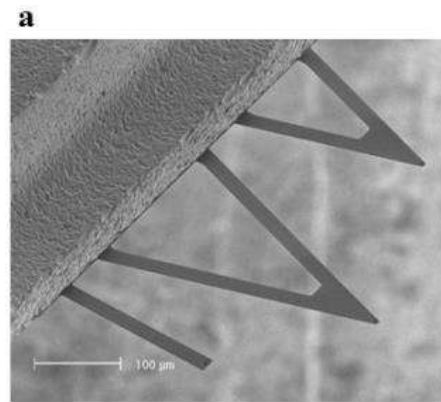
By altering tip geometry or chemistry, a multitude of both local and whole-cell studies can be performed on living cells in their native environments.

These studies induce a rapid response of cells through shape change, remodelling of the cytoskeleton and calcium signalling, which all depend on frequency, duration, magnitude and location of applied force

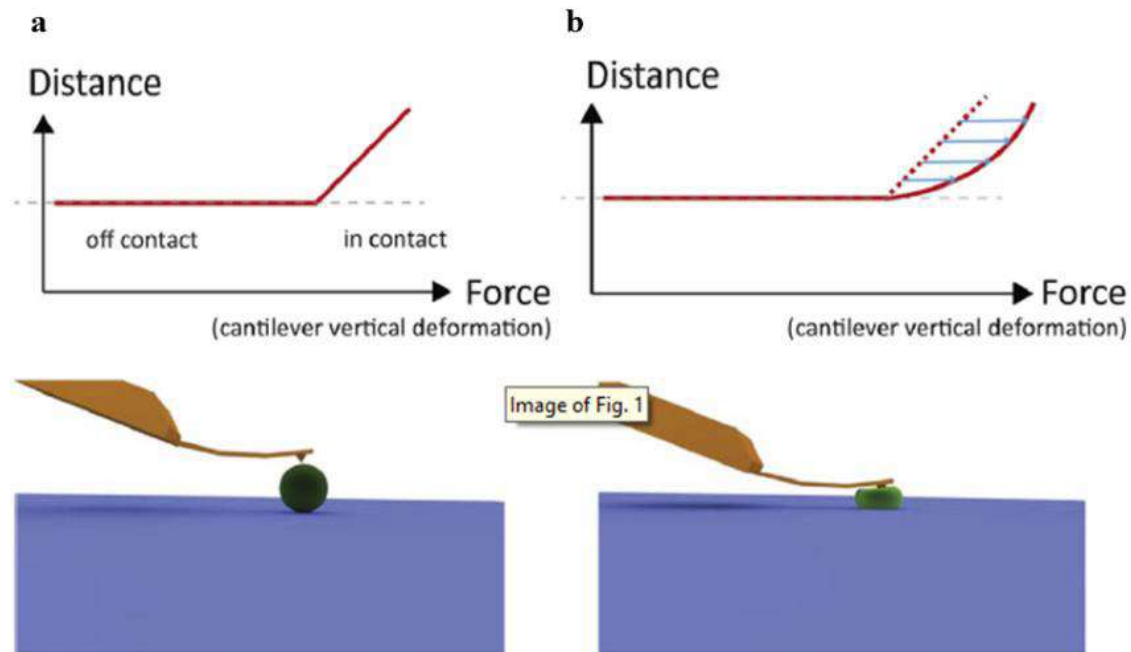


AFM and cell mechanics

AFM indentation data demonstrated that in many pathologies such as the anemia, diabetes, cardiomyopathies, Parkinson's and Alzheimer's diseases, cancer and many others, the mechanical properties of affected cells are perturbed resulting in a characteristic fingerprint for these diseases



AFM and cell mechanics



Before contact, the base of AFM cantilever - surface distance is the same as tip apex - surface distance.

From contact point on:

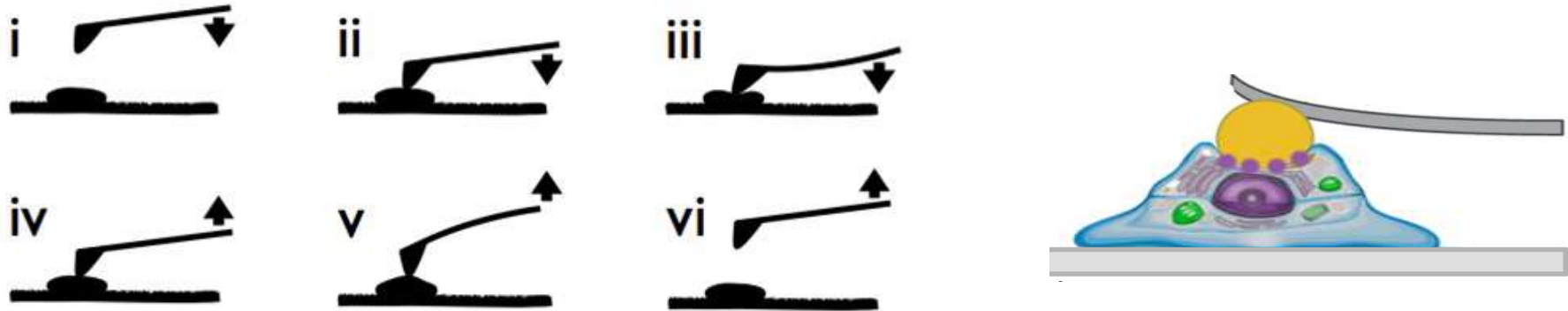
- if the material has **infinite rigidity**, tip-surface distance will be zero while base of the AFM - surface distance further reduces -- **cantilever deformation**
- if the material is **soft**, tip penetrates the surface. The entity of this penetration is inverse function of the stiffness of the sample.

Cantilever deflection due to the further reduction of the distance between the cantilever base and the surface has to be corrected by the distance the apex tip penetrate into the material

AFM Force-Spectroscopy

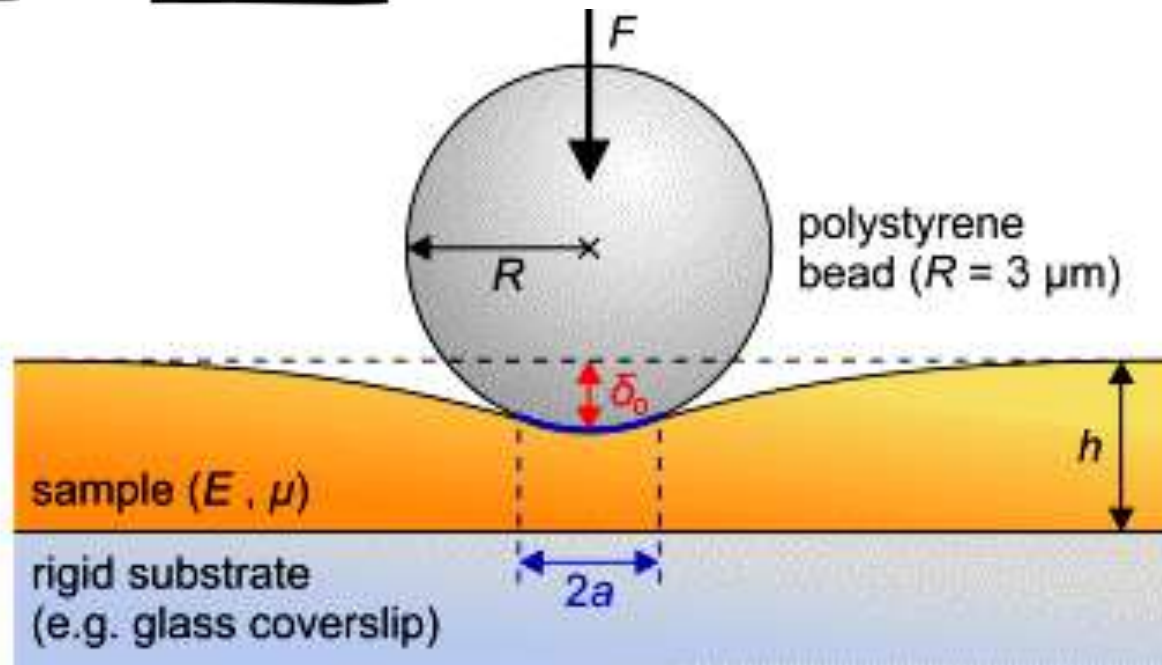
The most used is the Hertz model. The Hertz formalism is founded on the theory of linear elasticity and must satisfy a Hookean relationship which describes the elastic deformation of two sphere, where the relation between the applied force (F) and the resulting indentation is:

AFM Force-Spectroscopy



$$F = \frac{4}{3} \frac{E}{1-\mu^2} \sqrt{R \delta_0^3}$$

- F ... applied force
- R ... radius of the probe
- δ_0 ... indentation of the sample
- E ... elastic modulus
- μ ... POISSON'S ratio



An elastic sphere of radius R indents an elastic half-space to depth d , and thus creates a contact area of radius

$$a = \sqrt{Rd}$$

The applied force F is related to the displacement d by [4]

$$F = \frac{4}{3} E^* R^{\frac{1}{2}} d^{\frac{3}{2}}$$

where

$$\frac{1}{E^*} = \frac{1 - \nu_1^2}{E_1} + \frac{1 - \nu_2^2}{E_2}$$

and E_1, E_2 are the elastic moduli and ν_1, ν_2 the Poisson's ratios associated with each body.

The distribution of normal pressure in the contact area as a function of distance from the center of the circle is!

$$p(r) = p_0 \left(1 - \frac{r^2}{a^2} \right)^{\frac{1}{2}}$$

where p_0 is the maximum contact pressure given by

$$p_0 = \frac{3F}{2\pi a^2} = \frac{1}{\pi} \left(\frac{6FE^{*2}}{R^2} \right)^{\frac{1}{3}}$$

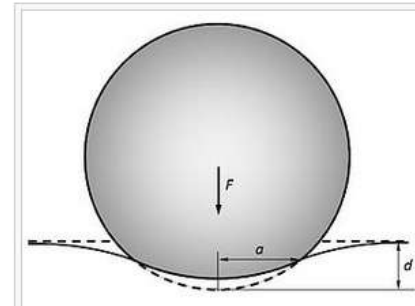
The radius of the circle is related to the applied load F by the equation

$$a^3 = \frac{3FR}{4E^*}$$

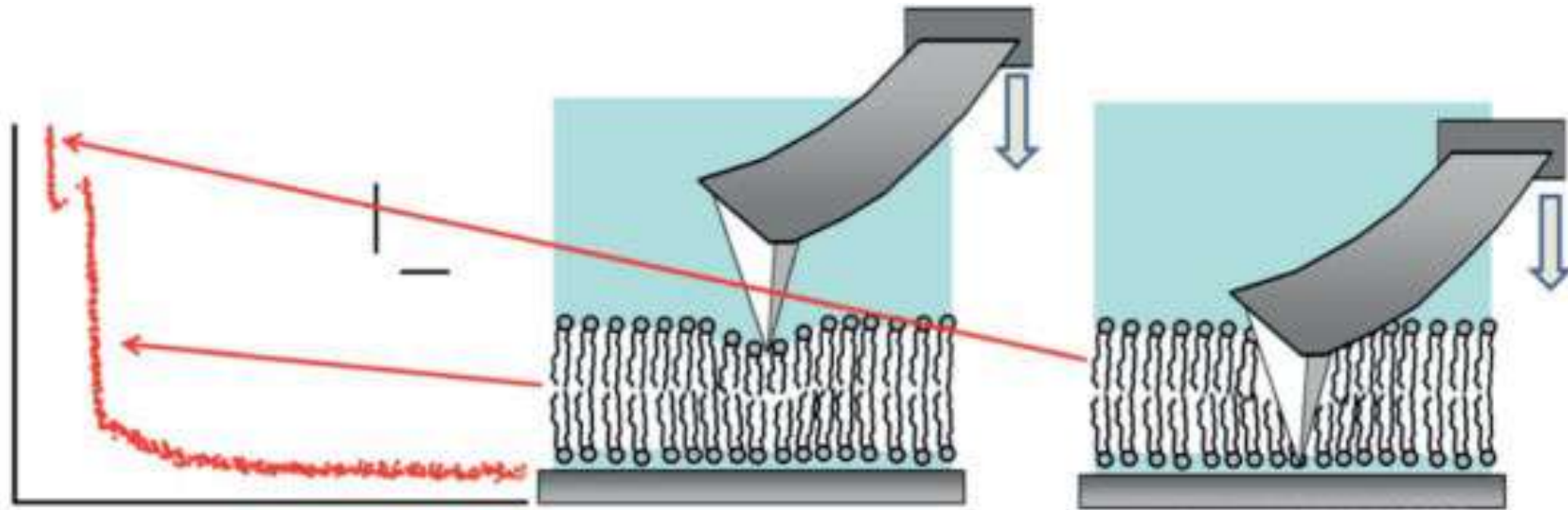
The depth of indentation d is related to the maximum contact pressure by

$$d = \frac{a^2}{R} = \left(\frac{9F^2}{16E^{*2}R} \right)^{\frac{1}{3}}$$

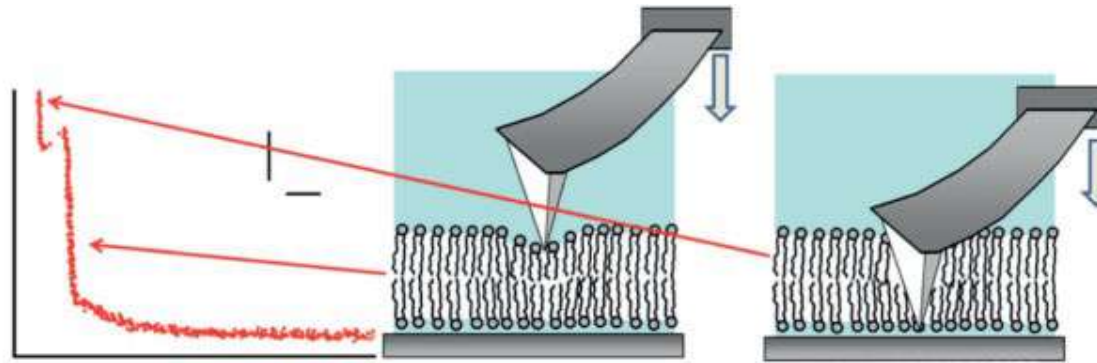
The maximum shear stress occurs in the interior at $z \approx 0.49a$ for $\nu = 0.33$.



The tip of an AFM is pressed on a supported lipid bilayer until indentation takes place. A discontinuity in the force curve appears when the tip instantaneously punches through the bilayer.

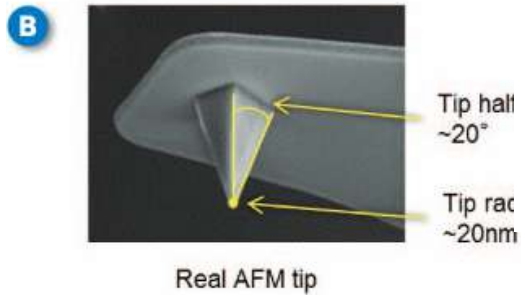


Scheme of a force curve performed on a supported lipid bilayer. The cantilever is moving at constant speed towards the bilayer. After a first long range interaction section which might include electrostatic and hydration forces, a contact region between the tip and the bilayer follows. This region can be considered of elastic deformation. After a threshold force is reached, the tip jumps in contact with the substrate by a process of plastic deformation (rupture) of the membrane.

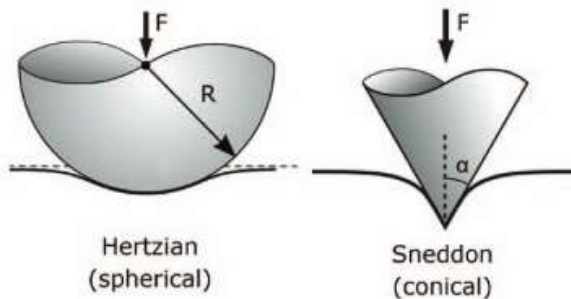
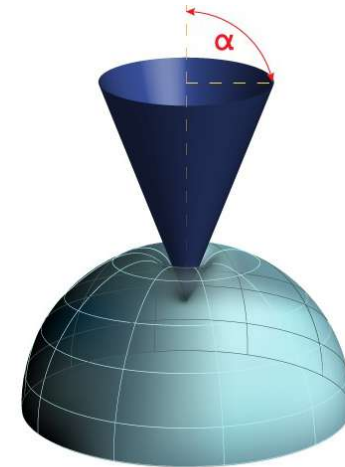


However, it has been shown that the above model is not appropriate in case of supported lipid bilayers.

Typical Features for Data Process



$$F = \frac{2}{\pi} \frac{E}{(1 - \nu^2)} \tan(\alpha) \delta^2$$



Equation 5: Sneddon model

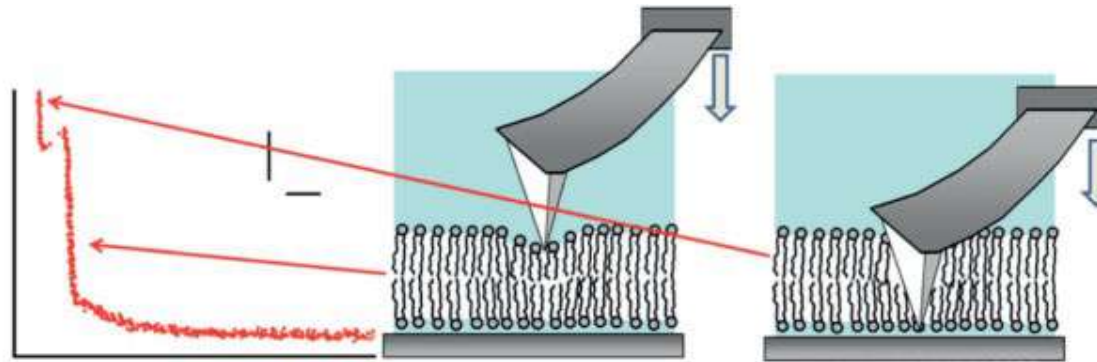
F = force (from force curve)

E = Young's modulus (fit parameter)

ν = Poisson's ratio (sample dependent, typically 0.2 - 0.5)

α = half-angle of the indenter

δ = indentation



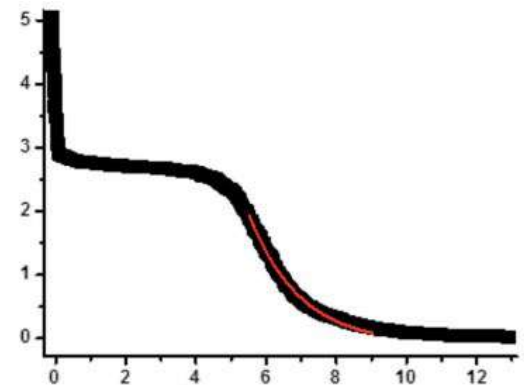
The difficulty stems from the small thickness of the lipid bilayer. Indeed, the presence of a rigid substrate supporting the bilayer can strongly influence the value of the Young modulus obtained by interpreting the stress-strain relation on the basis of the Hertz theory, especially in the case of high deformation ratio.

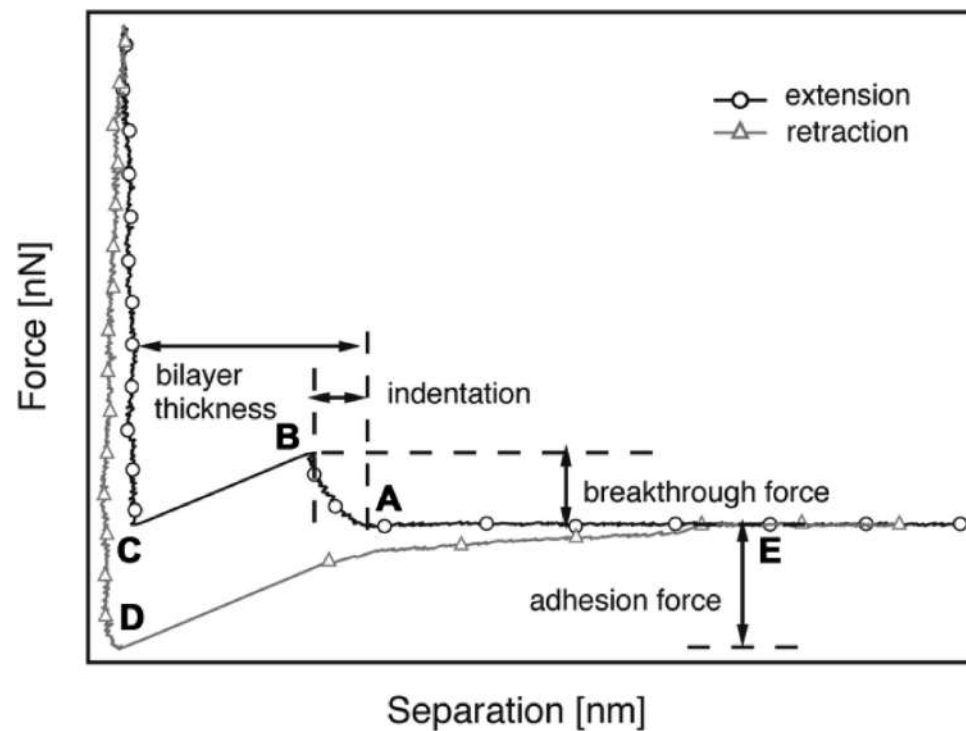
Another more plausible model to figure out a value for the spring constant of a lipid bilayer related to the area stretching modulus is that developed by Das et al. This model accounts for the presence of the two leaflets making up the bilayer, although it neglects the strong asymmetry in the physical properties of the two leaflets as due to the presence of the substrate.

This model is based on the fact that a spherical indenting AFS tip forces the lipid on a curved surface. As a consequence, the area stretching modulus of the lipid bilayer is involved. By calculating the Gibbs free energy cost for the deformation and its derivative with respect to tip movement, the authors obtained the following analytical expression for the applied force and the bilayer deformation:

$$F = \frac{\pi \kappa_A R}{4} \left(\frac{2z_0}{2d - z_0} \right)^2$$

where κ_A is the area stretching modulus, R is the diameter of the apical region of the AFM tip, $2d$ is the thickness of the bilayer and z_0 is the indentation. Figure 7.10 reports a force curve resulting from an average over more than 200 individual force curves obtained on a supported POPE bilayer at 27°C in 50 mM KCl. By fitting the previous equation to the experimental data in the contact region of the force curve (overlaid trace in figure 10) and assuming a tip apical radius ranging between 5 nm and 10 nm it is possible to extract a value for κ_A in the range 0.12 N/m ÷ 0.06 N/m. At 34°C the value for κ_A is between 0.16 N/m and 0.08 N/m whereas at 38°C it is between 0.14 N/m and 0.07 N/m. This analysis can also show that AFS is able to detect the softening effect of the phase transition in the contact region besides the decreased mechanical stability.





Spring constant:

$$F = \frac{4E\sqrt{R}}{3(1-\sigma^2)} \delta^{3/2}$$

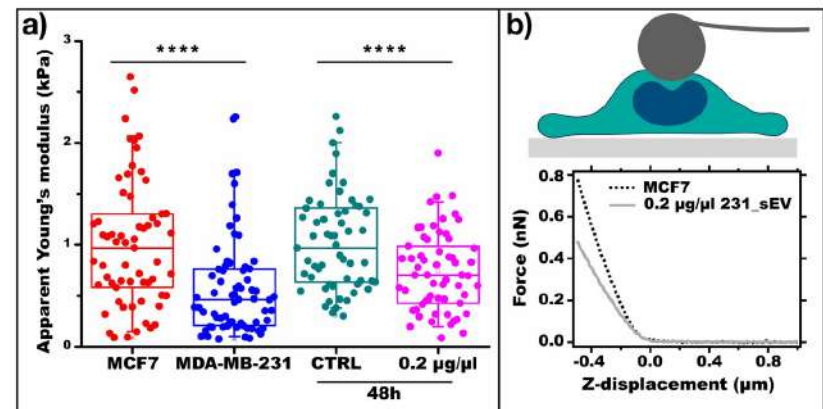
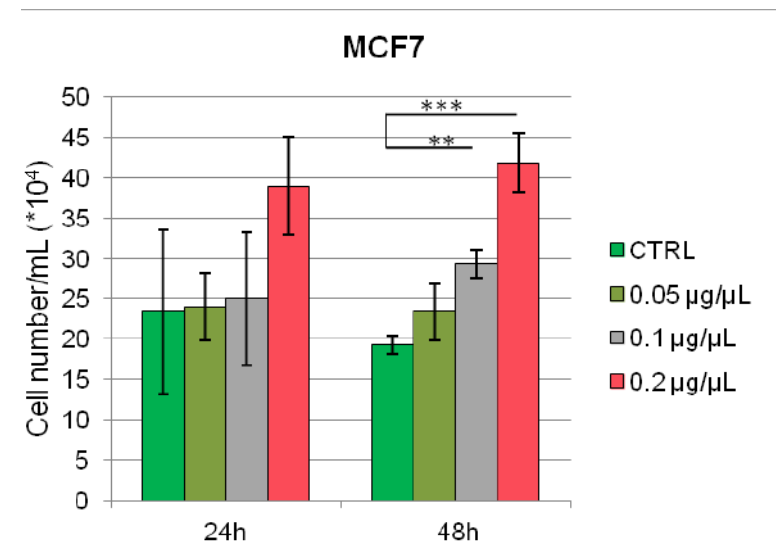
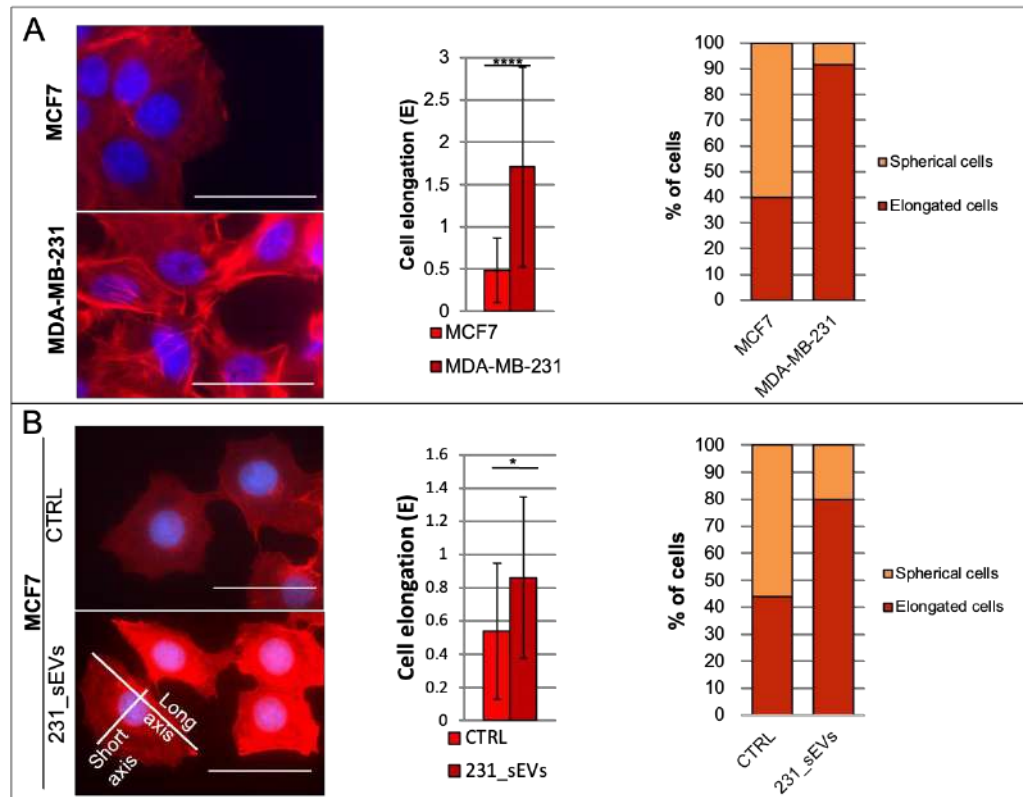
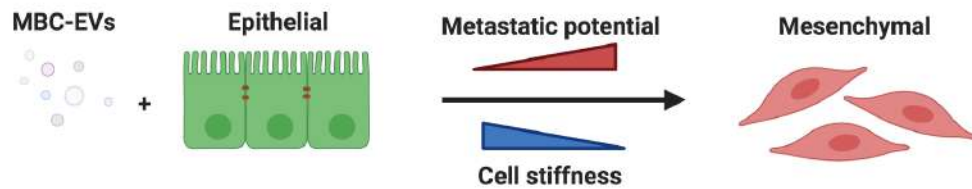
$$d = \frac{F}{k}$$

$$F = \frac{2E \tan(\alpha)}{\pi(1-\sigma^2)} \delta^2$$

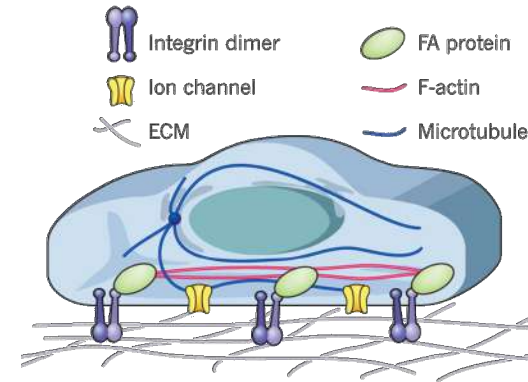
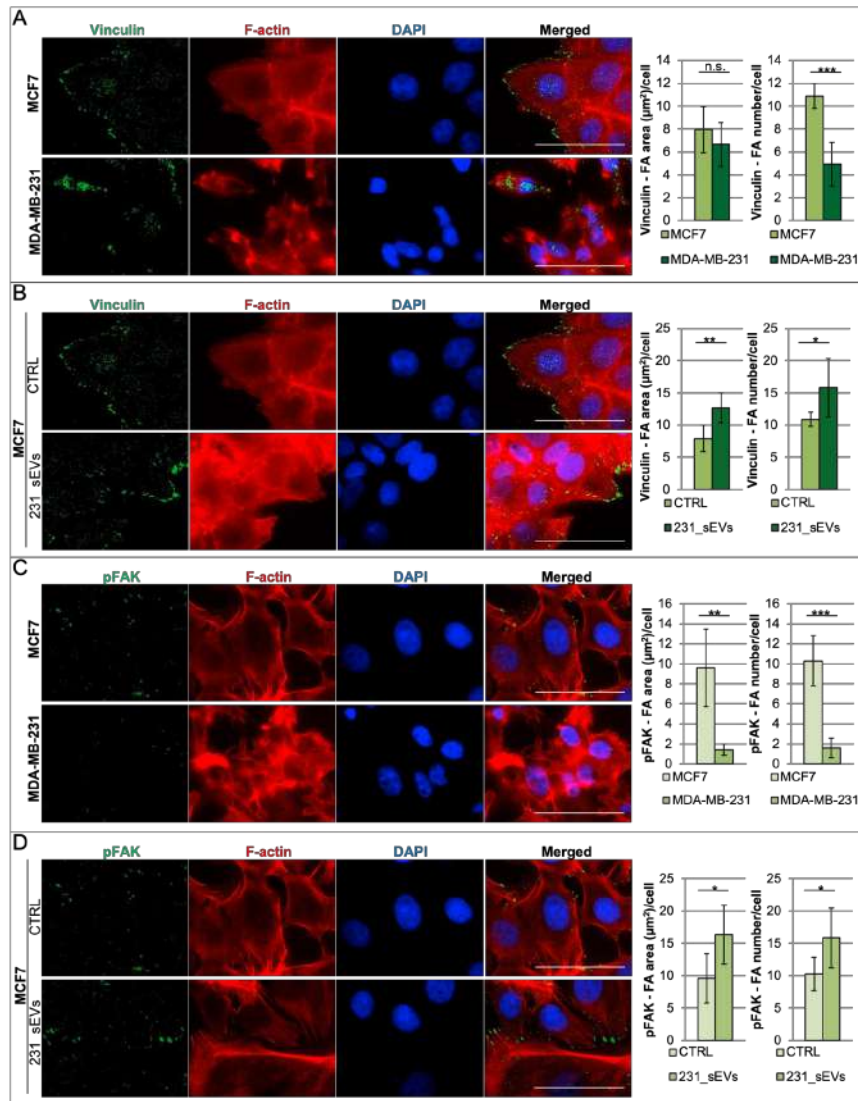
$$s = z - \frac{d}{c}$$

sEVs affect cellular functions

sEVs from Triple Negative Breast Cancer cells as regulators of breast cell biomechanical changes



sEVs affect cellular functions



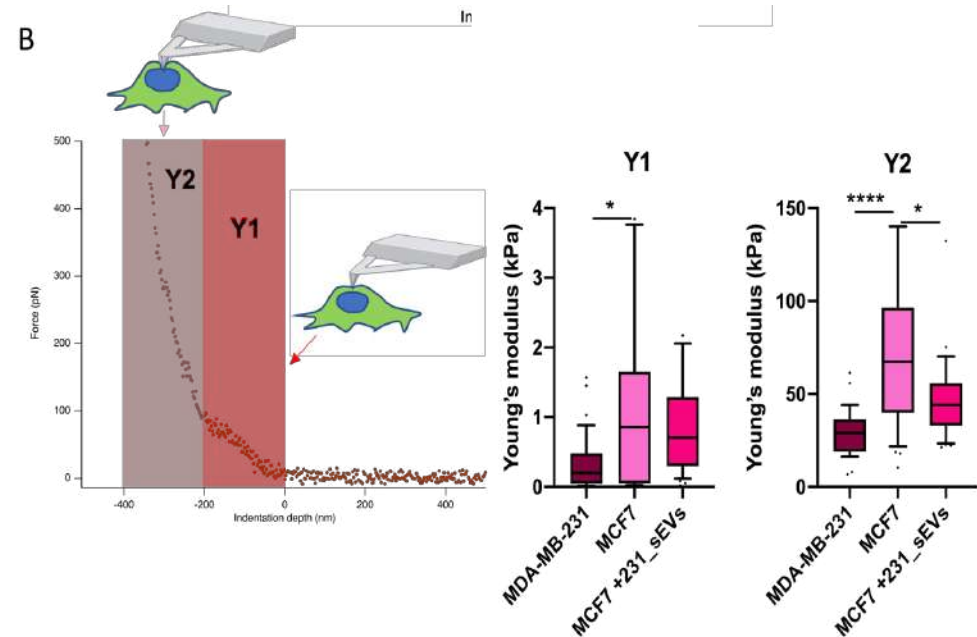
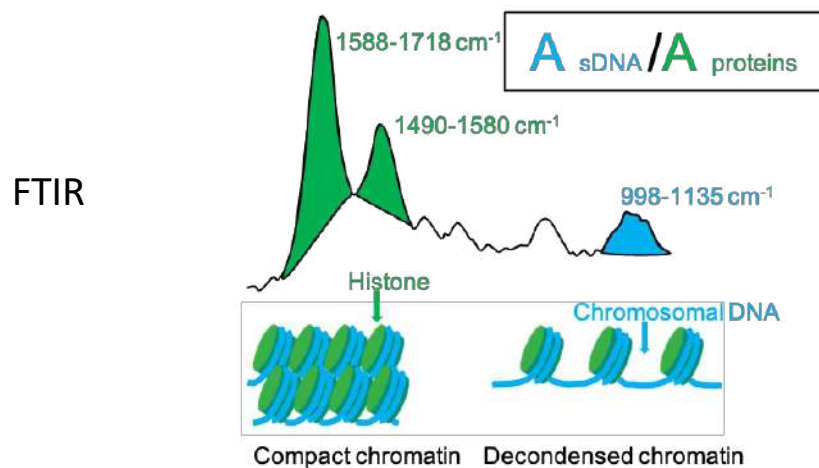
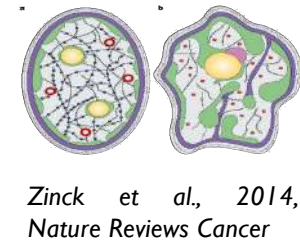
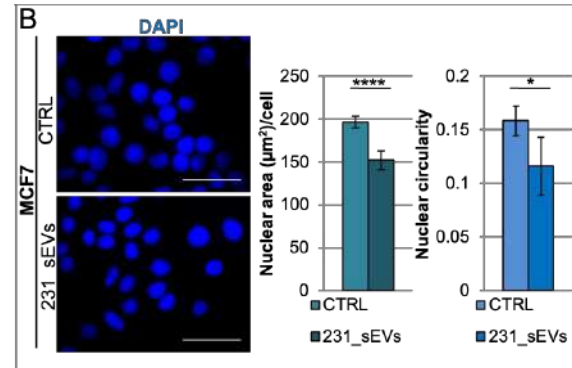
F-actin signal:
higher in 231
higher in 231_sEVs treated MCF7

FA density and size:
smaller in 231
higher in 231_sEVs treated MCF7

Different adhesion phenotype

Stiffness modulation: where it from?

- s-EVs induce modification of nuclear shape and size
- The Young modulus changes at the level of nucleus, not membrane-associated cortical fibers
- Chromatin decondensation might play a relevant role in biomechanical changes

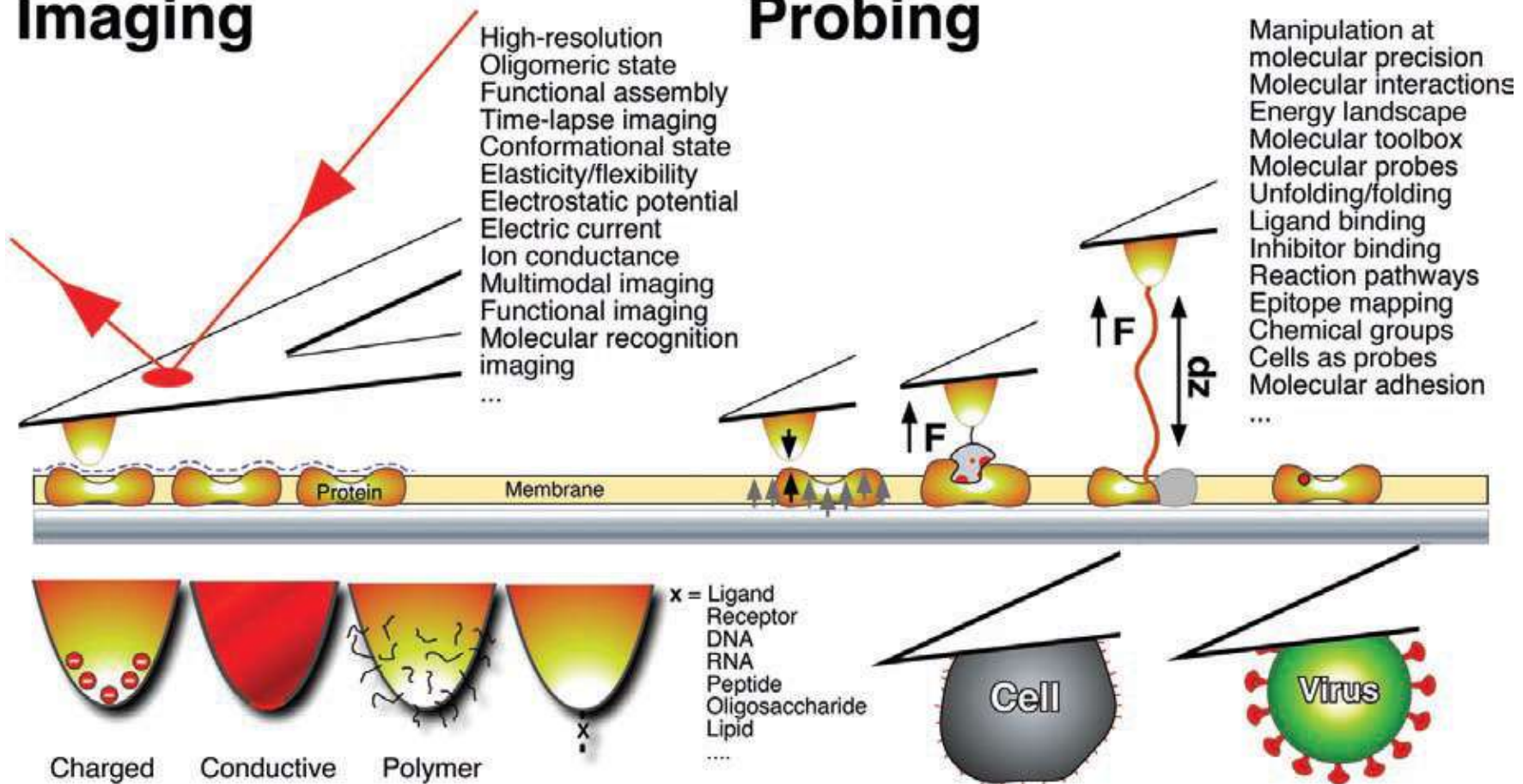


Protein pulling

AFM: lab on a tip

Imaging

Probing



Single molecule manipulation

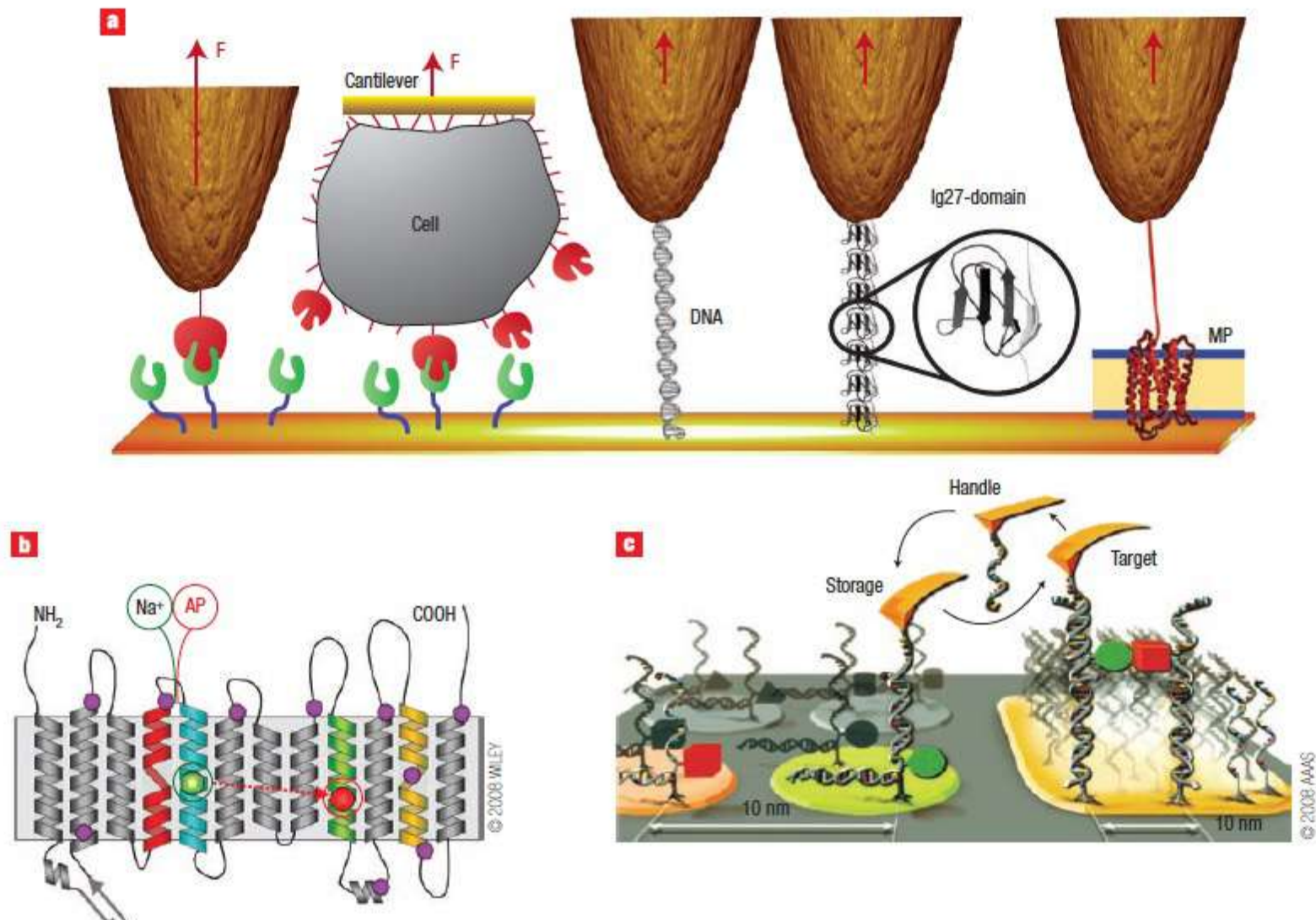
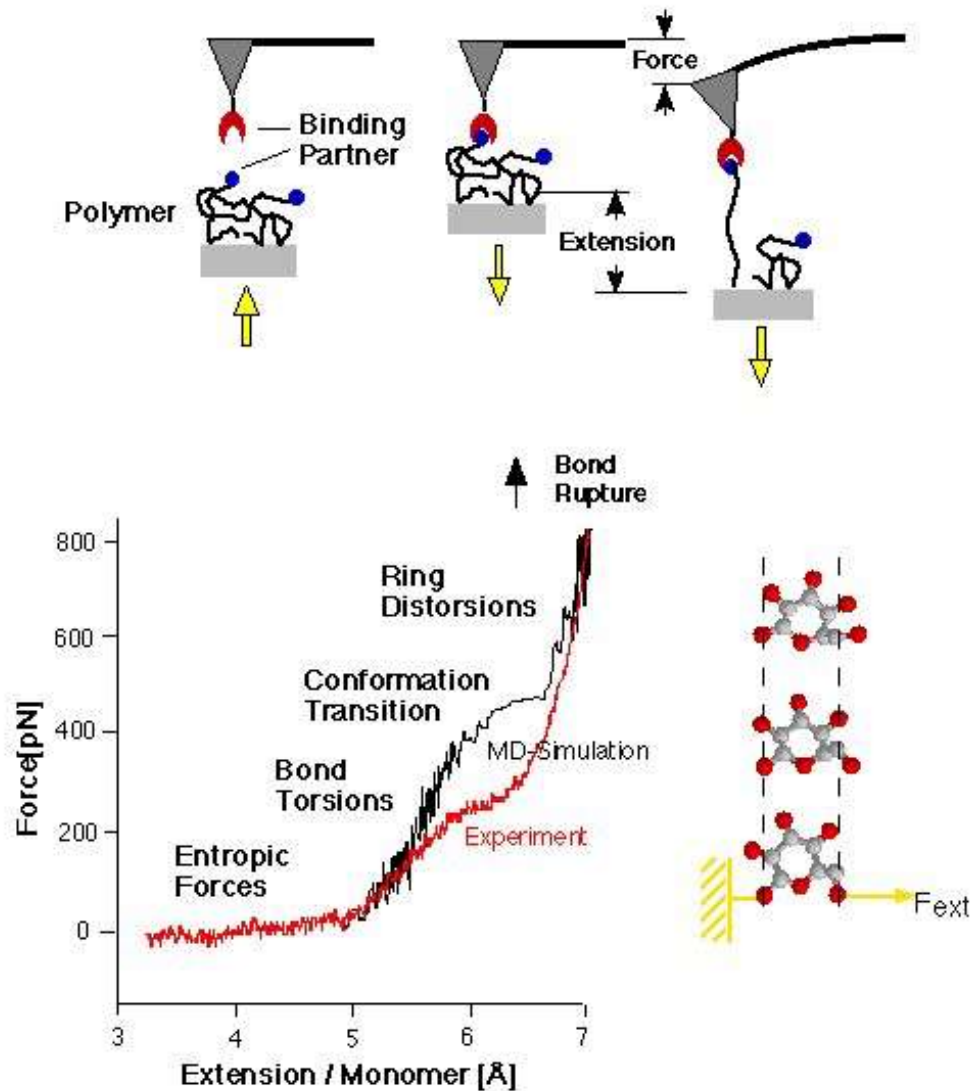
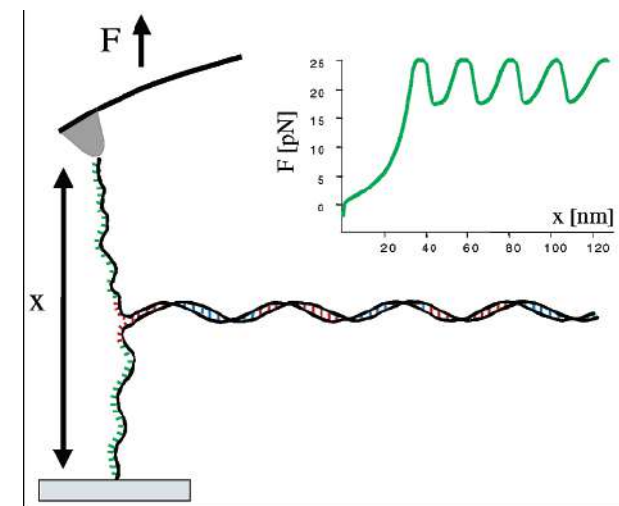
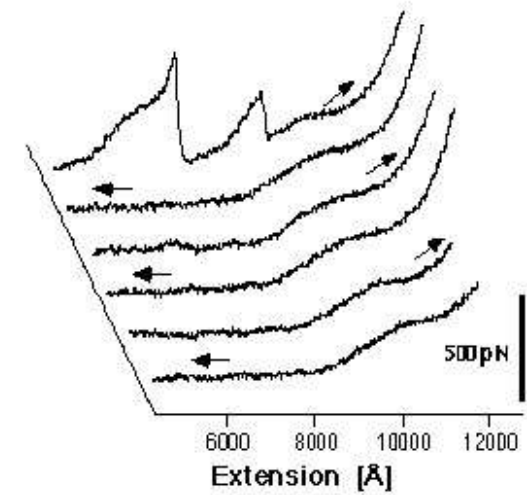


Figure 3 Single molecule manipulation, control and design. **a**, Applying AFM to probe interaction forces (F) of single biomolecules. These examples measure ligand–receptor interactions in their isolated form (left) and embedded in their cellular environment (probe replaced by a biological cell); stretching of a DNA molecule; unfolding of Ig27-titin; and unfolding of a membrane protein (MP). **b**, SMFS can detect and locate interactions (circles) on the structure of membrane proteins (here proton/sodium antiporter NhaA from *E. coli*). A ligand (Na^+ ion) or inhibitor (AP, 2-aminoperimidine) binding to the ligand-binding site (green circle) establishes different interactions activating (green circle) or deactivating (green and red circles) the antiporter (composed of 12 transmembrane helices). **c**, Single molecules can be mechanically assembled by picking up from discrete storage sites with a DNA oligomer at the AFM probe and depositing them at a target site with nanoscopic precision. Reproduced with permission from refs 52, 53 and 63.

Single molecule force spectroscopy



Reversible Extension of a Single Dextran Polymer

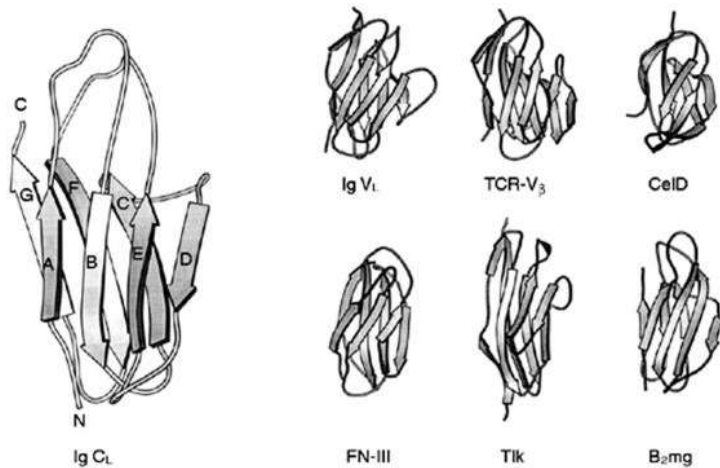


Single molecule manipulation

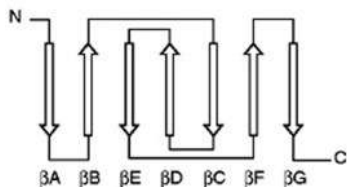
One common feature of many mechanical proteins is that they contain multiple, individually folded protein domains.

Two important examples are the **immunoglobulin (Ig)-type fold** and the **fibronectin-type fold** (the most common of which is fibronectin type 3 or FN-III).

Both are so-called **b-sandwich structures**: these domains might unfold and refold as proteins execute mechanical functions.



Force-induced extension of the **protein titin**, for example, which is responsible for the passive elasticity of muscle, can cause its constituent Ig and FN-III domains to unravel.



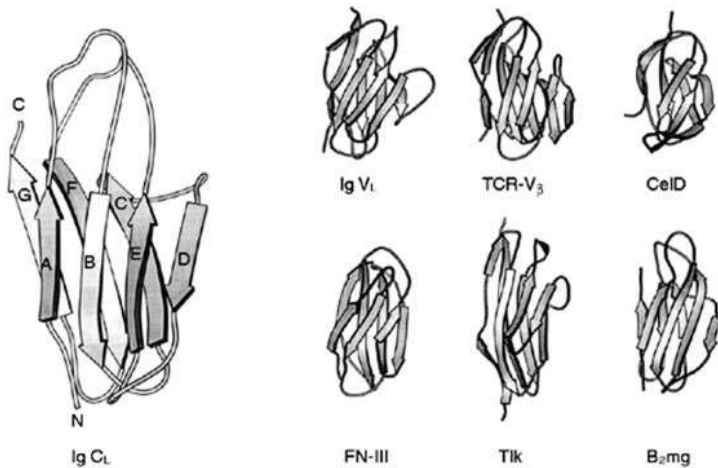
Structural diversity of Ig-type domains. The constant domain of antibodies (Ig C_L) represents the common core present in all Ig-like structures, composed of seven antiparallel β strands labeled A–F. The two-dimensional topological diagram (bottom, left) shows the connected Greek key motif of this structure.

Single molecule manipulation

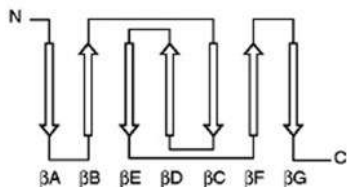
One common feature of many mechanical proteins is that they contain multiple, individually folded protein domains.

Two important examples are the **immunoglobulin (Ig)-type fold** and the **fibronectin-type fold** (the most common of which is fibronectin type 3 or FN-III).

Both are so-called **b-sandwich structures**: these domains might unfold and refold as proteins execute mechanical functions.

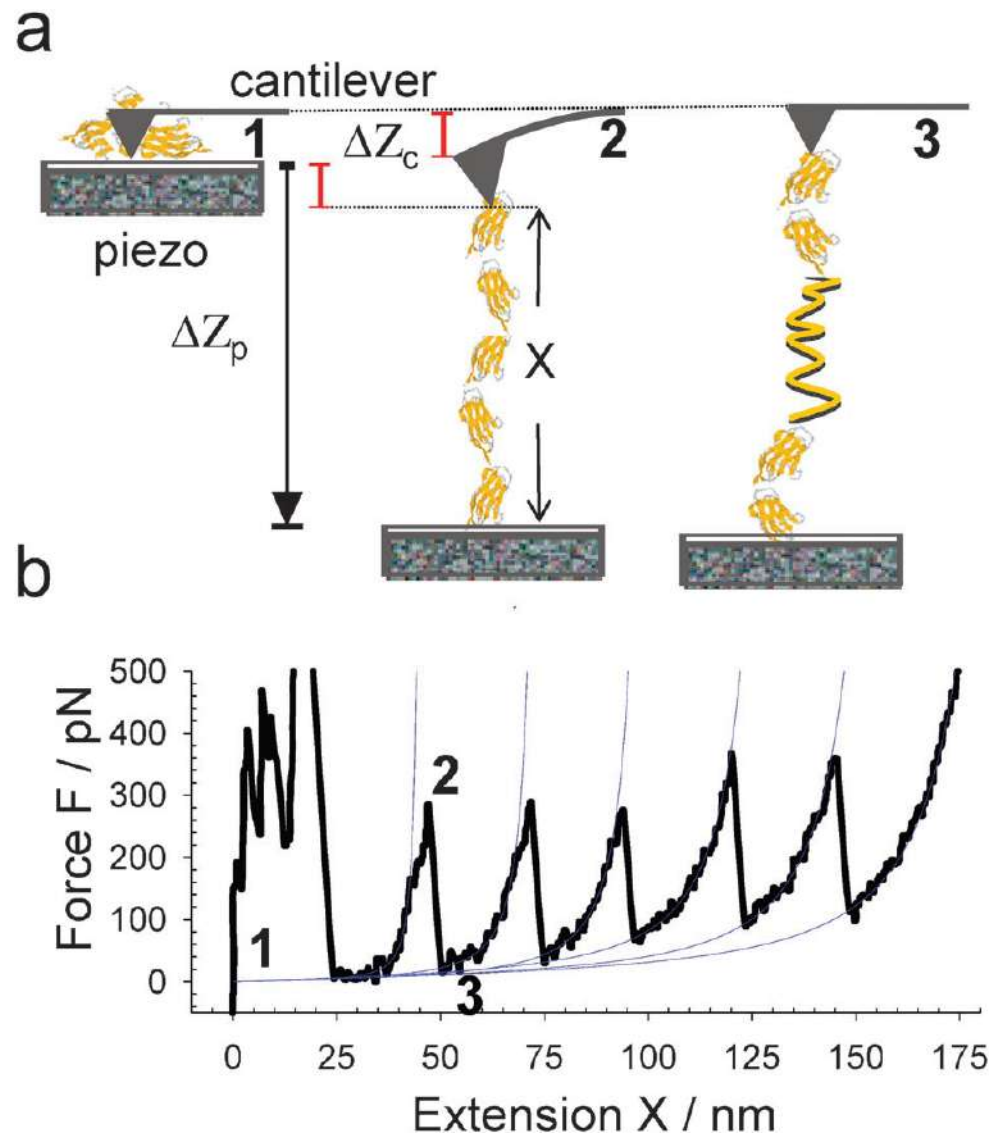


Unfolding and refolding of domains, as part of a particular mechanical function, could be **a mechanism by which tension is maintained as a protein is extended or relaxed**. Unfolding might also contribute to the function of fibronectin by exposing cryptic protein interaction sites that are important in ECM assembly.



Structural diversity of Ig-type domains. The constant domain of antibodies (Ig C_L) represents the common core present in all Ig-like structures, composed of seven antiparallel β strands labeled A–F. The two-dimensional topological diagram (bottom, left) shows the connected Greek key motif of this structure.

Single molecule manipulation

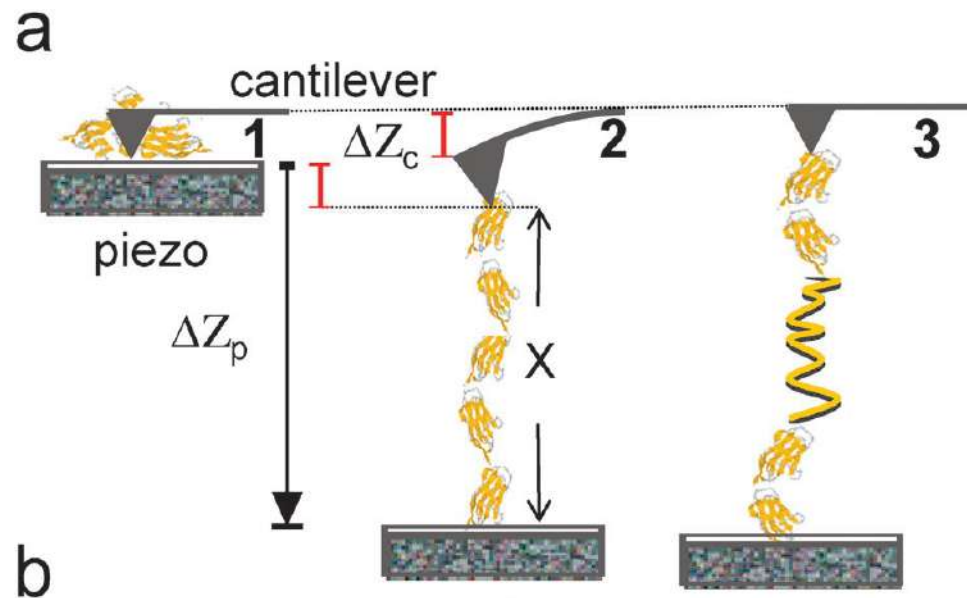


Mechanical proteins are frequently composed of either individually folded globular domains that are connected to each other by short flexible linkers (e.g. titin in muscle) or tightly stacked short helical segments that form elongated single-domain structures (e.g. ankyrin in the RBC skeleton), or longer helical domains that form coiled-coils structures (e.g. spectrin in the RBC skeleton, or myosin in muscle).

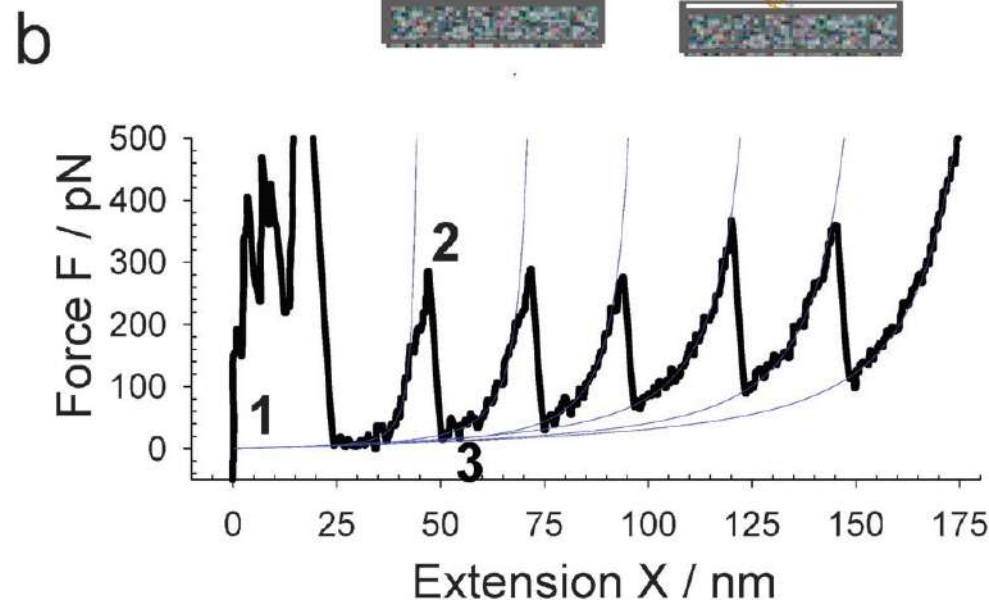
*P.E. Marszalek, Y. F. Dufrene
Chem. Soc. Rev., 2012, 41, 3523–3534*

Single molecule manipulation

Single-molecule techniques analyze individual members in complex, heterogeneous populations, enabling to reveal the diversity of hidden molecular behaviors and rare events.

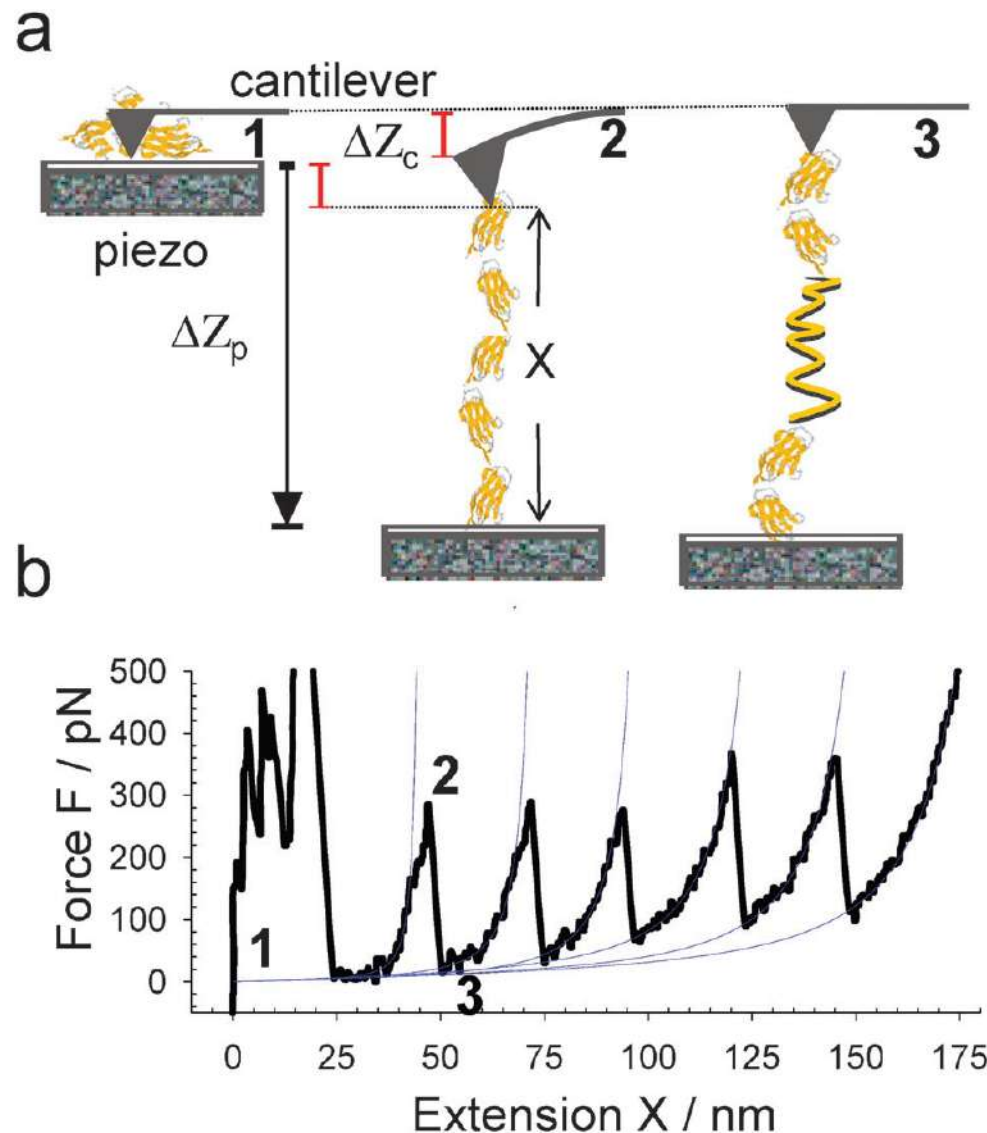


Single-molecule assays permit the direct measurement of the molecular elasticity of polysaccharides, proteins or nucleic acids, otherwise impossible, and the acceleration of certain molecular reactions, such as protein unfolding or ligand–receptor bond rupture.



$$X = \Delta Z_p - \Delta Z_c$$
$$F = k_c \Delta Z_c$$

Single molecule manipulation



The resolution of force measurements depends on the dimensions of the AFM cantilever (the smaller the better) and on the range of measured frequencies

using small cantilevers in the measurement bandwidth of 1 kHz, the **force noise** that limits the resolution can be as small as **3–5 pN** (resolution can be improved to below 1 pN)

$$X = \Delta Z_p - \Delta Z_c$$
$$F = k_c \Delta Z_c$$

How much should be the force to “break” a bond?

The energy of a molecular bond is approx $3 \text{ eV} = 360 \text{ KJ / mole} = 6 \times 10^{-19} \text{ J / bond}$

The length of a molecular bond is approx 0.3 nm or 3 Angstrom but to break a bond is sufficient to stretch it by less. Let us say 1 \AA

$$\text{ENERGY} = \text{FORCE} \times \text{DISTANCE}$$

$$\text{FORCE} = \text{ENERGY} / \text{DISTANCE} = 6 \times 10^{-19} \text{ J} / 0.1 \times 10^{-9} \text{ m}$$

$$= 600 \text{ pN} \quad \text{or} \quad \text{less than } 1 \text{ nN or } 10^{-9} \text{ Newton}$$

Single molecule manipulation

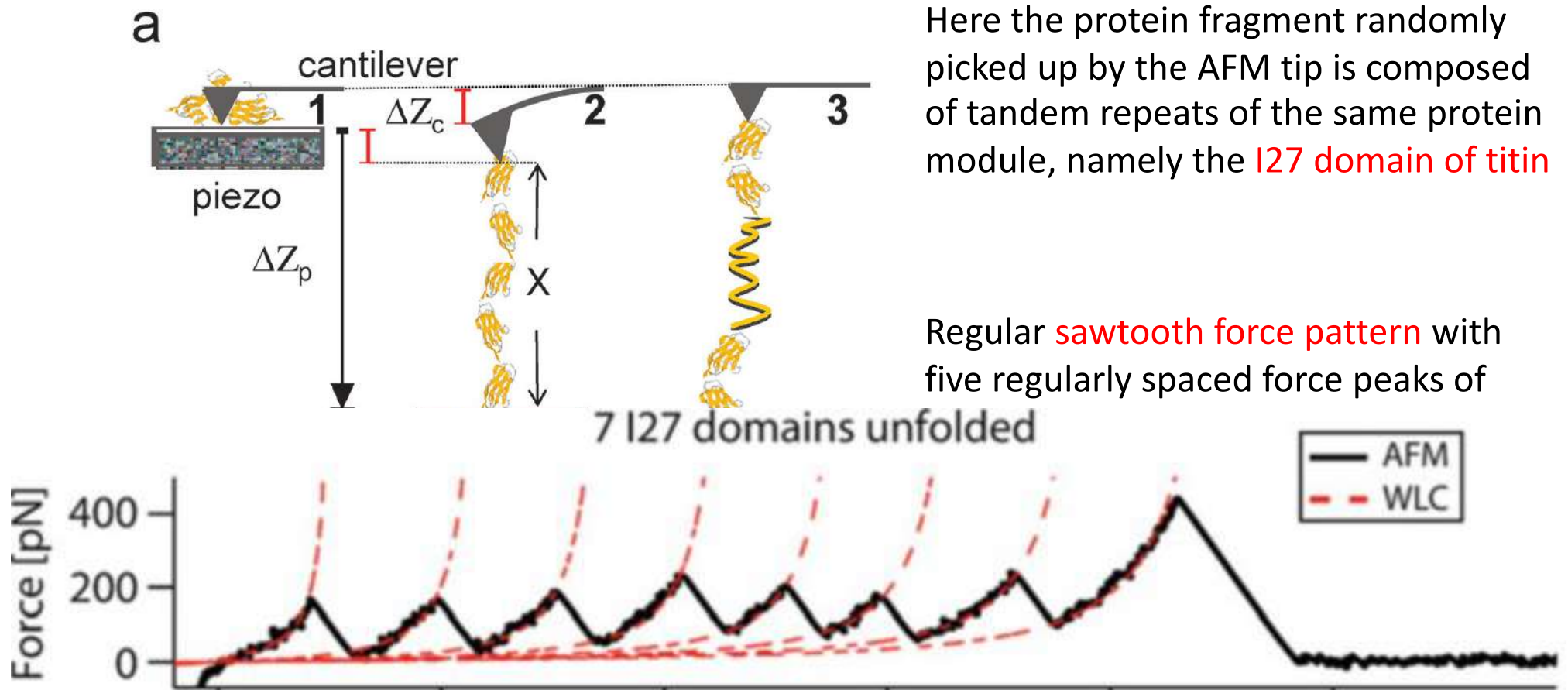
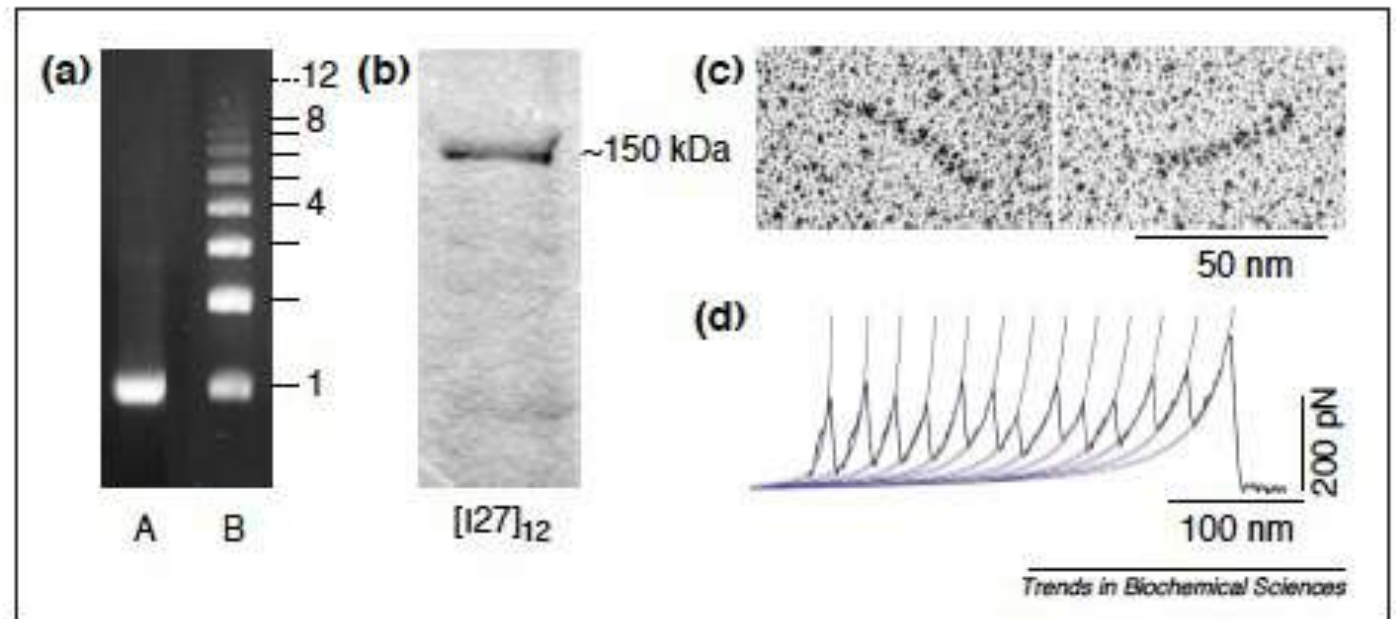
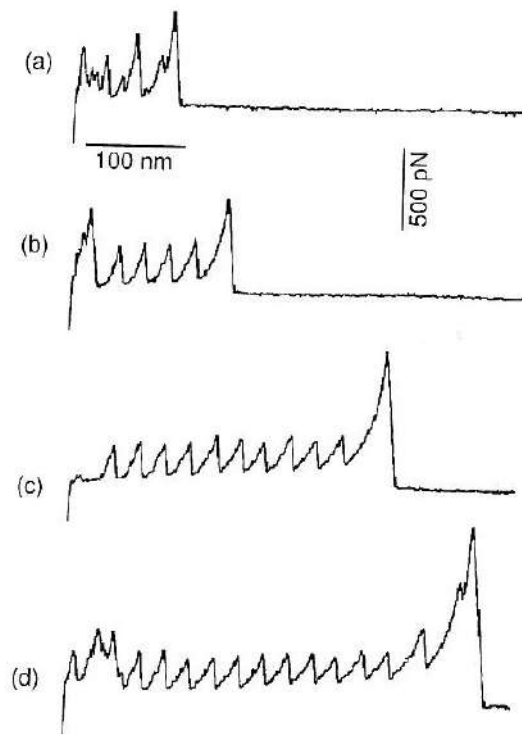


Fig. 33.5 Typical force–extension plot of the unfolding of a polyprotein consisting of seven I27 domains from the titin protein (also called I91 domains). Each peak corresponds to an unfolding event of a single domain. The unfolding force for each domain is ~ 200 pN. The dashed red line indicates a family of worm-like chain fits with a contour length spacing of 28.5 nm between unfolding events

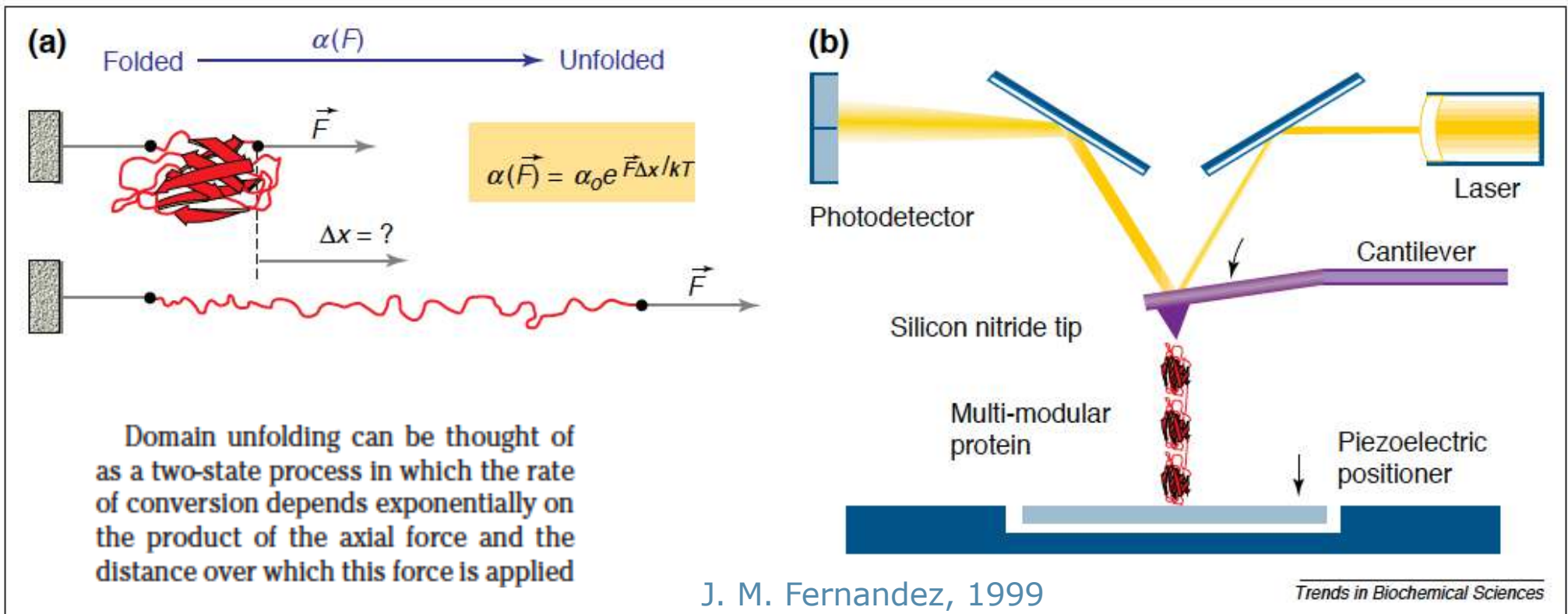
Polyprotein force spectroscopy

Engineered poly I27 Titin



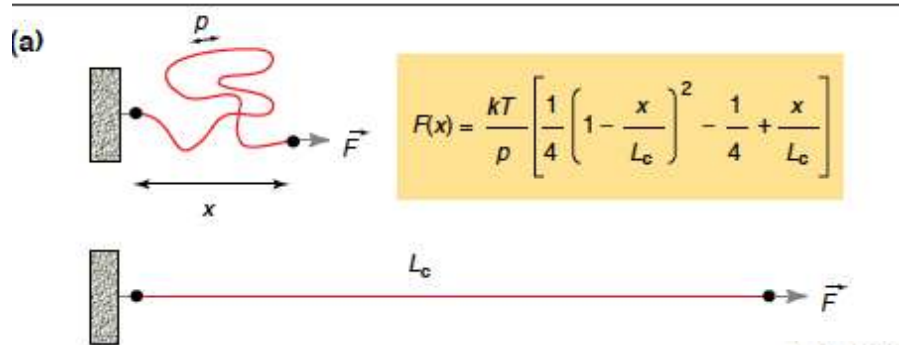
Protein force spectroscopy

When a polymer is relaxed, it forms a coiled structure (maximizes the entropy of its segments). Extension of the polymer generates an opposing force (reduction in entropy) called **ENTROPIC ELASTICITY**: small extensions require little force, resistance to extension rises rapidly as the polymer approaches its full length



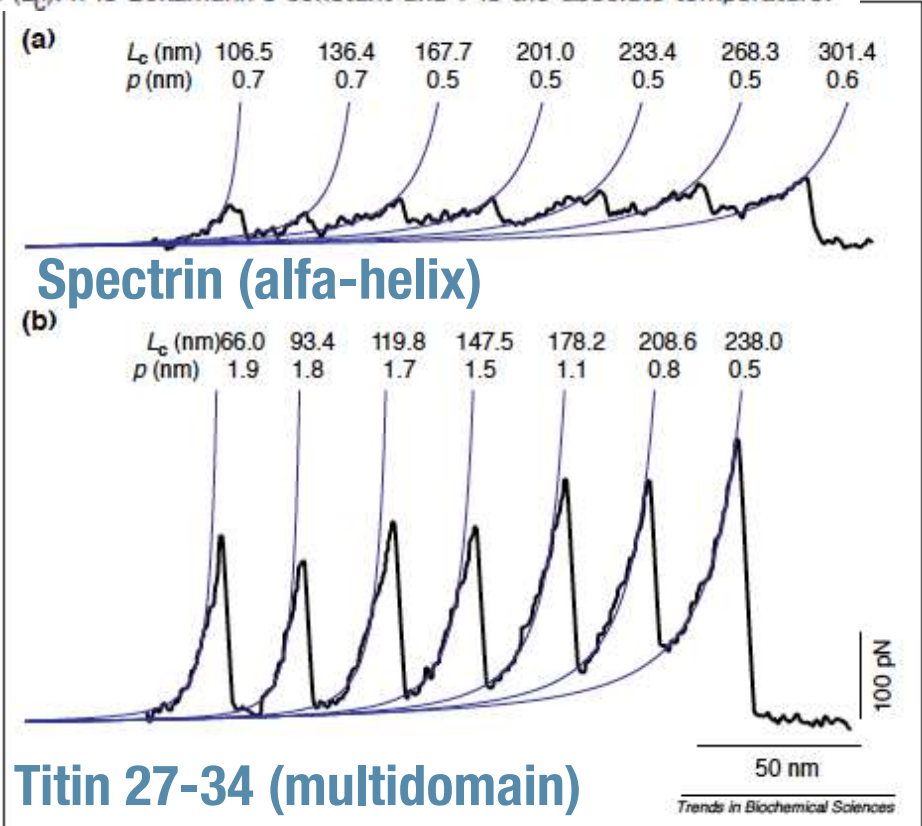
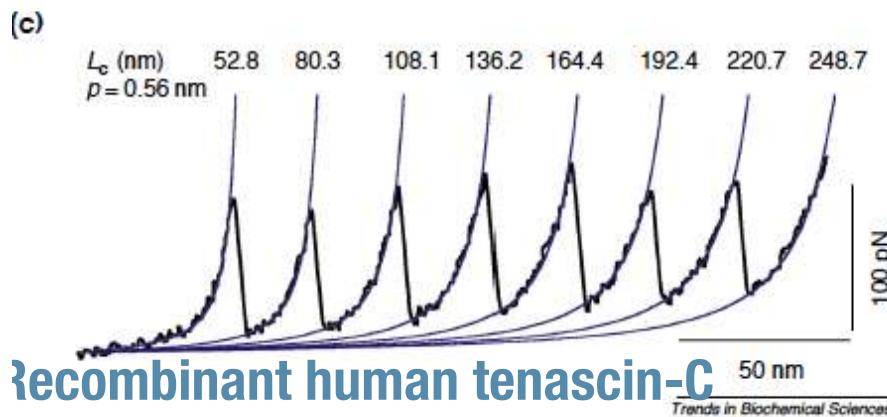
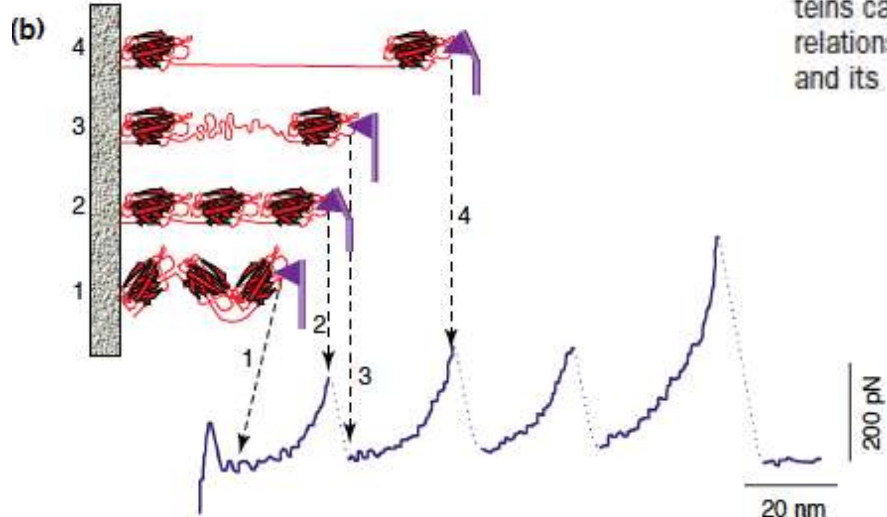
The unfolding of protein domains by an external force. **(a)** When axial stress is applied to a folded domain the protein will unravel. The inset shows an equation describing this transition, where F is the applied force, Δx is the distance over which the unfolding event occurs, α_0 is the rate constant in the absence of an applied force, k is Boltzmann's constant and T is the absolute temperature. Thus, the rate at which protein unfolding occurs increases exponentially with the applied force. This equation is similar to that describing the dissociation of non-covalent bonds placed under an external force^{38,39}. **(b)** The force-extension mode of the atomic force microscope (AFM). When pressed against a layer of protein attached to a substrate, the silicon nitride tip can adsorb a single protein molecule. Extension of a molecule by retraction of the piezoelectric positioner results in deflection of the AFM cantilever. This deflection changes the angle of reflection of a laser beam striking the cantilever, which is measured as the change in output from a photodetector.

Polyprotein force spectroscopy



At **small displacements**, reduction in the number of conformations gives rise to **entropic elasticity forces**
 At **large extensions**, tension in the molecular backbone may lead to **enthalpic elasticity effects** (bond deformation, rupture of intramolecular hydrogen bonds and even conformational changes of the entire molecule)

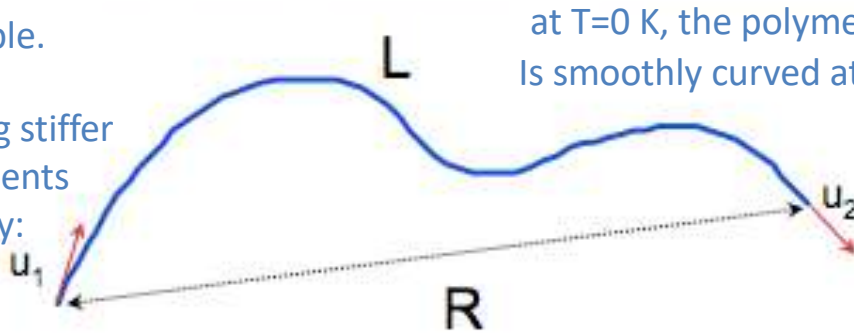
The entropic elasticity of proteins and domain unfolding. (a) The entropic elasticity of proteins can be described by the WLC (worm-like chain) equation (inset), which expresses the relationship between force (F) and extension (x) of a protein using its persistence length (p) and its contour length (L_c). k is Boltzmann's constant and T is the absolute temperature.



The behaviour of polymers under mechanical stress is described by the **worm-like chain (WLC) model of elasticity**

Equilibrium Statistic of a Worm-like Chain

Isotropic rod continuously flexible. The worm-like chain model is particularly suited for describing stiffer polymers, with successive segments displaying a sort of cooperativity: all pointing in roughly the same direction



at T=0 K, the polymer adopts a rigid rod conformation
Is smoothly curved at RT

$$\left\langle \vec{u}_1 \cdot \vec{u}_2 \right\rangle = e^{-\frac{L}{P}}$$

The persistence length of the molecule, P , is the decay length through which the initial orientation of the molecule persists. It is a measure of the stiffness of a polymer chain.

This model describes a polymer as a continuous string of a given total (or **contour length**). Bending of the polymer at any point influences the angle of the polymer for a distance, referred to as the **persistence length**, that reflects the polymer flexibility. The smaller the persistence length, the greater the entropy of the polymer and the greater the resistance to extension. The persistence length and the contour length comprise the adjustable parameters of the WLC model.

Single molecule force spectroscopy

The statistical model used for describing the elastic behavior of the polymer is the WORM-LIKE CHAIN (WLC) model (proteins, DNA/RNA) and the FREELY-JOINTED CHAIN (FJC) model (polysaccharides)

WLC model

the polymer is an irregular curved filament, **linear on the scale of the persistence length l_p** , which represents the stiffness of the molecule.

Molecules with low persistence length have a tendency to form coils.

Extension is limited by the **contour length L_c** of the molecule, **i.e.** the length of the linearly extended molecule without stretching the molecular backbone.

In this model, the force **F versus** extension **x** is approximately given by:

$$F(x) = k_b T / l_p [0.25(1 - x/L_c)^{-2} + x/L_c - 0.25]$$

Single molecule force spectroscopy

The statistical model used for describing the elastic behavior of the polymer is the WORM-LIKE CHAIN (WLC) model (proteins, DNA/RNA) and the FREELY-JOINTED CHAIN (FJC) model (polysaccharides)

FJC model

the polymer is considered as a series of rigid, orientationally independent statistical (Kuhn) segments, connected through flexible joints.

The segment length, or **Kuhn length l_k** , is a direct measure of the chain stiffness and is related to the contour length by $L_c = n l_k$.

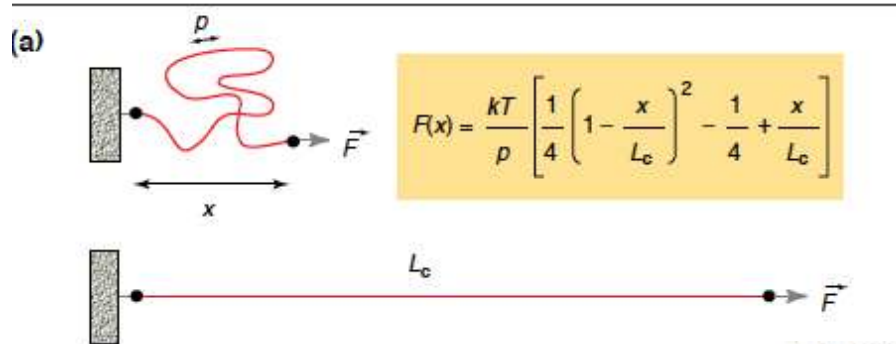
In this model, the extension x versus force F is approximately given by:

$$x(F) = L_c [\coth(Fl_k/k_b T) - k_b T / Fl_k]$$

And, allowing Kuhn segments can stretch and align under force with elasticity k_s :

$$x(F) = L_c [\coth(Fl_k/k_b T) - k_b T / Fl_k] [1 + nF/k_s L_c]$$

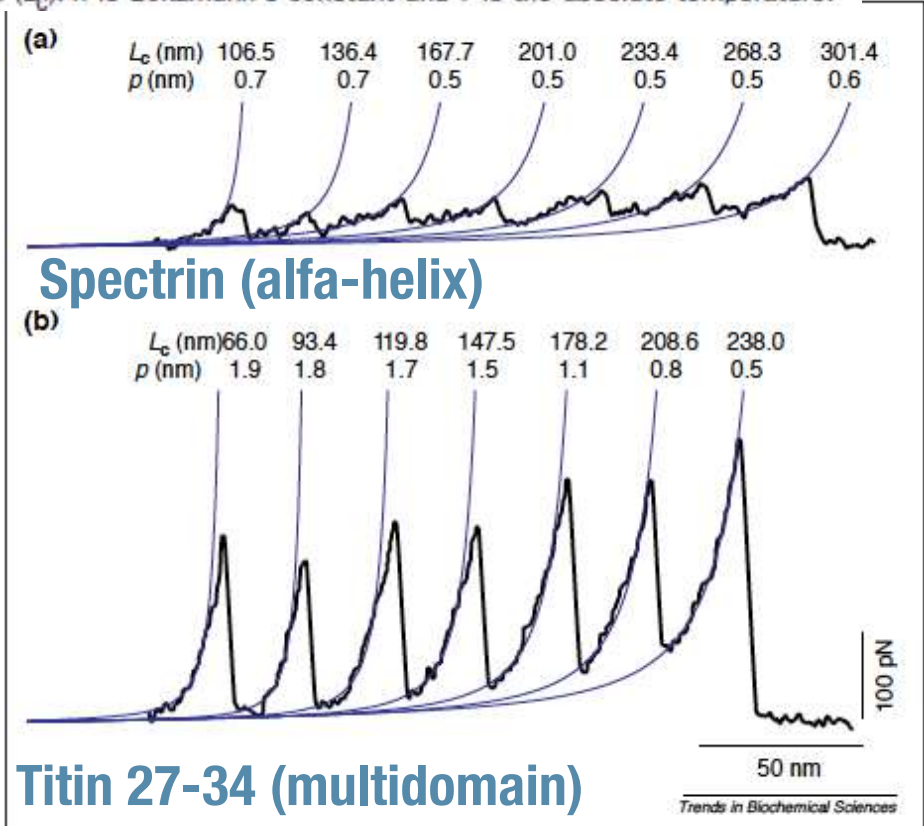
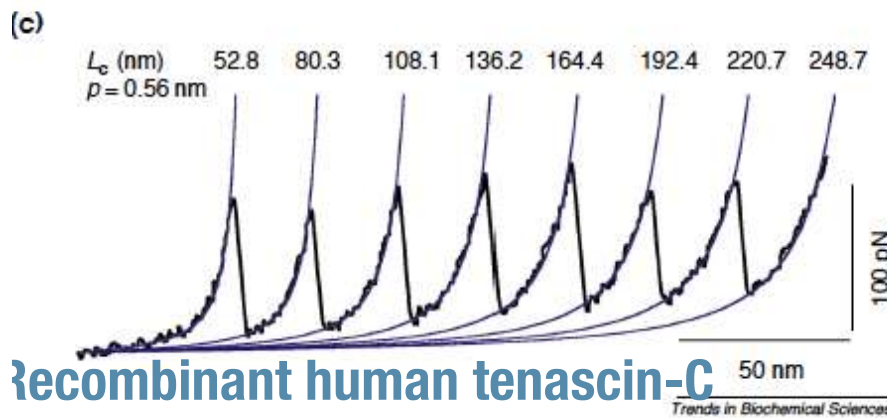
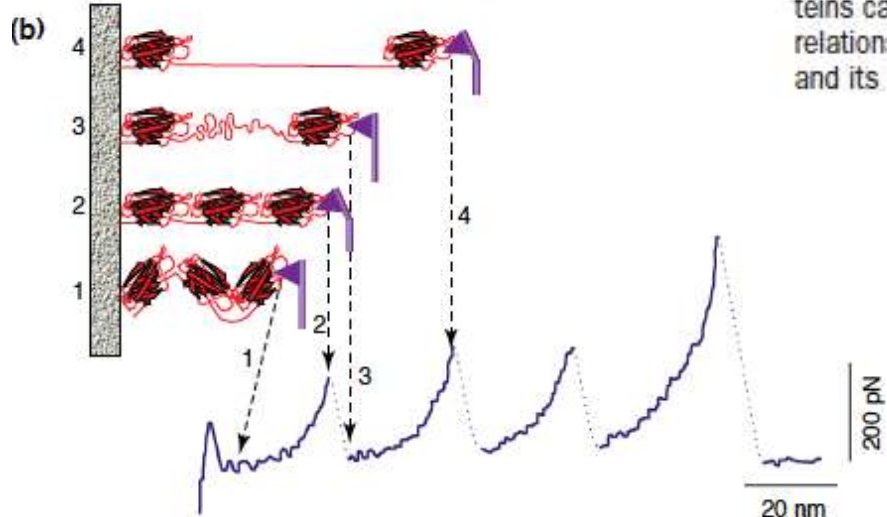
Polyprotein force spectroscopy



Interestingly, the measured unfolding forces generally increase with **extension speed**. Varying this parameter may provide an estimate of the **unfolding off-rate** and of the **width of the unfolding energy barrier**.

Reliable force data on a given molecule require recording several hundred force-curves using many independent tips and samples and proper model to fit data.

The entropic elasticity of proteins and domain unfolding. (a) The entropic elasticity of proteins can be described by the WLC (worm-like chain) equation (inset), which expresses the relationship between force (F) and extension (x) of a protein using its persistence length (p) and its contour length (L_c). k is Boltzmann's constant and T is the absolute temperature.



Unfolding-refolding

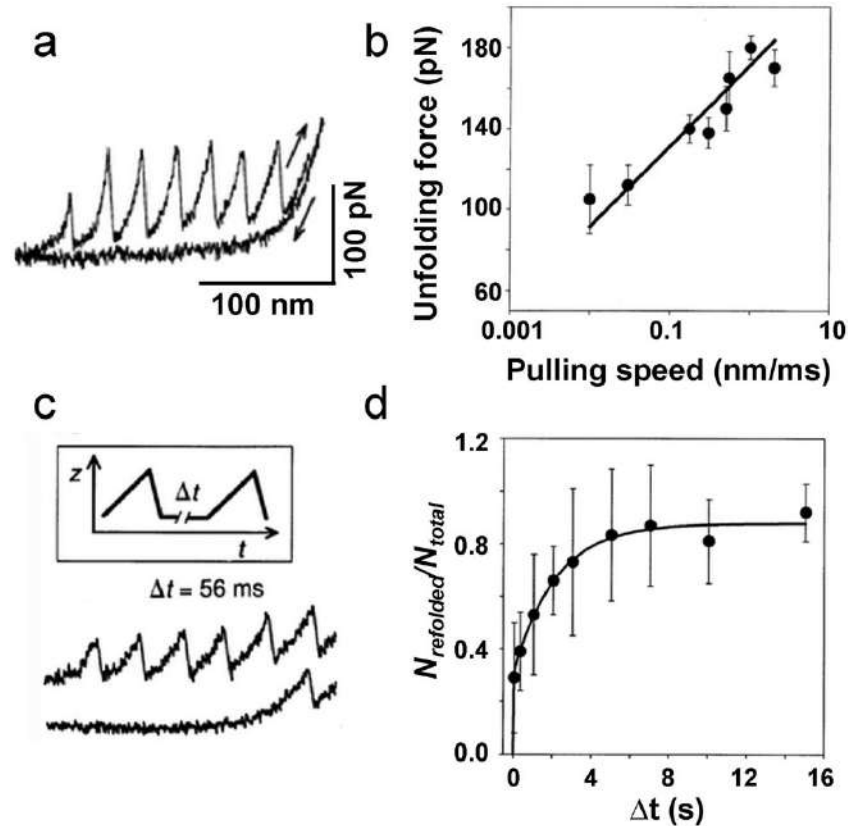
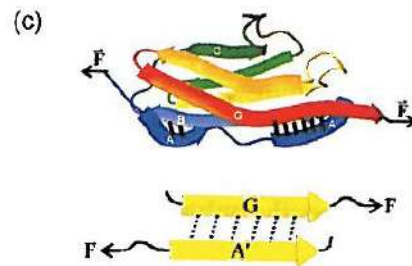
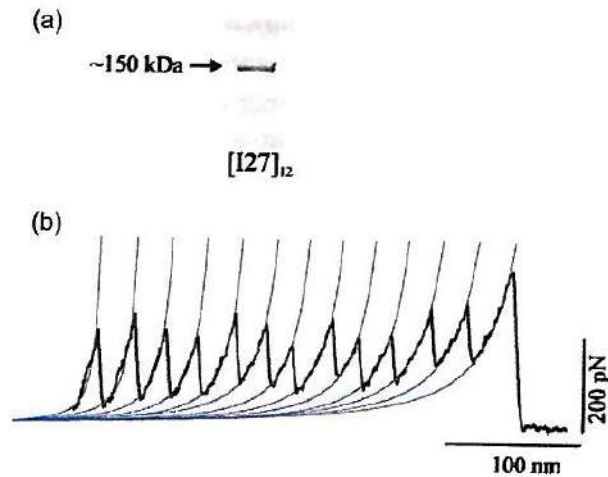


Fig. 3 Repeated unfolding and refolding cycles of tenascin. (a) The same TNfnAll fragment of tenascin was repeatedly stretched at various stretching speeds. (b) The average unfolding force *vs.* stretching speed. (c) A double-pulse experiment where the same molecule is stretched, relaxed for time Δt and stretched again. (d) The fraction of folded modules (counted from the second unfolding pulse) as a function of Δt .

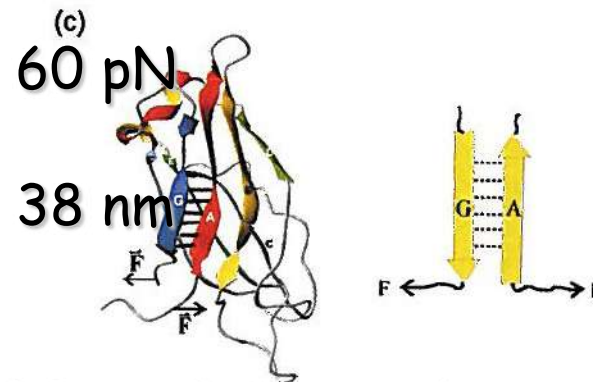
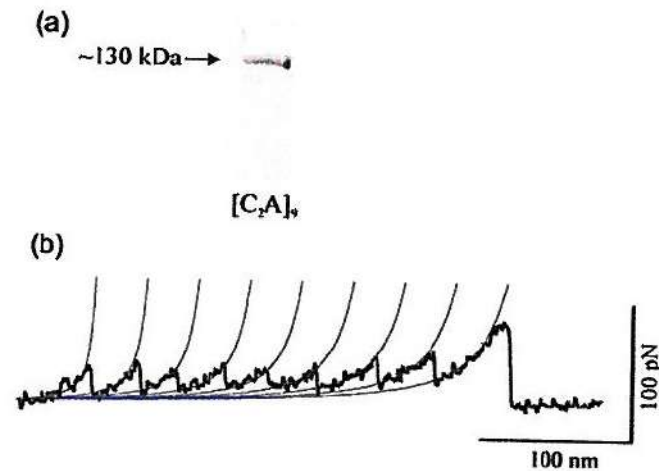
The data can be fitted using a Monte Carlo approach with a two-state model of the unfolding/refolding process, allowing the extraction of important parameters characterizing the unfolding reaction such as the distance to the unfolding transition state and the unfolding rate constant extrapolated to zero force

Polyprotein force spectroscopy



$F = 204 \text{ pN}$

$\delta Lc = 28 \text{ nm}$



Two proteins with "all beta" structure and β -sandwich topology
 -titin has seven β strands which fold face-to-face through backbone H-bonds and hydrophobic core interactions, perpendicular to stretching direction

-C2 β sandwich with 127 aminoacids arranged in 8 antiparallel strands. domains are in a zipper configuration